„Discrete solitons in media with saturable nonlinearity“

A Dissertation

for Obtaining a Doctoral Degree

in Natural Sciences

by

Milutin Stepić

from Zemun, Serbia and Montenegro

Presented to the Faculty of Mathematics and Natural Sciences of the Technical University of Clausthal

date of the oral exam

03. December 2004

Chairman of PhD Committee	Prof. Dr. Dieter Mayer
Supervisor	Prof. Dr. Detlef Kip
Reviewer	Dr. Ljupčo Hadžievski
Reviewer	Apl. Prof. Dr. Wolfgang Lücke

CONTENT

1. INTRODUCTION

Solitons represent localized structures which exist due to the exact balance between nonlinear self-interaction and dispersive and/or diffractive effects. They can be found in quite different nonlinear systems in nature such as fluids, optical fibers, Bose-Einstein condensates, etc. Mathematically, solitons are the exact particular solutions of various nonlinear partial differential equations, such as Korteweg-de Vries, Klein-Gordon, and Kadomtsev-Petviashvili equations. They have an infinite number of conserved quantities and demand an infinite phase space to exist. However, most nonlinear physical systems of importance are described with non-integrable evolution equations that have so-called solitary wave solutions. These localized structures, although with only few conserved quantities like power and Hamiltonian and in spite of radiation losses, exhibit a surprising robustness and vitality during their propagation and interactions. Especially in the optics community it is quite usual to neglect these differences between solitons and solitary waves and to use only the term soliton, which shall be performed through this thesis.

The first scientifically documented report about the beautiful phenomena of soliton formation originates from the Scottish naval engineer John Scott Russell [1], who observed "a wave of translation" while riding a few miles after it on horse back along a narrow barge channel near Edinburgh in Scotland in August 1834. Years later after this first observation he built a tank in his own garden and started to experiment with shallow water waves. Russell discovered that their shape can be described by a sech^2 function and determined that their peak amplitude is proportional to the velocity of the wave. However, at that time there was no equation describing such water waves and possessing solitary solutions. It took more than sixty years until Korteweg and de Vries in 1895 derived a nonlinear wave equation which describes the evolution of waves in a shallow one-dimensional (1D) water channel [2]. As a confirmation of Russel's experimental investigations they have shown theoretically that such a system admits solitary wave solutions.

From that time, being regarded unstable for all possible initial conditions solitons stayed dormant for decades. 1960 Gardner and Morikawa [3] have proved that these solutions are spatio-temporal stable structures for a wide set of initial conditions. Five years later Fermi, Pasta and Ulam have explored the mechanisms which lead to thermal equilibrium [4]. They numerically integrated the ordinary differential equations which describe a set of coupled anharmonic oscillators. Because of the equipartition of energy they thought that the nonlinearity would quickly cause energy redistribution among all the modes, but they found that only a very small number of modes were actually participating in the system dynamics. In the same year Zabusky and Kruskal, while studying the Fermi-Pasta-Ulam problem, rederived the Korteweg-de Vries equation as a continuum approximation [5]. They have numerically solved this equation for periodic boundary conditions and revealed that the solitary solutions of this equation interact elastically with each other. Exactly because of this particle-like property they named these solutions "solitons". In 1967 Gardner, Greene, Kruskal and Miura, while exploring the initial value problem for the Korteweg-de Vries equation, discovered a new method of mathematical physics based on the ideas of direct and inverse scattering [6]. One year later Lax generalized these ideas [7], and in 1971 Zakharov and Shabat proved that this method also can be applied to another physically significant nonlinear evolution equation, namely the nonlinear Schrödinger (NLS) equation [8]. Three years later Ablowitz, Kaup,

Newell and Segur showed that this method is analog to the Fourier transform for nonlinear problems. They called this procedure the inverse scattering transform [9].

Although solitons are observed in various nonlinear systems such as DNA[1] molecules [10] and Scheibe aggregates [11], in this thesis the accent is put on solitons in nonlinear optics. The realm of nonlinear optics consists of those phenomena where the optical properties of a material depend on the strength of the applied field. As only the laser light usually is intense enough to modify the optical properties of a dielectric material it is not surprising that the beginning of nonlinear optics is usually taken to be 1961, when Franken, Hill, Peters and Weinreich observed the generation of a second harmonic frequency by focusing a laser beam through crystalline quartz [12]. The idea that an optical beam may induce a waveguide and guide itself in it was suggested by Askary'an one year later [13]. Spatial self-focusing of optical beams due to third-order nonlinearities was for the first time experimentally analyzed in 1964 [14], while the first experiment on spatial solitons was reported one year later by Ashkin and Bjorkholm [15]. The existence of temporal optical solitons in lossless fibers was theoretically proposed by Hasegawa and Tappert in 1973 [16], and the first experimental realization in a long-distance all-optical transmission line was carried out by Mollenauer and Smith in 1988 [17]. Discrete solitons, which are the main objects of investigation in this thesis, were theoretically suggested by Christodoulides and Joseph 16 years ago in 1988 [18]. The first experimental observation of these localized structures, which possess a great potential in optical communications, was published only recently in 1998 [19].

In this thesis the dynamics of discrete solitons in media with a saturable type of the nonlinearity is investigated analytically, numerically, and experimentally. A more detailed classification of solitons with respect to their dimensionality, colour, coherence, and nonlinear mechanism is performed in the second chapter. Chapter 3 describes the connection between discrete solitons in periodic waveguides and band gap structures in solid state physics, including the phenomena of discrete diffraction and Bloch oscillations. Furthermore, a usual approach for describing discrete solitons in the first band-gap, the so-called tight-binding approximation, is tackled. In this approximation the system dynamics is represented by the discrete NLS (DNLS) equation. It is shown that a plane wave solution of this equation is modulationaly unstable and it might evolve to a discrete soliton. Subsequently, a rough classification of different discrete solitons is presented. Finally, at the end of this chapter, the stability of solitons is investigated.

In the next chapter the model equation, which describes the propagation of optical spatial pulses in discrete media with saturable screening photorefractive nonlinearity, is exposed. A few stationary unstaggered solutions are obtained and their stability with respect to small perturbations is investigated. The numerical examination of the stability of stationary soliton solutions reveals that such systems exhibit a cascade mechanism of saturation. A similar model equation which describes the propagation of optical pulses in discrete media with saturable photovoltaic, photorefractive nonlinearity is presented in Chapter 5. Also, the stability of different analytically discovered stationary staggered solutions is examined here.

Chapter 6 is devoted to the intrinsically localized modes (i.e., discrete screening and photovoltaic solitons) and the Peierls-Nabarro (PN) potential barrier, which can be roughly described as the energy difference between a localized mode centred on the site (mode A) and a localized mode centred between sites (mode B). It is discovered that this potential, opposite to discrete media with cubic nonlinearity, may change its sign, which has a strong influence on the stability of the modes A and B. The corresponding PN potential has multiple zeroes, which

[1] Deoxyribose nucleic acid.

enables increased mobility of discrete solitons across the system. New phenomena, such as stable propagation of mode B across the array and elastic interactions of discrete screening photorefractive solitons are presented.

Chapter 7 is reserved for experimental results. The procedure of channel waveguide formation in lithium niobate (LN) and strontium barium niobate (SBN) is explained at the beginning of this chapter. Experimental observations of discrete diffraction, diffraction-less propagation in LN nonlinear waveguide arrays, formation of stable discrete photovoltaic solitons as well as their steering across the array are demonstrated. Conclusions and possible directions for future investigations are given in Chapter 8.

2. CLASSIFICATION OF SOLITONS

A brief classification of solitons can be found in this Chapter. Parallels between spatial and temporal solitons are drawn. Differences between them are accented, too. Basic facts about two most investigated kinds of spatial solitons, namely quadratic and photorefractive solitons, are given. Finally, a brief overview of generic families of solitons is presented.

2.1 SPATIAL AND TEMPORAL SOLITONS

Optical solitary waves, i.e., spatial, temporal, and spatio-temporal solitons have been the subject of intense experimental and theoretical studies in the past few decades. Solitons, which are bounded or self-guided beams in space, or localized wave packets in time, emerge from a nonlinear change in the refractive index of a material induced by the light intensity distribution. When the combined effects of optical nonlinearity and beam diffraction (in case of spatial solitons) or chromatic pulse dispersion (in case of temporal solitons) exactly compensate each other, the beam or pulse propagates without any change in shape and is said to be self-trapped. On the other hand, so-called spatio-temporal solitons (or optical bullets) are the result of a dynamical balance between nonlinearity, dispersion, and diffraction, and are simultaneously localized both in time and space [20].

Nonlinear effects responsible for soliton formation in fibres are usually weak and Kerr-like, i.e., the induced local refractive index change Δn_r is directly proportional to the light intensity I, $\Delta n_r = n_2 I$, where n_2 is the Kerr coefficient. Here, the evolution of the complex amplitude of the electrical field envelope can be fairly well described by virtue of a cubic NLS equation. Depending on the sign of the group-velocity dispersion, two different types of localized solutions can be found: bright and dark temporal solitons. Bright solitons in optical silica fibers, which always possess a positive Kerr coefficient n_2, exist in the anomalous dispersion regime, while dark solitons may be observed in the regime of normal dispersion [15, 21]. Similarly, spatial solitons in planar waveguides or bulk media always experience normal diffraction, i.e., the beam diverges during propagation. Here, the involved nonlinearity can be either positive (so-called self-focusing media) [22] or negative (self-defocusing media) [23], which, again, enables the existence of bright and dark localized solutions.

When the group velocity dispersion in an optical fibre is anomalous or, analogously, when the nonlinearity of a bulk medium is self-focusing, a uniform continuous wave is modulationally unstable and breaks up in a train of localized pulses in fiber or beams in the spatial case, respectively [24, 25]. In the case of normal group velocity dispersion in fibres or self-defocusing nonlinearity in bulk media bright solitons do not exist. Here initially localized temporal pulses experience enhanced dispersion, resulting in light induced chirping (self-phase modulation) and broadening of the pulse. In the spatial case, linear dispersion is enhanced by the defocusing nonlinearity. Thus, uniform, constant amplitude waves are modulationally stable and localized states (dark solitons) may appear only as a dip on a continuous wave background [26].

The dimensionless NLS equation can be written in the form

$$i\frac{\partial U}{\partial z} + \frac{1}{2}\frac{\partial^2 U}{\partial x^2} \pm |U|^2 U = 0, \tag{2.1}$$

where + stands for the self-focusing nonlinearity while – is for the self-defocusing nonlinearity. The normalized, slowly varying wave envelope is U, the transverse coordinate is x, and z represents the propagation coordinate. Within the 1D NLS model, a bright stationary soliton of amplitude A_0 is described by

$$U(x,z) = \frac{A_0}{\cosh(A\,x)} \exp(i\,A_0^2\,z), \tag{2.2}$$

while a dark soliton with a boundary condition $|U(x \to \pm\infty)| = U_\infty$ has the form

$$U(x,z) = U_\infty \tanh(x) \exp(i\,A_0^2\,z). \tag{2.3}$$

As one can see in Fig. 2.1, bright solitons have a constant phase and vanishing asymptotic amplitude, while dark solitons have a phase jump of π across the centre and finite tails.

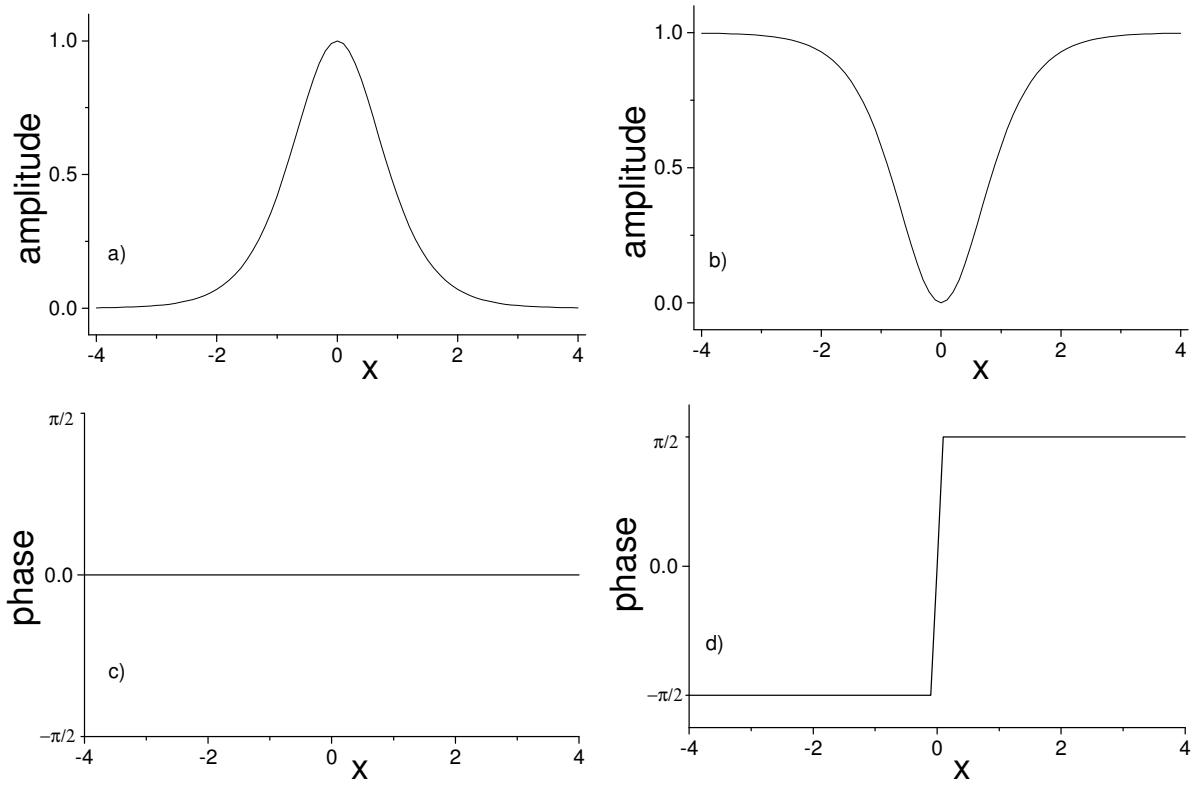

Fig. 2.1 *Amplitude and phase profiles of bright (a, c) and dark NLS solitons (b, d).*

Although, at first sight, temporal and spatial solitons possess several similarities in their theoretical treatment, there are two important differences one should bear in mind. Firstly, while in fibres (because of the small dispersion of pulses) the refractive nonlinearity is always rather weak, in bulk media linear diffraction is not a small dynamical factor, which means that the required nonlinearity for soliton formation should be significantly higher. Because of that, different models with saturable nonlinearity are often applied [27, 28]. On the other hand, what sets spatial solitons apart from their temporal analogues is their dimensionality. Temporal solitons in fibres are described by a (1+1) D NLS equation, while spatial solitons are (2+1) D objects. The nomenclature $(m+1)$ D means that the beam diffracts in m dimensions while it propagates in one dimension. The fact that the spatial domain exhibits a higher dimensionality

leads to several interesting processes and phenomena with no temporal counterpart. Examples are soliton spiralling [29], vortex solitons [30, 31], rotating vector solitons [32], etc. The main reason for such a disproportion is the fact that the number of various nonlinear mechanisms that can support spatial solitons is much larger than for temporal solitons.

2.2 REALM OF SPATIAL SOLITONS

Besides the Kerr-based solitons a few new classes of solitons are discovered till now. For example, spatial solitons can form in liquid crystal waveguides, which possess reorientational nonlinearity [33], or in media with a resonant nonlinearity [34]. But, certainly, quadratic and photorefractive solitons are the most investigated objects within the soliton family, which may be explained by the relative simplicity of the experimental realizations in these materials.

2.2.1 Quadratic solitons

These coherent structures consist of multi-frequency waves which are mutually coupled via second order nonlinearity. They were proposed by Sukhorukov and Karamzin in 1976 [35], while Torruellas and co-workers experimentally observed them in 1995 [36]. Here the beam-trapping occurs as an outcome of the rapid energy exchange between the fundamental and second harmonic, which preserves the spatial width and the power of the beam. Quadratic solitons are found to be stable in both bulk media [37] and slab waveguides [36].

Quadratic solitons can be also generated during the second harmonic generation process with the fundamental beam only [38]. Their significance lies in the fact that they revealed that in nonlinear optics soliton formation can be achieved by virtue of nonlinear wave mixing. Contrary to experiments using KTP[2] crystals [37], where the exact phase-matching condition has to be chosen, in $LiNbO_3$ waveguides (1+1) D quadratic solitons with only a small amount of second harmonic were generated [39]. In this so-called cascading limit only a tiny amount of second harmonic wave amplitude is necessary in order to induce a nonlinear phase shift to the fundamental beam. Here the effective nonlinearity depends on the phase-mismatch and is tunable both in sign and magnitude. Moreover, the rigid phase-matching conditions are here not important at all.

2.2.2 Photorefractive solitons

Photorefractive solitons attract the biggest attention both in soliton and optical communication community. They were predicted by Segev and co-workers in 1992 [40]. Due to the small optical power required for their generation (micro watt level) it is easy to obtain them experimentally even with continuous wave lasers and standard optical equipment, and an almost full control of the relevant parameters can be obtained in the experiment. The formation time of these solitons can be as short as milliseconds and below. In many experiments, the magnitude of the saturable nonlinearity of photorefractive crystals can be easily driven by

[2] Potassium titanium oxide phospate ($KTiOPO_4$).

adjusting the applied external electrical field. Furthermore, in some photorefractive media there are enough scattering centres to monitor the beam propagation visually.

To the class of photorefractive solitons belong photovoltaic [41, 42], quasi steady-state [40, 43], and screening solitons, which have been predicted and observed ten years ago [44, 45]. Quasi steady-state solitons appear during the slow screening process of a field applied externally to a photorefractive crystal. They are transient in nature and their most prominent features are their independence of the absolute light intensity and the capability of trapping in both transverse dimensions. Photovoltaic solitons exist in materials that are both photovoltaic and photorefractive. This type of solitons stem from photovoltaic currents that generate space charge fields and corresponding index perturbations, analogous to the nonlinearity in a saturable absorber.

Screening solitons appear in the steady state, after the external field is screened non-uniformly as a result of a transversely non-uniform intensity distribution. The physical mechanism which lies beyond the generation of screening solitons is rather complicated and therefore the interested reader is directed to some of the articles where this is explained in detail [46, 47]. The mechanism includes several processes with a retarded temporal response. Both charge separation and the subsequent generation of a space charge electric field under the influence of an external beam require a finite time which is proportional to the dielectric relaxation time. Due to the charge transportation over macroscopic distances via diffusion and/or drift this mechanism is also anisotropic and non-local. This type of solitons is interesting for steering and waveguide applications. Once the index distribution responsible for the self-trapping is established, stronger beams of longer wavelength with low photorefractive sensitivity can be guided by these index waveguides [48], provided that they are at wavelengths where the absorption is small. The waveguides induced by these solitons can be made permanent by suitable fixing techniques. Moreover, one might erase and overwrite them by electrical repoling the crystal or by bringing its temperature near a crystalline phase transition [49].

2.3 GENERIC FAMILIES OF SOLITONS

Apart from these above mentioned solitons in bulk materials, in other physical systems, there exist more generic families of solitons that are not directly related to specific media. Some examples are discrete solitons, incoherent solitons, cavity solitons, multi-component vector solitons, and spatio-temporal solitons. In this section some basic properties of these solitons are described, with the exception of discrete solitons, which are in the focus of this thesis and which are treated in more detail in the next chapter.

2.3.1 Incoherent solitons

In systems with cubic (Kerr) and quadratic nonlinearity the nonlinear response of the medium is basically instantaneous with respect to changes in the optical field parameters. Anyway, some nonlinearities, such as photorefractive and thermal one [50], have a rather slow response time. In the case that this time is much longer than random fluctuations in the phase of an optical field it is possible to obtain so-called incoherent solitons. These self-trapped spatially incoherent wave-packets were observed in a slowly-responding photorefractive crystal by Mitchell and co-workers in 1996 [51]. That discovery broke the dogma that all solitons are

solely coherent structures. One year later the effect of self-trapping was confirmed also for a both spatially and temporally incoherent white light beam of an evanescent light bulb [52].

A spatially incoherent monochromatic beam consists of speckles that are caused by a randomly varying phase distribution in time. The envelope of this beam is defined by virtue of the time-averaged intensity. As all speckles contribute to diffraction, in the limit when the size of the speckles is much smaller than the beam diameter, diffraction is driven not by the beam's envelope but by the size of speckles, i.e., by the degree of spatial coherence. Obviously, such beams cannot self-trap in media with an instantaneous nonlinear response, because each speckle forms a small lens in the medium and captures a small part of the beam, thus fragmenting the envelope of the beam. But, if the nonlinearity has a response time much longer than the phase fluctuation time across the beam, the nonlinearity responds to the time-averaged envelope and not to the instantaneous speckles. In order that an incoherent soliton occurs two additional conditions have to be satisfied. Firstly, the speckled (multimode) beam should be able to induce, via the nonlinearity, a multimode waveguide and, secondly, this multimode beam must be able to guide itself in its own induced waveguide [53].

2.3.2 Vector solitons

Vector solitons consist of two or more modes (components) that mutually self-trap in a nonlinear medium. So, strictly speaking, quadratic solitons, which consist of a conglomerate of the first and the second harmonic, can be regarded as vector solitons. A key prerequisite for forming a stationary vector soliton is that the interference among the components does not contribute to the nonlinear index change Δn_r. If this is not fulfilled the induced waveguides do not possess a constant shape during propagation and thus the components self-trapped within are not stationary [54].

Vector solitons, which were first suggested by Manakov in 1974 [55], may be composed of two orthogonally polarized components in a nonlinear Kerr medium in which cross-phase modulation (action of one component on the other) is identical to self-phase modulation (nonlinear action of a field component on itself). Under these assumptions, the solitons form an integrable system, in which they interact fully elastically and preserve Hamiltonian, power, and linear momentum. Manakov-type vector solitons were first demonstrated in AlGaAs waveguides in 1996 [56].

There are two other techniques for generating stationary vector solitons. In the first approach, each field component has a different frequency, and the frequency difference between the two components is much larger than the nonlinearity relaxation time [57]. In the second type, the field components are mutually incoherent [58].

Multi-component vector solitons can also consist of different modes of their jointly induced waveguide [59], and their total intensity profile can have multiple humps [60, 61]. Photorefractive vector solitons also exist in a form of hybrid structures where one component is dark and the other one is bright [62, 63]. Finally, two-dimensional (2D) dipole vector solitons, which are composed of a 2D dipole mode and a bell-shape component, are experimentally observed [64], too.

2.3.3 Cavity solitons

Cavity solitons are localized structures trapped between reflecting surfaces [65]. Spontaneous formation of intricate patterns in optical cavities is under continuous investigation since the invention of the laser [66]. These patterns naturally originate from random perturbations (i.e., noise). Some particular frequencies are selected from the noise because they experience higher gain, and, via feedback in the cavity, stabilize and form a transverse pattern. Different picturesque structures, such as bright and dark hexagons, shock waves, spirals, and vortices, have been discovered [67]. Such cavity effects have been observed in various nonlinear systems such as thermal nonlinearities, quadratic nonlinearities in optical parametric oscillators, atomic two-level systems, and three-level systems with gain. Two characteristic features distinguish patterns in a cavity from patterns arising during one-way propagation: the existence of a set of resonant frequencies and the existence of a threshold for pattern formation. In laser cavities, pattern formation exhibits considerably different features above, at, or below the oscillation threshold. These patterns are highly dependent on the "detuning", i.e., by the difference between the frequency of the light beam and the nearest resonant frequency of the cavity.

2.3.4 Spatio-temporal solitons

A self-trapped wave packet which is localized both in time and space is named an optical light bullet. These spatio-temporal solitons can be found only in materials which, for a given width of the optical pulse, have a spatial diffraction length comparable to the dispersion length in time and that are both equal to the nonlinear length. These objects, which preserve their shape in all dimensions, have been predicted by Silberberg in 1990 [20].

Within the slowly varying envelope approximation, such multi-dimensional pulses are predicted to be unstable [68, 69]. They are categorized as (2+1) D or (3+1) D objects, depending on whether diffraction is limited to one dimension, as in a planar waveguide, or to two dimensions in a bulk medium. However, such mathematical collapse is, by virtue of other higher-order effects such as third order dispersion and multi-photon absorption, usually avoided in reality and experimental observation of optical bullets has been published recently in 1999 [70].

3. DISCRETE SOLITONS

This Chapter is devoted to discrete solitons which can be found in different inherently discrete and nonlinear systems. Phenomenon of discrete diffraction, which balances nonlinear self-focusing or self-defocusing, is explained here. Analogy with band gap structure and Bloch oscillations is elaborated, too. Working approximation, which describes the effect of linear coupling between adjacent elements in nonlinear arrays within this thesis, is so-called tight binding approximation. Topology of discrete solitons within this approximation is tackled. Finally, remarks on different methods of investigation of soliton stability are given, with emphasis on bright solitons in DNLS model.

3.1 DISCRETE DIFFRACTION

Discrete solitons are a specific class of spatial solitons, which arise in bulk or planar waveguides due to the interplay between a linear correlation effect (diffraction) and nonlinear phase modulation. In discrete systems the linear correlation is achieved by evanescent coupling between modes in adjacent elements. This evanescent coupling resembles diffraction because it spreads an excitation of finite width across the system and thus may be named discrete diffraction [19].

The spreading may be mathematically delineated by an infinite set of coupled-mode equations with nearest-neighbour interaction [18]:

$$i\frac{d E_n}{d z} + \Pi E_n + C(E_{n+1} + E_{n-1}) = 0, \tag{3.1}$$

where E_n is the complex amplitude of the electrical field envelope in the n-th element, Π is the propagation constant, and C is the coupling constant between two adjacent elements of the system. This coupling constant is proportional to an overlap integral of the two modes. If the only one element (for simplicity the central one, i.e., $E_0 = E_n(n=0),\ E_{\pm n} = 0$ for $n \neq 0$) is initially excited at $z = 0$, the above equation has the following analytical solution [71]:

$$E_n(z) = E_0\, i^n \exp(i\Pi z)\, J_n(2Cz), \tag{3.2}$$

where $J_n(2Cz)$ is the Bessel's function of the first kind of order n. Asymptotically ($z \to \infty$), the field tunnels away from the central element. As a result most of the energy is concentrated in two distinct outermost lobes, which is completely opposite to "usual" diffraction in continuous media where most of the light is concentrated around the centre of the beam.

In order to understand discrete diffraction, it is worthwhile to remember firstly the continuous case. One may consider the propagation of a scalar plane waves of the form $U(\vec{r}) = A_0 \exp(i\vec{k}\cdot\vec{r})$ in two-dimensional free space, where $\vec{k}$ is the wave vector. It points along the normal to the plane wave phase fronts and has the magnitude $k = 2\pi n_r / \lambda_0$, where λ_0 is the wavelength in vacuum. The diffraction relation of the time independent wave equation $k_z(k_x) = \sqrt{k^2 - k_x^2}$ can be derived from simple geometrical considerations. If one assumes that the beams are not too narrow, it is possible to work within the paraxial

approximation, where the transverse wave vector component satisfies $k_x << k$, and obtain [72]:

$$k_z(k_x) = k - \frac{k_x^2}{2k}. \tag{3.3}$$

Each spectral component k_x of a finite beam is accumulating phase differently during propagation. The amount of phase gained by each component after propagating a distance z is $\Phi(z, k_x) = k_z(k_x)\, z$. A group of transverse components centred at component k_x is shifted in transversal direction by an amount $\Delta x = -\partial\Phi / \partial k_x = -z(\partial k_z / \partial k_x)$. The beam broadens because of the divergence between the different displacements $\Delta x(k_x)$. This divergence is the magnitude of diffraction (or the diffraction coefficient), which can be calculated as:

$$D = -\frac{1}{z}\frac{\partial^2\Phi}{\partial k_x^2} = -\frac{\partial^2 k_z}{\partial k_x^2}. \tag{3.4}$$

The diffraction in free space, within the paraxial limit, is $D_{FP} \approx 1/k$. This value does not depend on the transverse wave vector component k_x and is always positive (normal diffraction). Unlike dispersion, which is material dependant and can be either positive (normal dispersion) or negative (anomalous dispersion) thus enabling both dark and bright temporal solitons, here only bright spatial solitons can occur in materials with a focusing nonlinearity.

In analogy with continuous diffraction (and dispersion in temporal case), discrete diffraction is best described by plane wave excitations of an infinite array. The diffraction relation may be derived from the coupled-mode equation (3.1), which can, for example, be regarded as the optical analog of the continuous model of tight binding of electrons in a one-dimensional atomic lattice [73]. Here the linear diffraction relation is:

$$k_z(k_x) = \Pi + 2C\cos(k_x d), \tag{3.5}$$

where d represents the distance between the centres of two adjacent elements and $k_x d$ is the so-called Bloch momentum. The direction of this vector quantity is determined by the angle at which the beam is launched into the system. The diffraction relation given in equation (3.5) is periodic and thus there exists an infinite number of components k_x for each k_z, equally separated by $2\pi/d$. Because of this periodicity, it may be sufficient to restrict k_x to the first Brillouin's zone ($|k_x| \leq \pi/d$) only. Spatial diffraction curves, which are given by equations (3.3) and (3.5), are presented in Fig. 3.1.

The periodic diffraction relation:

$$D = 2C d^2 \cos(k_x d), \tag{3.6}$$

which may be obtained from the Eq. (3.5), significantly influences the propagation of plane waves. Similar as dispersion, discrete diffraction can change its sign. Diffraction is anomalous in the region $\pi/2 < |k_x d| < \pi$, while it disappears for the Bloch momentum $|k_x d| = \pm\pi/2$. The sign and value of diffraction can be controlled either by launching a beam at a particular angle or by concatenating pieces with different signs of diffraction [74-76].

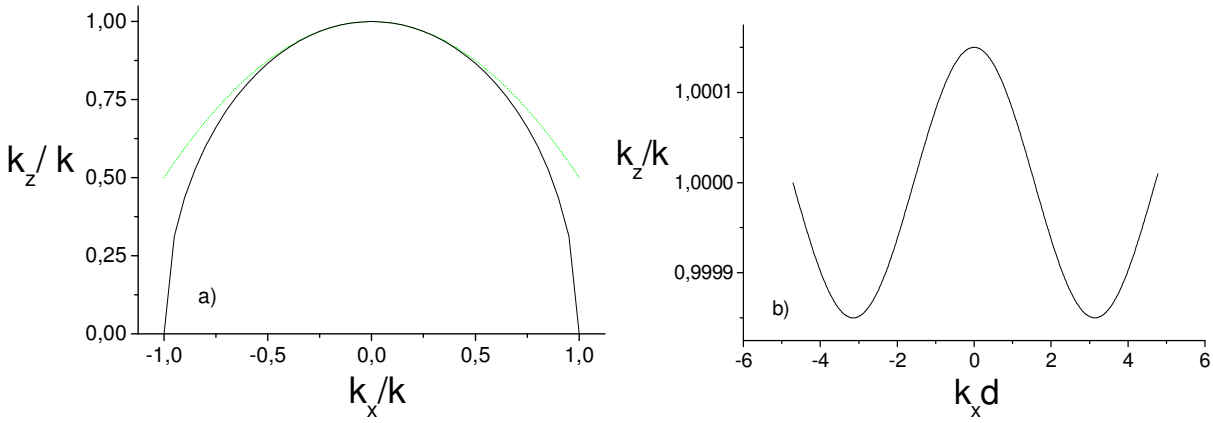

Fig. 3.1 *Diffraction curves. a) Propagation angle versus spatial frequency for diffraction in a homogeneous medium (green dotted line: paraxial approximation, solid line: non-paraxial case), and b) discrete diffraction. Only discrete diffraction exhibits inversion of curvature around* $k_x d = \pm\pi/2$.

3.2 BAND GAP STRUCTURE AND BLOCH OSCILLATIONS

As a direct consequence of the discrete translational symmetry the underlying physical mechanism which leads to discrete diffraction in homogeneous system is the band structure of the dispersion relation (3.6). Bloch [77] and Zener [78] have investigated how the field dynamics change if this discrete nonlinear system becomes inhomogeneous. This can be achieved, for example, through introduction of a linear variation in the refractive index across the waveguide array. Bloch and Zener have explored how do electrons behave in crystal lattices when a linear potential (DC field) is applied, and suggested the occurrence of periodic (Bloch) oscillations. These oscillations are caused by field-induced acceleration of electrons travelling through the periodic potential. When the electron reaches the boundary of the Brillouin's zone it experiences Bragg's reflection and a subsequent deceleration by the DC field. Finally it stops, which completes one period of oscillation.

Bloch oscillations are experimentally observed in various discrete systems, such as electrons in semiconductor super-lattices [79], and in waveguide arrays with linearly growing effective index of individual guides, which accounts for the strength of the linear potential [80]. The latter can be regarded as a modified version of Eq. (3.1) with $\Pi = p\,n$, where p represents the strength of the linear potential. This modified model equation allows for localized solutions of identical form which are named Wannier-Stark states. These states have equally spaced eigenvalues (the Wannier-Stark ladder). Therefore, arbitrary input field distributions excite a certain set of Wannier-Stark states and the superposition of these localized states leads to a periodic recurrence of the input field after a propagation distance $z = 2\pi\, j / p$ where j is an integer.

In the small amplitude or linear regime an optical pulse travelling in a waveguide array is subjected to a periodic potential and, as already mentioned in the former section, the dispersion relation (3.6) is organized as a succession of allowed bands and band gaps in which propagating modes do not exist. An example of this band structure within the first Brillouin's zone is presented in Fig. 3.4 [81]. Waves can only travel if their eigenvalues fall inside an allowed band. The corresponding modes are called Floquet-Bloch modes. The bands originate

from either guided modes, which are bound within the waveguide and decay outside, or radiation modes, which oscillate in the space between waveguides. On the other hand, waves whose eigenvalues fall in the band gaps decay exponentially in the transverse direction. Waveguide arrays can be seen as a chain made of potential wells, where each of them has a single bound state. Thus, the first band arises from the guided modes while all higher bands originate from radiation modes.

The Floquet-Bloch waves extend over the whole array, thus an excitation of a localized wave packet (a superposition of Floquet-Bloch waves) leads to diffraction (broadening) of this packet during propagation. As mentioned already, diffraction in periodic systems can be either normal or anomalous, depending whether the corresponding Bloch momentum is close to the centre or the edge of the (first) Brillouin's zone.

Under nonlinear conditions the optical field perturbs the refractive index, which induces a defect within the waveguide lattice. Consequently, the eigenvalue of this defect-like state moves into the band gap. Positive defects (increased refractive index or deeper potential well) attract normally diffracting Floquet-Bloch waves, while negative defects attract anomalously diffracting waves. When a localized wave packet that induces a defect is also an eigenmode of the complete potential (lattice plus induced defect) the propagation of the wave packet is stationary, i.e., a discrete lattice soliton forms. As the power of this optical field increases the eigenvalue penetrates deeper into the gap, which results in a more confined and transversely immobile discrete soliton.

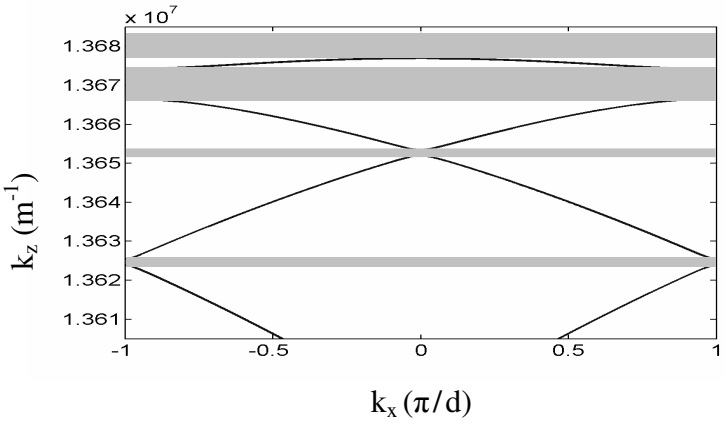

Fig. 3.2 *Reduced (i.e. folded into the first Brillouin's zone) band-gap diagram of a typical waveguide array. The grey regions represent the gaps* [81].

Generally, transversely immobile discrete solitons can be categorized into those with zero Bloch momentum at the centre of the band, and those close to the edge of the Brillouin's zone where the Bloch momentum is $k_x d = \pm\pi$. At the base of the first band of Fig. 3.2, the curvature of the dispersion curve is such that discrete diffraction is normal. Thus, in-phase (unstaggered) bright discrete solitons exist in arrays with self-focusing nonlinearity while analog dark solitons exist in arrays with self-defocusing nonlinearity. At the edges of the band the dispersion curve possess negative curvature and the discrete diffraction is anomalous. Here dark staggered (π out of phase) discrete solitons exist in self-focusing arrays while corresponding bright solitons demand a self-defocusing nonlinearity.

Theoretically estimated (a) and experimentally observed (b) modal shapes of pure Floquet-Bloch modes excited in the first four bands are presented in Fig. 3.3. Obviously, the Floquet-Bloch modes which belong to higher bands have much of their energy distributed between the waveguides, with an increasing number of oscillations.

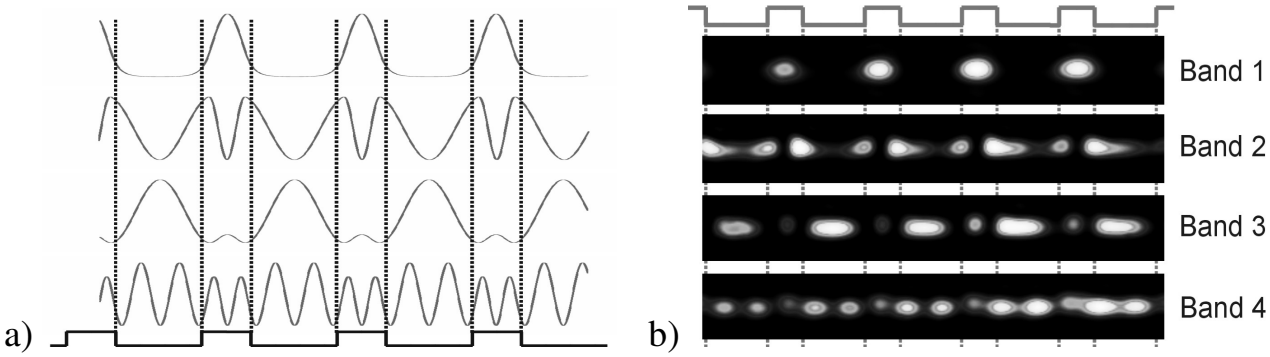

Fig. 3.3 *a) Theoretically estimated form of Floquet-Bloch modes in the first four bands, b) magnified photographs of the light intensity at the output face of the waveguide array (after* [81]*).*

3.3 DISCRETE SOLITONS IN TIGHT-BINDING APPROXIMATION

3.3.1 Mathematical model

If the waveguides of an array are sufficiently separated the Floquet-Bloch functions which belong to the first allowed band of the array may be described by virtue of either coupled-mode theory [82, 83] or tight-binding approximation [84-86]. The coupled-mode theory is based on a decomposition of the electrical field into backward and forward propagating components, under the condition of the Bragg's resonance. On the other hand, the tight-binding approximation corresponds to the case of weakly coupled fundamental modes excited in each waveguide of the array. The waveguide modes discretely interact with each other through evanescent coupling. In case of Kerr nonlinearity, the dynamics of spatial optical solitons can be described by virtue of the following discrete nonlinear Schrödinger equation:

$$i\frac{d\,E_n}{d\,z} + C(E_{n+1} + E_{n-1}) + \mathrm{X}\,|\,E_n\,|^2\;E_n = 0, \tag{3.7}$$

where E_n, as before, represents the amplitude of the envelope of the electric field at lattice site n, C is the coupling constant between two adjacent elements of the system, while X is the nonlinear coefficient. This equation represents a system of linearly coupled nonlinear ordinary differential (or, shorter, difference-differential) equations and depicts only one transmission band which is surrounded by two semi-infinite band gaps. It possesses only two conserved quantities (integrals of motion), namely the power (L^2 norm[3] or number of quanta)

[3] Lebesgue's norm of square integrable functions on the interval (a,b) is $\|\,f\,\|_{L^2} = \sqrt{\int_a^b |\,f(x)\,|^2\;dx}$.

$$P = \sum_{n=1}^{N} | E_n |^2, \tag{3.8}$$

and the Hamiltonian

$$H = -\sum_{n=1}^{N} \left[C(E_n^* E_{n+1} + E_n E_{n+1}^*) + \mathrm{X} | E_n |^4 \right]. \tag{3.9}$$

These two quantities are especially valuable for double checking of the accuracy of the corresponding numerical simulations. The existence of only two integrals of motion in a system with N degrees of freedom means that this model equation is not fully integrable and hence does not have pure soliton solutions. However, it is possible to find approximate long-live stationary solitary solutions, whose stability will be investigated in the next sections.

3.3.2 Modulational instability of plane waves

Many nonlinear systems exhibit an instability that leads to self-induced modulation as an outcome of the interplay between dispersive and nonlinear effects. This so-called modulational instability (MI) has been investigated in quite diverse fields such as plasmas [87, 88], nonlinear optics [18, 23-26, 89-96], solid state physics [97-101], and fluids [102, 103]. In plasmas and nonlinear crystals it may cause the filamentation of an initial laser beam while in optical fibres with anomalous group velocity dispersion it manifests itself as a break-up of a continuous wave into a train of ultra-short pulses (soliton trains) which can be observed experimentally [24].

The nonlinear evolutional equation (3.7) possesses stationary, array-independent (uniform) solutions of the form $E_n(z) = E_H \exp[i(q\,n + \nu_H\, z)]$, which obey the following nonlinear dispersion relation:

$$\nu_{UN} = 2C\cos(q) + \mathrm{X} E_H^2. \tag{3.10}$$

If the stationary solution is unstaggered, i.e., the phase difference between adjacent elements is zero, one gets $q = 0$ and $\eta = \cos(q) = 1$. On the other hand, when the phase difference between adjacent elements is $q = \pi$, which means that adjacent elements oscillate π out of phase, we obtain $\eta = -1$. Keeping this in mind one may rewrite the above dispersion relation as:

$$\nu_H = 2C\eta + \mathrm{X} E_H^2. \tag{3.11}$$

The strong localization condition demands that the nonlinearity prevails over linear coupling. From this equation it is possible to see that bright, strongly nonlinear, localized modes may exist only for ν which lies outside the linear bands. To examine the stability of this uniform solution it is necessary to add small perturbations which, for sake of simplicity, will be taken to be in phase with the stationary solution. By substituting $E_n(z) = [E_H + \delta_n(z)]\exp(i\nu_H\, z)$ (where $|\delta_n(z)| << E_H$) in Eq. (3.7) and after linearization it is possible to get the following evolution equation for the perturbations:

$$i\frac{d\delta_n}{dz} + \eta C(\delta_{n+1} + \delta_{n-1} - 2\delta_n) + \mathrm{X} | E_H |^2 (\delta_n + \delta_n^*) = 0. \tag{3.12}$$

These small, in-phase, complex perturbations can be taken in the form $\delta_n = \delta \exp(i Q n)$, where Q is the wave vector of modulation and $\delta = a + i b$. Assuming that $a, b \propto \exp(-i \omega z)$ one can obtain the following dispersion relation:

$$\omega^2 = 8C \sin^2\left(\frac{Q}{2}\right)\left[\eta \frac{\mathrm{X}}{2} | E_H |^2 - C \sin\left(\frac{Q}{2}\right)\right]. \tag{3.13}$$

In order that MI occurs the condition $\eta \, \mathrm{X} > 0$ must be fulfilled, i.e., unstaggered solutions ($\eta = 1 > 0$) require a focusing nonlinearity ($\mathrm{X} > 0$), while staggered solutions ($\eta = -1 < 0$) exist only in media with self-defocusing nonlinearity.

3.4 TOPOLOGY OF DISCRETE SOLITONS

As mentioned in the previous section, the evolution of slowly varying envelopes of guided-mode fields in a homogeneous discrete system with Kerr nonlinearity and within the approximation of nearest neighbour interaction can be described by virtue of a dimensionless DNLS equation (3.7). In this paragraph, a categorization of various *strongly localized* stationary solutions of Eq. (3.7) is given.

If one considers a stationary solution of the form $E_n = F_n \exp(i \nu z)$ the DNLS equation (3.7) is reduced to the following infinite set of coupled algebraic equations:

$$-\nu F_n + C(F_{n+1} + F_{n-1}) + \mathrm{X} F_n^3 = 0. \tag{3.14}$$

By solving this system approximately for strong localization i.e., by reducing it to a finite number of equations one may identify localized stationary solutions of different topologies. In this thesis only the classification of bright discrete solitons will be given.

3.4.1 On-site (odd) bright discrete solitons

These solitons, which are centred on the elements of the system (see Fig. 3.4 below), may be readily separated in four different groups:

a) symmetric odd unstaggered ($\Gamma > 0$) solitons (SOU) are roughly caricaturized as:

$$F_{SOU} = A(..., 0, f_1^A, 1, f_1^A, 0, ...), \tag{3.15a}$$

b) antisymmetric odd unstaggered solitons (AOU) solitons are described by:

$$F_{AOU} = A(..., 0, f_2^A, 1, 0, -1, -f_2^A, 0, ...), \tag{3.15b}$$

c) symmetric odd staggered ($\Gamma < 0$) solitons (SOS) have the following form:

$$F_{SOS} = A(..., 0, -|f_1^A|, 1, -|f_1^A|, 0, ...), \tag{3.15c}$$

d) while antisymmetric odd staggered solitons (AOS) are sketched by:

$$F_{AOS} = A(..., 0, -|f_2^A|, 1, 0, -1, |f_2^A|, 0, ...). \tag{3.15d}$$

Here the soliton amplitude A represents an arbitrary constant which determines the power and thus the degree of localization of the stationary solution.

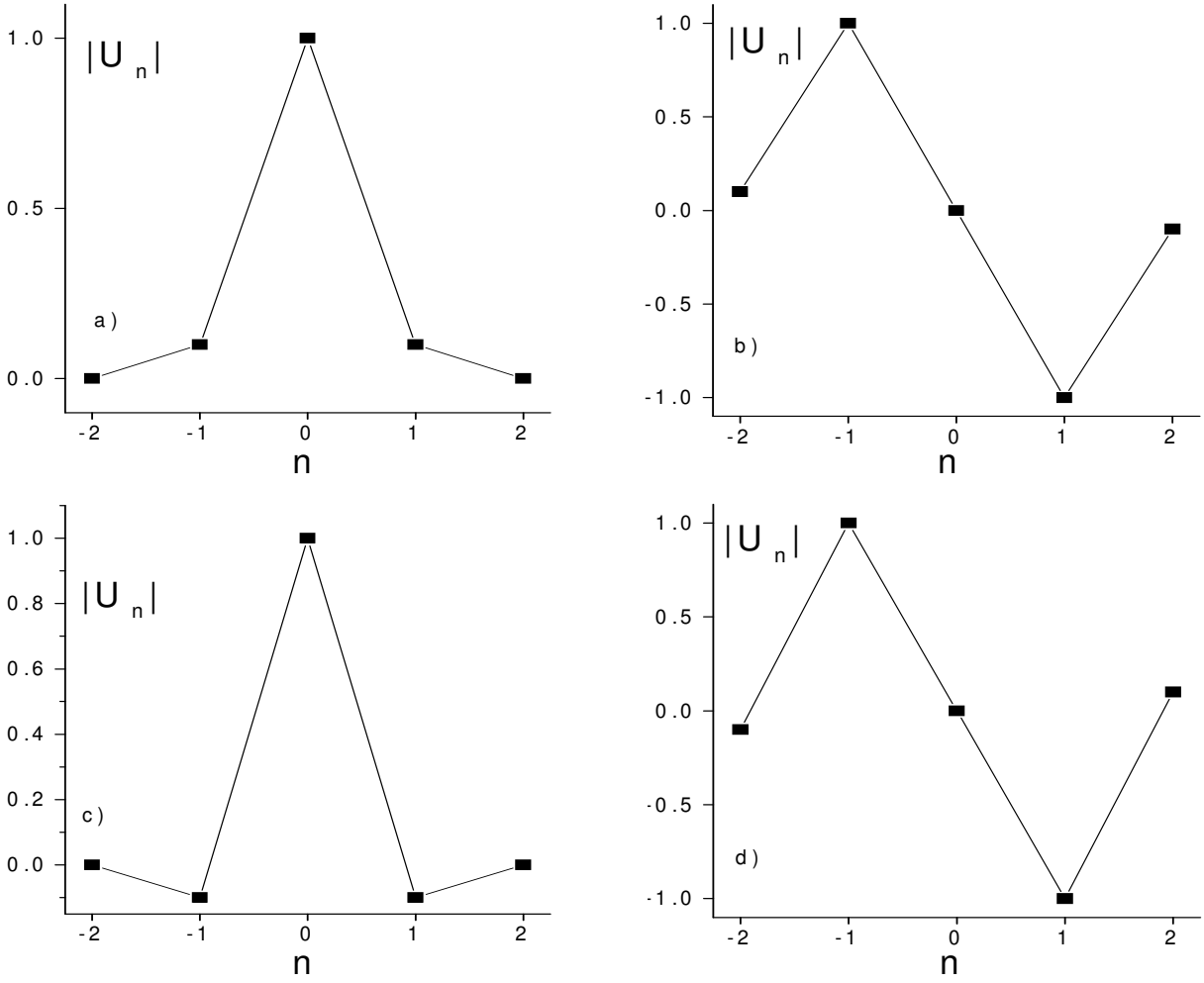

Fig. 3.4 *Odd (on-site) bright discrete solitons: unstaggered a) symmetric and b) antisymmetric, and staggered c) symmetric and d) antisymmetric.*

3.4.2 Inter-site (even) bright discrete solitons

These stationary, strongly localized solutions centred between the elements of the system can be found in the following four different forms:

a) even unstaggered (EU) solitons

$$F_{EU} = B(...,0, f_2^B, 1, 1, f_2^B, 0, ...), \tag{3.16a}$$

b) even staggered (ES) solitons

$$F_{ES} = B(...,0, -|f_2^B|, 1, -1, |f_2^B|, 0, ...), \tag{3.16b}$$

c) twisted unstaggered (TU) solitons

$$F_{TU} = B(...,0, f_2^B, 1, -1, -f_2^B, 0, ...), \tag{3.16c}$$

d) and, finally, twisted staggered (TS) solitons

$$F_{TS} = B(...,0,-|f_2^B|,1,1,-|f_2^B|,0,...). \tag{3.16d}$$

These solutions are sketched in Fig. 3.5. Lines represent just a guide to the eye. One can notice that twisted solitons do not possess odd counterpart.

Beside these eight species of discrete bright solitons, whose linear stability will be shortly outlined in next section, there are so-called topological and flat-top solitons. More about them can be found in [104].

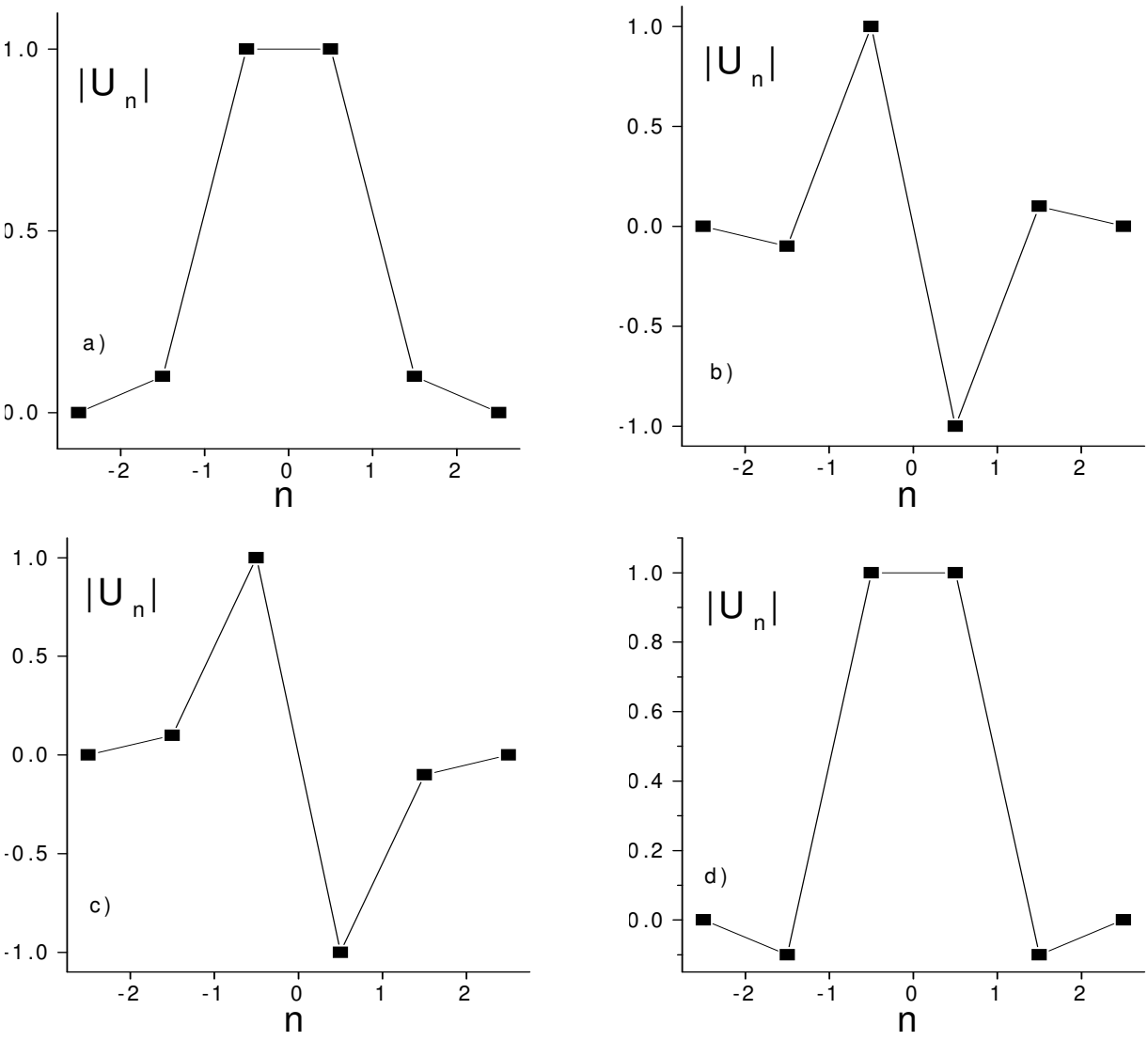

Fig. 3.5 *Even (inter-site) bright discrete solitons: a) unstaggered, b) staggered, c) twisted unstaggered, and d) twisted staggered.*

3.5 STABILITY ANALYSIS

3.5.1 General remarks on soliton stability

Due to the fascinating mathematical properties of soliton solutions such as, for example, the elastical mutual interaction, the soliton concept is applied to many nonlinear systems like plasmas [105, 106], solid state physics [107, 108], biology [109, 110], astrophysics [111], etc. Theoretical and analytical investigations of solitons in real physical systems provoked the intensive examination of solitons in the presence of perturbations.

With respect to the sort of perturbations, the soliton stability problem can be naturally separated in two groups [89]. To the first group belongs the soliton stability problem under perturbations which have the same dimensionality as the initial soliton [18, 23-26, 87-103, 112-114], while the other group encloses the soliton stability problem with respect to perturbations which change (in fact, increase) the dimensionality of the problem [27, 89, 115-118].

Generally, solitons can be represented by the four parameters amplitude, frequency shift, initial phase, and initial position. Thus, their behaviour in the presence of perturbations may be depicted by a set of time dependent evolution equations for these parameters. One can get these evolution equations by (1) a perturbative method for the conserved quantities such as energy or momentum, by (2) the averaged Lagrange's method of variation of the action integral [119-123], or (3) by the perturbation of the inverse scattering transformation [124].

The second method for soliton stability investigation is based on the analysis of the linear eigenvalue problem which can be obtained by linearization of the corresponding dynamical equations around the exact soliton solutions [125-127]. As the exact solution depends only on a few parameters one might separate variables and reduce the analysis of the corresponding linear problem to the analysis of eigenvalue spectra of adequate differential operators. Usually, the problem of determination of these eigenvalues is rather complicated, thus the different analytical methods for finding their approximative unstable values and specification of conditions which are necessary for the onset of instability are used. These approximative methods are based on a Taylor's expansion around the marginally stable states which are given by the condition $\Gamma = 0$, where Γ is the gain of the perturbation ($\omega = \Omega + i\Gamma$).

The examination of the stability of continuous-discrete systems, such as arrays of Josephson junctions [128] or nonlinear fiber arrays and photonic crystals [25, 90-91, 96, 129-131], have started to attract a growing interest recently. In such systems it is possible to explore simultaneously both, the evolution of the form of the localized solution and the redistribution of energy among the elements of the system.

In the following section the linear stability analysis of discrete solitons within the DNLS model is presented. Corresponding results on stability of discrete bright solitons within the model with saturable nonlinearity will be exhaustively investigated in Chapters 4 and 5.

3.5.2 Linear stability analysis of bright discrete solitons in media with Kerr nonlinearity

The stability of different types of discrete solitons is of special interest for two reasons. Foremost, as the DNLS equation (3.7) is non-integrable, these solitons are only the

approximate solutions. Therefore, the question arises whether they will evolve into an exact, stationary, stable solution of Eq. (3.7) or not. On the other hand, dynamics of optical pulse propagation in nonlinear fibres or waveguide arrays can be fairly well described with the DNLS equation. As these optical systems potentially play a great role in future all-optical devices for switching [132-140], steering [141-143], and storage [144], it is necessary to find out the boundaries between stable and unstable solutions in the corresponding parameter space. In this thesis two different stability methods are used. Here (and again in Chapters 4 and 5) a linear stability analysis is performed, while the second method, which relies on the Peierls-Nabarro potential, will be explained in more detail in Chapter 6.

By inserting patterns of different bright discrete solitons in the dispersion relation (3.13) it is possible to realise that even staggered and unstaggered solutions (Eq. 3.16 a, b) are unstable. These solitons move slightly across the array and transform into the corresponding stable odd solitons (Eq. 3.15 c, a). This transformation was observed experimentally and exploited for discrete beam steering in [145]. On the other hand, twisted unstaggered and staggered solitons (Eq. 3.16 c, d), which do not possess topological analog among odd solitons, are stable provided that the localization is sufficiently strong [100]. Beyond some critical value, the onset of instability displays a delocalization or spreading of the mode.

4. DISCRETE SCREENING PHOTOREFRACTIVE SOLITONS

This chapter is devoted to the theoretical description of discrete, bright, and unstaggered solitons in systems which exhibit a screening nonlinearity of the saturable type within the first band-gap. Examples for media with such a saturable nonlinearity are photorefractive crystals such as SBN61 ($Sr_{0.61}Ba_{0.39}Nb_2O_6$), where the magnitude of the nonlinear refractive index change is limited by a maximum value of the light-induced space charge field, which can be in turn adjusted by an external electric field. Homogeneous and various soliton-like stationary solutions are obtained from the model equation and their stability with respect to small perturbations is investigated. It is revealed that such systems exhibit a cascade mechanism of saturation, which strongly influences dynamics of soliton solutions.

4.1 THEORETICAL MODEL

The optical pulse propagation in 1D equidistant nonlinear photorefractive waveguide arrays with saturable nonlinearity can be modelled, within the nearest neighbor approximation and with neglected influence of diffusion of charge carriers, by virtue of the following discrete version of the Vinetskii-Kukhtarev equation [146]:

$$i\,\frac{\partial U_n}{\partial \xi} + \frac{1}{2h^2}\left(U_{n-1} + U_{n+1} - 2U_n\right) - \beta_{SC}\,\frac{U_n}{1+\left|U_n\right|^2} = 0, \tag{4.1}$$

where U_n is the wave function in the n-th nonlinear element ($n = 1,\ldots, N$) while, in the case of periodic boundary conditions ($U_{N+1} = U_1$), $h = (L–N\,w)/(N\,x_0)$ is the normalized distance between two elements, and w represents the width of a single waveguide. Here $\xi = z/(k\,x_0^2)$ is a dimensionless coordinate along which the beam propagates, x_0 is an arbitrary spatial width, $k = 2\pi\, n_{reo}/\lambda_0$ is the wave number with the unperturbed extraordinary refractive index n_{reo} and light wavelength λ_0. Furthermore $\beta_{SC} = (kx_0 n_{reo})^2\, r_{33} E_{ext}/2$ is a positive parameter. Here r_{33} is the electro-optic coefficient, $E_{\mathrm{ext}} \approx V/L$, where V is a constant bias voltage and L is the width of the nonlinear crystal along the x-direction. The ferroelectric c-axis of the photorefractive crystal coincides with the x-direction. It is also assumed that the incident laser beam is polarized along the c-axis and that the applied electric field E_{ext} has a component only in the same direction. This equation, in fact, represents a system of linearly coupled nonlinear ordinary differential equations, which are not integrable in the general case. It possesses two conserved quantities, the Hamiltonian

$$H = \sum_{n=1}^{N}\left[\beta_{SC}\,\ln\left(1+\left|U_n\right|^2\right) + \frac{\left|U_{n-1}-U_n\right|^2}{2h^2}\right], \tag{4.2}$$

and the number of quanta (power or L^2 norm)

$$P = \sum_{n=1}^{N}\left|U_n\right|^2. \tag{4.3}$$

In the small amplitude limit ($|U_n|^2 << 1$) this equation passes into the well-known 1D DNLS equation with Kerr nonlinearity. It means that Eq. (4.1), under proper conditions, also describes

various real discrete structures like a chain of tighten atoms [147, 148], the model of dynamics in globular proteins and some molecular crystals [10, 149], arrays of Josephson junctions [128, 150], polarons in condensed-matter physics [151-153], and pulse propagation in short fibre arrays where dispersion can be neglected [135].

Hereinafter the study is restricted to planar homogeneous arrays of waveguides where the parameters are chosen to correspond to photorefractive SBN61 substrates. This nonlinear crystal possesses excellent optical properties and large nonlinear electro-optic coefficients [154,155]. Usually SBN61 crystals are both a few mm long (z-direction) and wide (x-direction). The unperturbed extraordinary refractive index for SBN61 is $n_{reo} = 2.35$ while the relevant electro-optic coefficient is $r_{33} = 280$ pm/V. This crystal is sensitive to light in the blue and green spectral region. The arbitrary scaling length x_0 is set to 8 μm.

In the linear regime in which the nonlinear term can be neglected, one may expect to observe the effect of discrete diffraction. In Fig. 4.1 an example of a simulation of discrete diffraction in an SBN61 waveguide array is given. The corresponding system parameters are the number of elements in the array $N = 41$, the normalized distance between the elements $h = 0.5$, and the nonlinear coefficient $\beta_{SC} = 18.2$. In the diagram τ denotes the normalized propagation coordinate ($\tau = \xi / 2h^2$). An initially strongly localized excitation tends to spread over the whole array because of the discrete translational symmetry of the infinite array.

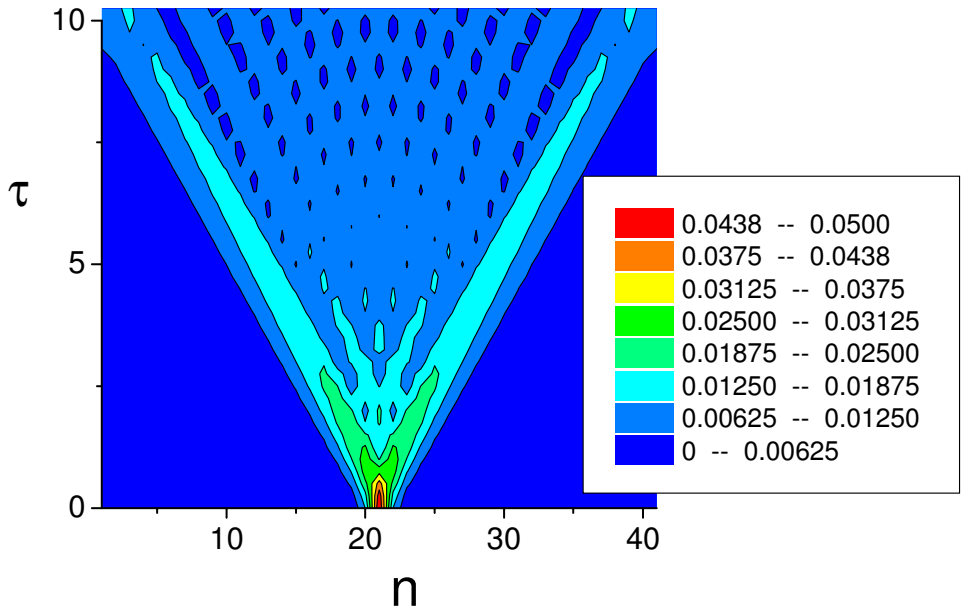

Fig. 4.1 *Discrete diffraction in a one-dimensional SBN61 waveguide array (top view[4]). The number of elements in the array is* $N = 41$ *while the initial value of the non-dimensional pulse amplitude is* 0.05.

As explained in Section 3.1, due to the periodicity of the corresponding dispersion relation, it is possible to observe diffraction-less propagation. The corresponding numerical result, with the Bloch momentum set to $k_x d = \pi/2$ and with the same values of all parameters as in Fig. 4.1, is depicted in Fig. 4.2.

[4] This form of presentation (either in colour or in grey scale) will be often used within the thesis. Numbers in the square represent the corresponding intensity of the pulse.

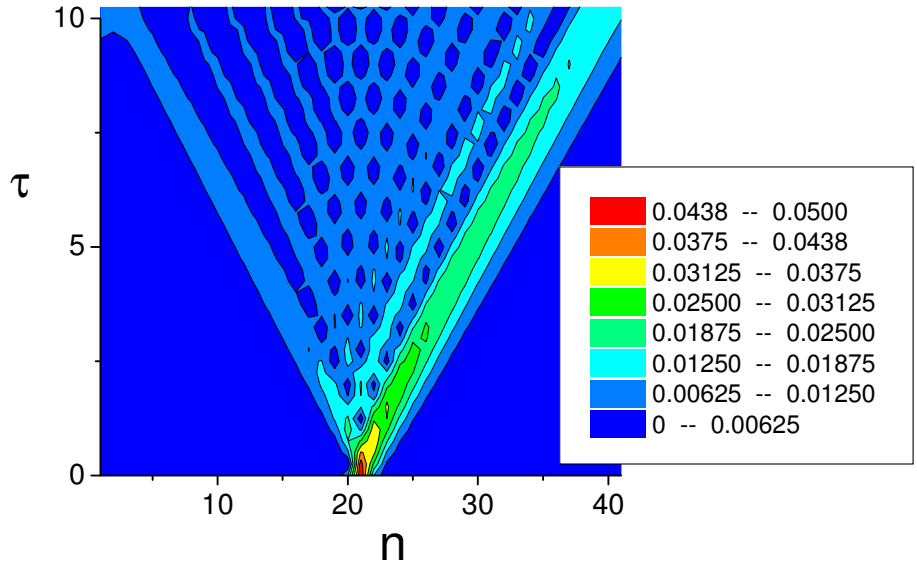

Fig. 4.2 *Diffraction-less propagation in a nonlinear SBN61 waveguide array. The number of elements in the array is N* = 41 *while the initial value of the non-dimensional pulse amplitude is* 0.05.

4.2 STATIONARY SOLUTIONS

Stationary solutions of the discrete Vinetskii-Kukhtarev equation (4.1) are of significant importance because they represent some of the available attractors of a nonlinear system. Within a linear theory, it shows up that both the exponential perturbations' growth rate and the threshold amplitude for the onset of instability depend on the wave number (and/or on the nonlinear frequency shift) of the stationary solution. There are a lot of reports about the linear stability of these stationary solutions in discrete [18, 94, 98, 100, 127, 129, 137, 148, 156-158], continuous [68, 69, 159], as well as in continuous-discrete systems [25, 90, 101, 114, 130]. For any set of the system's parameters β_{SC} and h there are $3N$ possible stationary solutions such as homogeneous, oscillatory, soliton, and multi-soliton solutions. In this thesis the existence and stability of the simplest homogeneous and soliton solutions are explored.

4.2.1 Homogeneous solutions

It is possible to find the following exact oscillatory wave solution of Eq. (4.1)

$$U_{OSC} = \pm\sqrt{\frac{\beta_{SC} + 2h^{-2}\sin^2(qh/2) - v}{v - 2h^{-2}\sin^2(qh/2)}}\exp(-ivz + iqnh), \tag{4.4}$$

where q is a discrete wave number and v is the nonlinear frequency shift. The amplitude of this solution is real if $2h^{-2}\sin^2(qh/2) < v < \beta_{SC} + 2h^{-2}\sin^2(qh/2)$, and the corresponding existence region is of width β_{SC}. It is also possible to find an exact, homogeneous unstaggered solution

$$U_{HU} = |U_{HU}| \exp(-i v \xi) = \pm \sqrt{\frac{\beta_{SC} - \nu}{\nu}} \exp(-i\nu\xi). \tag{4.5}$$

This simple array-independent solution is a special case of the oscillatory one, where $q=0$ is taken. If $0<\nu<\beta_{SC}$ its constant amplitude is real and, opposite to the corresponding solution in Kerr-like media, it has a limited existence range due to the saturable nature of the nonlinearity. The unstaggered homogeneous solution is represented in Fig. 4.3 for two different values of the parameter β_{SC}.

Additionally, a staggered homogeneous solution of the following form

$$|U_{HS}| = \sqrt{\frac{\beta_{SC} + 2h^{-2} - \nu}{\nu - 2h^{-2}}} \tag{4.6}$$

represents another possible stationary solution of Eq. (4.1).

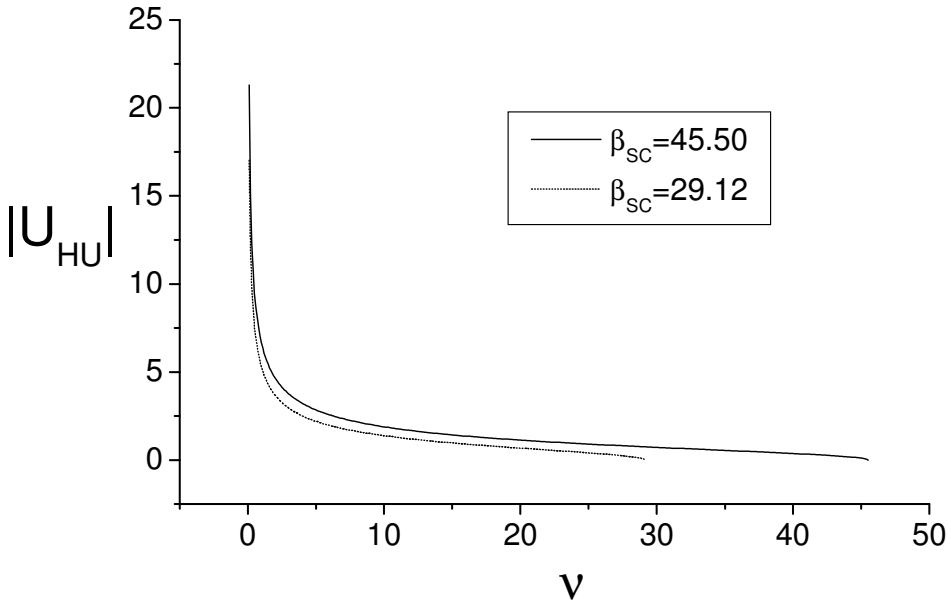

Fig. 4.3 *Unstaggered homogeneous solution U_{HU} for two different values of the parameter β_{SC}.*

4.2.1.1 Stability of the homogeneous solutions

In order to investigate the linear stability of a homogeneous unstaggered solution one may follow a standard procedure and introduce a small complex, array-dependent, in-phase perturbation around this solution $U_n = (|U_{HU}| + \delta_n)\exp(-i v \xi)$, where $\delta_n = (a + ib)\cos(2\pi n / N)$, and $|\delta_n| << |U_{HU}|$. Substitution into Eq. (4.1), after linearization with respect to the small perturbations and use of Fourier's transform *a, b* ~ exp*(−iωξ)*, leads to the following dispersion relation

$$\omega^2 = \frac{4}{h^2}\sin^2\left(\frac{\pi}{N}\right)\left(\frac{1}{h^2}\sin^2\left(\frac{\pi}{N}\right)-\nu\left(1-\frac{\nu}{\beta_{SC}}\right)\right). \tag{4.7}$$

In the small amplitude regime this result coincides (after a simple adjustment of notations and for wave number $q=0$) with the dispersion relation (Eq. 10) in Ref. [98], where a general approach to modulational instability of discrete nonlinear systems with cubic nonlinearity is described. A sufficient condition for the unstaggered homogeneous solution to become modulationaly unstable is $\omega^2<0$, which, together with the facts that $N\approx 100$ and $h\approx 1$, results in the next instability frequency band:

$$\nu \in \left(\frac{1}{h^2}\sin^2\left(\frac{\pi}{N}\right),\ \beta_{SC}-\frac{1}{h^2}\sin^2\left(\frac{\pi}{N}\right)\right). \tag{4.8}$$

In the very narrow frequency bands $\Delta\nu = h^{-2}\sin^2(\pi/N)$ at the ends of the existence interval this solution is stable with respect to the given form of the perturbation. Note that in these regions instabilities might occur under some other kinds of perturbations. The above result is valid in the limit $4\sin^2(\pi/N)/(\beta_{SC}\ h^2)\rightarrow 0$. The dispersion relation in Eq. (4.7) defines the instability growth rate spectra for the frequency band in Eq. (4.8).

On the other hand, using this procedure gives results in the corresponding dispersion relation for the staggered homogeneous solution:

$$\omega^2 = \frac{4}{h^2}\sin^2\left(\frac{\pi}{N}\right)\left(\frac{1}{h^2}\sin^2\left(\frac{\pi}{N}\right)+\frac{(\nu-2h^{-2})^2}{\beta_{SC}}\right). \tag{4.9}$$

As this expression is always positive, one may conclude that the staggered homogeneous solution is stable with respect to the given form of the small, in-phase, array-independent perturbations.

In order to confirm our analytical results we have numerically solved Eq. (4.1) by a sixth-order Runge-Kutta procedure with regular checking of the conserved quantities P and H. For the initial conditions (ξ = 0) in the numerical calculations a perturbed stationary homogeneous solution (Eq. (4.5)) in the form

$$U_n = U_{HU}+\delta_n = U_{HU}+\varepsilon U_{HU}\cos\left\{\frac{2\pi}{N}\left[n-\left(\frac{N}{2}+1\right)\right]\right\}, \tag{4.10}$$

is used. Here, ε is a small parameter which is set to $\varepsilon = 0.001$. The growth rates Γ ($\omega = \Omega + i\Gamma$) are numerically estimated from the early stage of the time evolution of the electric field across the waveguide array.

An example of the time evolution of the electric field across a waveguide array with $N=41$ elements and a nonlinear frequency shift $\nu=2$ is shown in Fig. 4.4, illustrating the development of the modulation instability of the homogeneous unstaggered solution. The values of the systems' parameters are $\beta_{SC} = 18.2$ and $h = 0.5$, which correspond to the blue light from an Argon ion laser with a wavelength of 488 nm, an externally applied electrical field E_{ext}=4.5 kV/cm, and an inter-element distance of 4 μm.

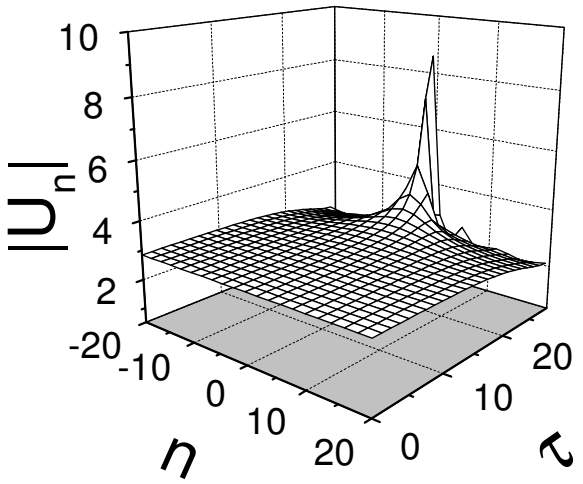

Fig. 4.4 *Example of the time evolution of the electric field across a SBN61 waveguide array with* $N = 41$. *System's parameters are* $\beta_{SC} = 18.2$ *with* $h = 0.5$ *while* $\tau = \xi / 2h^2$.

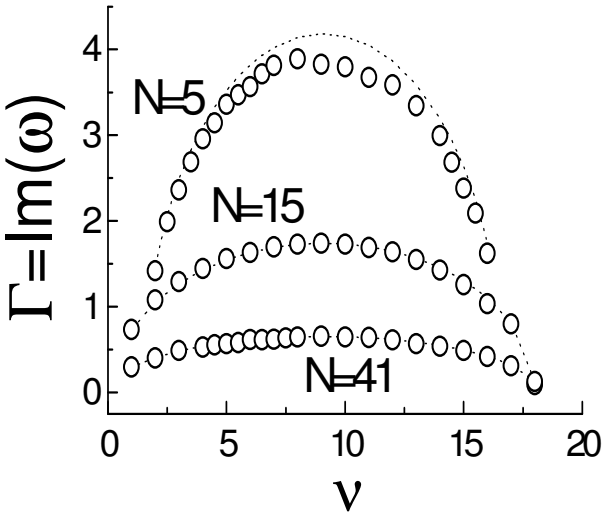

Fig. 4.5 *Comparison of the numerical (circles) and analytical (dotted line) results for the growth rate spectra* Γ *for the nonlinear SBN61 waveguide arrays with* N=5, 15, *and* 41 *elements*.

The numerically estimated and analytically calculated values of the growth rates Γ in the central waveguide are plotted in Fig. 4.5 over the instability region, which is given by Eq. (4.8) for Ω=0 and for arrays with N =5, 15, and 41 elements. The agreement between the numerical and analytical results is fairly good with only small discrepancies for the array with $N = 5$ waveguides in the region of medium values of v.

This result indicates the presence of exponentially growing modes in the system, giving no predictions about the subsequent nonlinear evolution stage. It is shown that discrete systems with Kerr nonlinearity, instead of a collapse behaviour that is observed in the multi-dimensional continuous case [68, 69], exhibit a quasi-collapse behaviour leading to the formation of localized structures in the form of discrete solitons [127, 129]. The Kerr nonlinearity is just the small amplitude limit of the saturable nonlinearity, therefore a similar quasi-collapse process and existence of bright unstaggered 1D discrete screening solitons, where the energy is localized only in-between a few central waveguides of the nonlinear array, is fully expected.

4.2.2 Soliton solutions

Similar as for Kerr-like media [127, 129, 139] it is possible to find an approximate expression for narrow discrete photorefractive solitons. From Eq. (4.1) it is possible to get the following five species of discrete solitons:

a) symmetric odd unstaggered (SOU) solitons, which are given by Eq. (3.15a) and Fig. 3.4a, have the form

$$|U_n| = \sqrt{\frac{\beta_{SC} + h^{-2} - \nu}{\nu - h^{-2}}}, \quad |U_{n\pm m}| = \frac{|U_n|}{2h^2(\beta_{SC} + h^{-2} - \nu)^m}, \tag{4.11}$$

where n denotes the dominant element (although n is quite arbitrary, it is usual to choose $n=0$) while $m=1, 2, \ldots$. The result for the neighbours is valid only under the restriction that $|U_m|^2 \to 0$. Such localized states are possible neither in the small amplitude regime nor in the over saturation regime.

b) antisymmetric odd unstaggered (AOU) solitons, which are given by Eq. (3.15b) and Fig. 3.4b, have a form [5]

$$U_0 = 0, \quad |U_{\pm 1}| = \sqrt{\frac{\beta_{SC} + h^{-2} - \nu}{\nu - h^{-2}}}, \quad |U_{\pm 1 \pm m}| = \frac{|U_{\pm 1}|}{2h^2(\beta_{SC} + h^{-2} - \nu)^m}, \tag{4.12}$$

c) even unstaggered (EU) solitons, which are represented by Eq. (3.16a) and Fig. 3.5a, which are given by

$$|U_{\pm 1}| = \sqrt{\frac{\beta_{SC} + 0.5h^{-2} - \nu}{\nu - 0.5h^{-2}}}, \quad |U_{\pm 1 \pm m}| = \frac{|U_{\pm 1}|}{2h^2(\beta_{SC} + h^{-2} - \nu)^m}, \tag{4.13}$$

d) even staggered (ES) solitons, which are sketched by Eq. (3.16b) and Fig. 3.5b, with the form

$$|U_{\pm 1}| = \sqrt{\frac{\beta_{SC} + 1.5h^{-2} - \nu}{\nu - 1.5h^{-2}}}, \quad |U_{\pm 1 \pm m}| = \frac{|U_{\pm 1}|}{2h^2(\nu - h^{-2} - \beta_{SC})^m}, \tag{4.14}$$

e) even, twisted unstaggered (TU) solitons (see Eq. (3.16c and Fig. 3.5c)), which are described by

$$|U_{\pm 1}| = \sqrt{\frac{\beta_{SC} + 1.5h^{-2} - \nu}{\nu - 1.5h^{-2}}}, \quad |U_{\pm 1 \pm m}| = \frac{|U_1|}{2h^2(\beta_{SC} + h^{-2} - \nu)^m}, \tag{4.15}$$

All of them possess a limited interval of allowed solitons frequencies. The width of these intervals depends on the ratio between β_{SC} and $0.5h^{-2}$. For example, in the case $\beta_{SC} < 0.5h^{-2}$ twisted unstaggered solitons do not exist while only symmetric and antisymmetric unstaggered solitons can exist in the same frequency interval $(h^{-2}, \beta_{SC} + h^{-2})$. Even staggered solution exist in a region with lower frequencies, $(\beta_{SC} + h^{-2}, \beta_{SC} + 1.5h^{-2})$, while even unstaggered solution can be found in a region with higher solitons frequencies, $(0.5h^{-2}, \beta_{SC} + 0.5h^{-2})$. In this thesis only the case when $\beta_{SC} > 1.5h^{-2}$ is investigated. The corresponding frequency intervals where these analytical solutions can be found are represented in Table 4.1.

$(0.5h^{-2}, h^{-2})$	$(h^{-2}, 1.5\ h^{-2})$	$(1.5\ h^{-2}, \beta_{SC}+0.5\ h^{-2})$	$(\beta_{SC}+0.5\ h^{-2}, \beta_{SC}+h^{-2})$	$(\beta_{SC}+h^{-2}, \beta_{SC}+1.5\ h^{-2})$
EU	SOU, AOU, EU	SOU, AOU, EU, TU	SOU, AOU, TU	ES

Tab. 4.1 *Frequency intervals for different types of solitons. For the notation recall the Section 3.4.*

[5] One has to combine together either only upper or only lower signs. The same hold for Eqs. (5.11)-(5.14).

In this thesis special attention is paid to the two symmetric unstaggered solutions, namely the odd (SOU) and even (EU) one. These simple localized structures should be easily observed experimentally.

Fig. 4.6 depicts the intensity distribution along the central part of the nonlinear waveguide array for $v = 5$, $\beta_{SC} = 18.2$, and for three different values of the waveguide distance h. The symbols denote the intensity in each waveguide, while the lines represent just a guide to the eye. In the case $h = 1.5$ the waveguides are well separated and there is almost no coupling between them resulting in a discrete odd unstaggered soliton where the energy is almost completely concentrated in the central waveguide. Decreasing the distance will increase the coupling, thus small satellites in the first neighbours form and the discrete photorefractive soliton starts to spread. By further reducing the distance, more and more elements of the array are excited, thus the localized structure becomes wider. Obviously, in the saturation region, where these solitons become broad, it is not justified to neglect the amplitude of the first neighbours in comparison to the amplitude of the central element. By solving Eq. (4.1) for the case $v = h^{-2}$, with the following corrected amplitude ratios $|U_0| > |U_1| >> |U_2| \rightarrow 0$, one can get the next approximate expressions for the pulse amplitudes in the three central elements of the nonlinear array

$$|U_0| = \pm\sqrt{\frac{\beta_{SC}^2 h^4 - 2 \pm \beta_{SC} h^2 \sqrt{4 + \beta_{SC}^2 h^4}}{2}}\,,$$
$$|U_1| = \beta_{SC} h^2 \frac{A_0}{1 + A_0^2}\,. \tag{4.16}$$

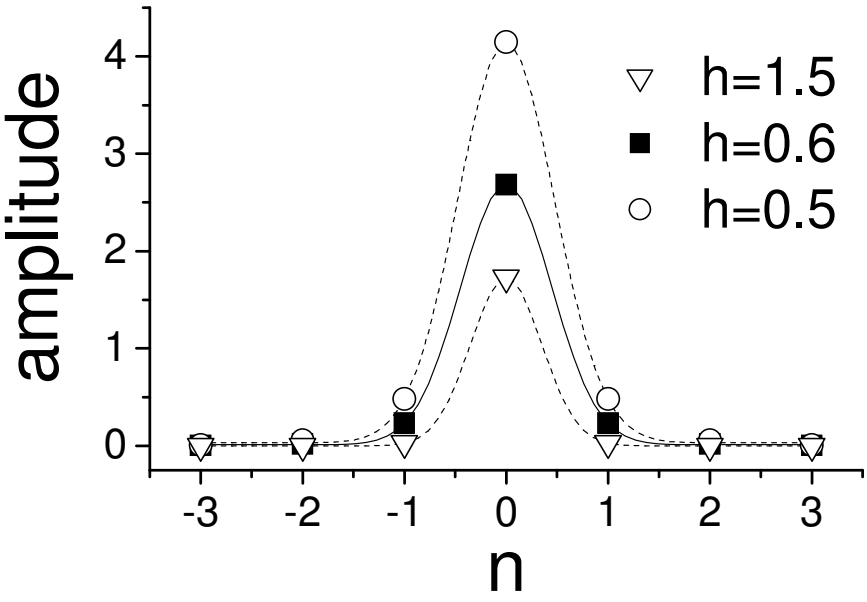

Fig. 4.6 *Intensity patterns of discrete odd unstaggered solitons for three different values of the waveguide distance h. The symbols denote the intensity in each waveguide while lines represent a guide to the eye.*

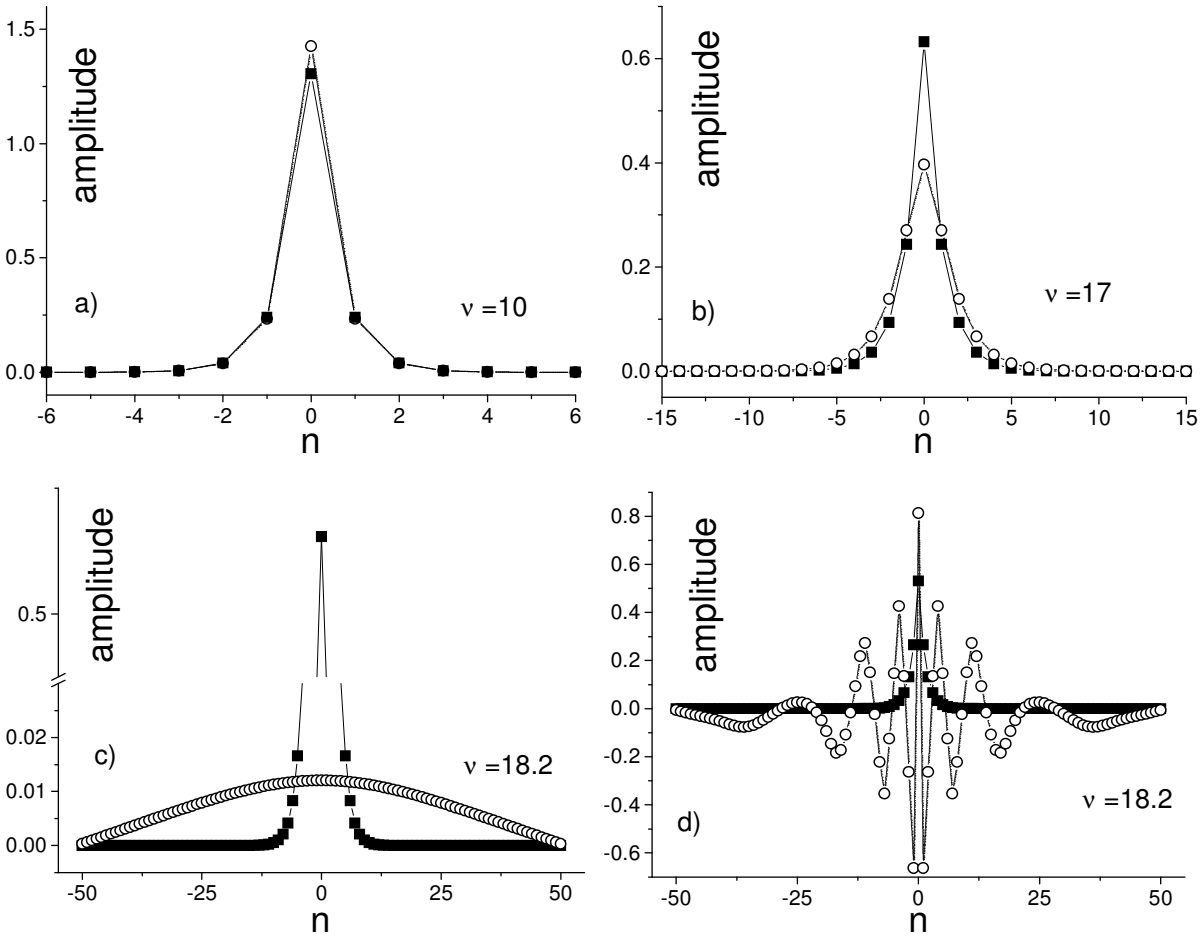

Fig. 4.7 *Amplitude of discrete screening odd unstaggered soliton ($\beta_{SC} = 18.2$, $h = 0.5$) versus waveguide number n for a) $v = 10$, b) $v = 17$, and c, d) $v = 18.2$. The numerical results are given by circles while the analytical predictions are given by squares.*

Fig. 4.7 depicts a comparison between analytical and numerical results for the possible stationary states of discrete screening unstaggered solitons which are all located in the centre of the array with $N = 101$ elements. The numerical procedure is based on the modified Powell's hybrid algorithm (shooting method). For intermediate frequencies (Fig. 4.7a) narrow discrete solitons are formed. By lowering the soliton amplitude the numerical simulations suggest a widening of the localized structures (Fig. 4.7 b). It is interesting to mention that for the same initial conditions in the small amplitude or Kerr regime, numerics reveals that both localized and oscillatory solutions are possible (Fig. 4.7 c, d). In this region the slopes of the curves are very small and practically all the corresponding soliton solutions are marginally stable.

In Fig. 4.8 a typical example of a discrete photorefractive odd unstaggered soliton propagation along an array with $N = 101$ is presented. The focus is put on the central part of the array. Similar patterns are achieved in a wide interval of v for discrete solitons given by Eq. (4.11). Note that a qualitatively similar behaviour, where the input beam evolves into a stable discrete soliton, is obtained with initially narrow Gaussian, sech, and nearly rectangular pulses (which are more natural in the experiment). It is appropriate to underline that the parameters in Fig. 4.6, i.e. a waveguide distance of 3 μm and $E_{ext} = 9$ kV / cm, are very close to the practically achievable values in the crystal SBN61. For higher values of v oscillatory solutions, which are given by Eq. (4.4) and presented in Fig. 4.7, are also observed.

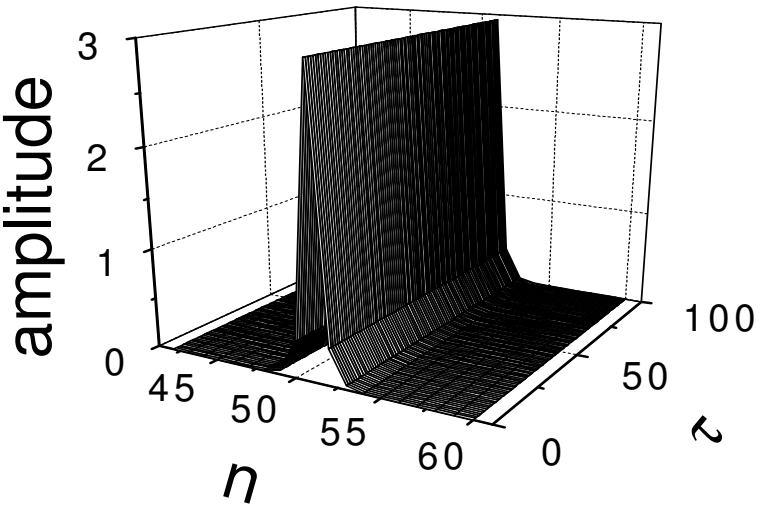

Fig. 4.8 *Propagation of a discrete odd unstaggered soliton along the array with* $N = 101$, $\beta_{SC} = 36.4$, *and* $h = 0.375$.

4.2.2.1 Stability of symmetric unstaggered soliton solutions

In order to examine the stability of localized structures one may apply a Vakhitov-Kolokolov [159] criterion which gives the answer about the system's stability with respect to small longitudinal perturbations. With the assumption that the system's total power P is shared only between three waveguides one may obtain

$$P_{SOU} = \frac{1 + 2h^4 (\beta_{SC} + h^{-2} - v)^2}{2h^4 (v - h^{-2})(\beta_{SC} + h^{-2} - v)}. \tag{4.17}$$

According to [159, 94] this localized structure is stable with respect to small longitudinal perturbations if the power P is a monotonically decreasing function for any value of the frequency v. This is both a necessary and sufficient condition for the stability in our discrete system [157]. The analytical form for the power P of discrete screening solitons located in the centre of the lattice as a function of the nonlinear frequency shift v is presented in Fig. 4.9a (full line). As the power is a monotonically decreasing function of v one might conclude that bright 1D discrete screening solitons are stable with respect to small perturbations. In the small amplitude regime this result confirms a conclusion about the stability of the corresponding nonlinear mode (odd, unstaggered, and symmetric) from Ref. [100], where the stability of strongly localized modes was investigated by virtue of a direct linear analysis.

In order to study the dynamics of a discrete system in media with saturable nonlinearity it is necessary to use numerical simulations, because Eq. (4.1) is not integrable in the general case. These numerical results are especially valuable in the deep saturation regime where our approximate theoretical solution fails. The numerically calculated power P is given in Fig. 4.9a (green dotted line). The agreement with our analytical results is fairly good, except in the big amplitude regime. However, despite a small bend near the left asymptote ($v = h^{-2}$), the curve is still monotonically decreasing, thus confirming the stability of symmetric odd unstaggered solitons.

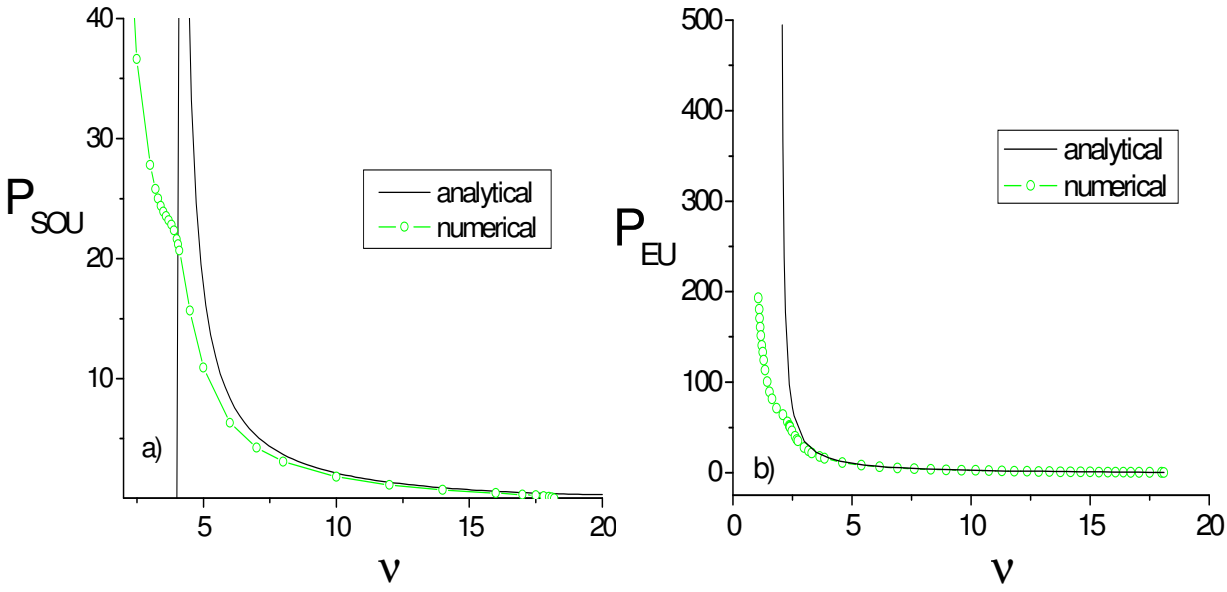

Fig. 4.9 *Power of discrete symmetric screening soliton P as a function of nonlinear frequency* ν *for* $\beta_{SC} = 18.2$ *and* $h = 0.5$. *a) Odd unstaggered, and b) even unstaggered.*

With the same assumptions as above the power of even unstaggered discrete screening solitons can be roughly estimated as

$$P_{EU} = 2\frac{(\beta_{SC} + 0.5h^{-2} - \nu)}{(\nu - 0.5h^{-2})}\left(1 + \frac{1}{4h^4(\beta_{SC} + h^{-2} - \nu)^2}\right). \tag{4.18}$$

This approximate analytical result, which confirms the linear stability of even unstaggered solitons, is represented by the full line in Fig. 4.9b. The corresponding numerical result is given by a green dotted line. Once again, one can observe a small bend in the big amplitude region.

If one recalculates the soliton power in case of a very large (infinite) arrays the result for the symmetric odd unstaggered solution reads:

$$P_{SOU} = |U_0|^2 \frac{(2h^2\beta_{SC} + 2 - 2h^2\nu)^2 + 1}{(2h^2\beta_{SC} + 2 - 2h^2\nu)^2 - 1}, \tag{4.19}$$

where $|U_0|^2$ can be obtained from Eq. (4.11). The power of the other four soliton solutions has the joint form:

$$P = |U_{\pm 1}|^2 \frac{(2h^2\beta_{SC} + 2 - 2h^2\nu)^2}{(2h^2\beta_{SC} + 2 - 2h^2\nu)^2 - 1}, \tag{4.20}$$

where the appropriate $|U_{\pm 1}|^2$ may be obtained from Eqs. (4.12-15).

Keeping in mind that the power, as a sum of positive numbers, has to be positive it is clear that the transition to an infinite array brings in the following restrictions on the soliton frequency: $\nu < \beta_{SC} + 0.5\,h^{-2}$ and $\nu > \beta_{SC} + 1.5\,h^{-2}$. Consequently, the even staggered soliton solution is physically unreal, while the interval of the existence of the approximate analytical odd staggered solutions is limited to $(h^{-2}, \beta_{SC} + 0.5h^{-2})$.

4.3 CASCADE MECHANISM OF THE SATURATION

The behaviour of discrete odd unstaggered solitons in the regime of saturation will be examined in detail in this Section. In Fig. 4.10, where the dependence of the soliton amplitude on the frequency for the central element and its first and second neighbours is presented, one can notice a gradual transition to the saturation regime [96].

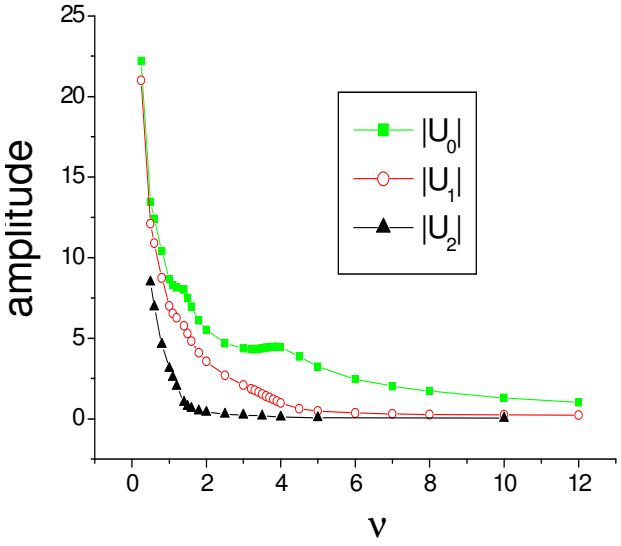

Fig. 4.10 *Amplitude in the central waveguide and its first and second neighbours versus frequency ν for the same waveguide parameters as in Fig.* 4.9.

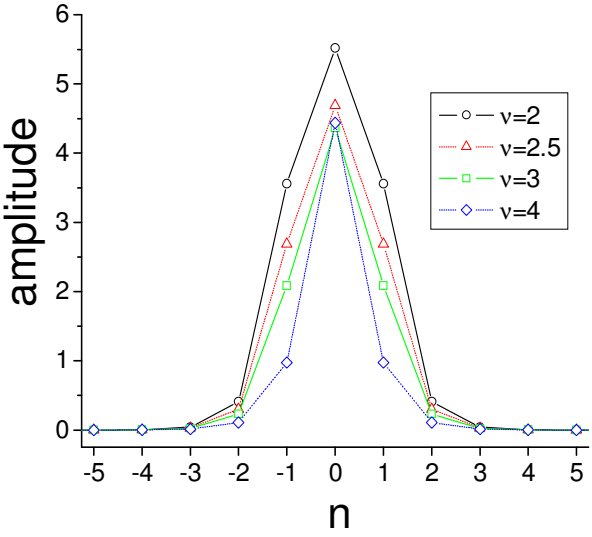

Fig. 4.11 *Amplitude of discrete screening odd unstaggered soliton (β_{SC} = 18.2, h = 0.5) versus number n in the regime of deep saturation.*

The central element goes first into saturation at $\nu \approx 4$, while the amplitude of its neighbours keeps rising monotonically till $\nu \approx 1.5$, where the first neighbours go in the saturation, too. This cascade saturation mechanism can explain the observed bend of the numerical curve for $\nu \approx 4$ in Fig. 4.9a. Indeed, the amplitude of the central element of the discrete soliton grows with the increase of the power P until saturation is reached. The further increase of P is an outcome of the growing amplitudes of the first neighbours. It is plausible to expect that the amplitudes of the second neighbours etc., behave in a similar manner. Thus increasing P does not lead to continuous energy localization into a single waveguide element and its decoupling from the rest of the array, as in the case of discrete media with cubic nonlinearity. Instead, it leads to the widening of the localized structure shown in Fig. 4.11. Moreover, by replacing β_{SC} = 18.2 and h = 0.5 in Eq. (4.1) we obtain $|U_0|$ = 4.545 and $|U_1|$ = 0.955, while the corresponding numerical values are $|U_0|$=4.439 and $|U_1|$=0.976.

Analogously, a cascade mechanism of saturation can be introduced also for the even unstaggered mode B. Here, this phenomenon occurs for higher values of the solitons power because the elements of the nonlinear array have to saturate in pairs.

5. DISCRETE PHOTOVOLTAIC PHOTOREFRACTIVE SOLITONS

In this part of the thesis a second class of discrete photorefractive solitons, namely discrete photovoltaic solitons are investigated in detail analytically. Nonlinear optical materials where these types of solitons may exist are photovoltaic photorefractive crystals such as LN ($LiNbO_3$) or lithium tantalate ($LiTaO_3$). Here, the emphasis is placed on stability properties of bright symmetric odd and even staggered solitons in which the adjacent elements are out of phase. Despite existence of two zeroes of PN potential the cascade mechanism of saturation could not be observed in such systems.

5.1 THEORETICAL MODEL

The scalar wave equation for the slowly varying amplitude of the optical field in steady state two-dimensional systems with a nonzero photovoltaic current and with electrons as the sole charge carriers is given by [41, 42]:

$$i\frac{\partial A_x}{\partial z}+\frac{1}{2k}\frac{\partial^2 A_x}{\partial x^2}+\frac{k\Delta n_r(A_x)}{n_{ro}}A_x=0. \tag{5.1}$$

Here k is the wave number, n_{ro} is the unperturbed ordinary refractive index while, mathematically, the nonlinear refractive index perturbation due to the Pockels' effect can be represented by:

$$\Delta n_r=\alpha\frac{I}{I+I_D}, \tag{5.2}$$

where the intensity $I=|A_x|^2$, the dark irradiance $I_D=G/c$ (G is the dark generation rate while c is the photo-ionization cross section), and $\alpha=-n_{ro}{}^3 r E_{PV}/2$ ($r=r_{33}$ is the effective electro-optic Pockels' coefficient, while E_{PV} is the photovoltaic field constant).

By the following set of substitutions $s=x/x_0$, $\xi=z/(kx_0{}^2)$, and $A_x=\sqrt{I_D}U$, where x_0 is the arbitrary width, the starting wave equation can be transformed into the non-dimensional evolution equation of the form:

$$i\frac{\partial U}{\partial \xi}+\frac{1}{2}\frac{\partial^2 U}{\partial s^2}-\beta_{PV}\frac{|U|^2U}{1+|U|^2}=0. \tag{5.3}$$

with $\beta_{PV}=k^2x_0{}^2|\alpha|/n_{ro}$. After the usual discretization this equation reads [160]:

$$i\frac{\partial U_n}{\partial \xi}+\frac{1}{2h^2}\left(U_{n-1}+U_{n+1}-2U_n\right)-\beta_{PV}\frac{|U_n|^2U_n}{1+|U_n|^2}=0, \tag{5.4}$$

where h and U_n have the same meaning as in Chapter 4.

Like the model equation (4.1), which describes the evolution of discrete screening solitons, this equation does not belong to the group of the integrable equations, too, because it has only two conserved quantities P and H, while the number of unknowns in this system of ordinary differential equations is N. The expression for the power P coincides with the result of Eq. (4.3), while the Hamiltonian is given by:

$$H = \sum_{n=1}^{N} \left\{ \beta_{PV} \left[\left| U_n \right|^2 - \ln\left(1 + \left| U_n \right|^2\right) \right] + \frac{\left| U_{n-1} - U_n \right|^2}{2\, h^2} \right\}. \tag{5.5}$$

In the next sections this model equation will be examined on the example of a waveguide array in a photovoltaic photorefractive LN crystal. The corresponding material parameters are $r = 32 \times 10^{-12}$ m/V, $n_{ro} = 2.20$ (for a wavelength $\lambda_0 = 514.5$ nm). In LN crystal photovoltaic field of $E_{PV} = 250$ kV/cm can be easily achieved. The arbitrary scaling length x_0 is again set to 8 μm, as in Chapter 4.

In the linear regime the last term in Eq. (5.4) can be neglected. An illustration of the discrete diffraction in a waveguide array in lithium niobate is given in Fig. 5.1, while the diffraction-less propagation (with the same amplitude and with the Bloch momentum $k_x d = \pi/2$) is given in Fig. 5.2.

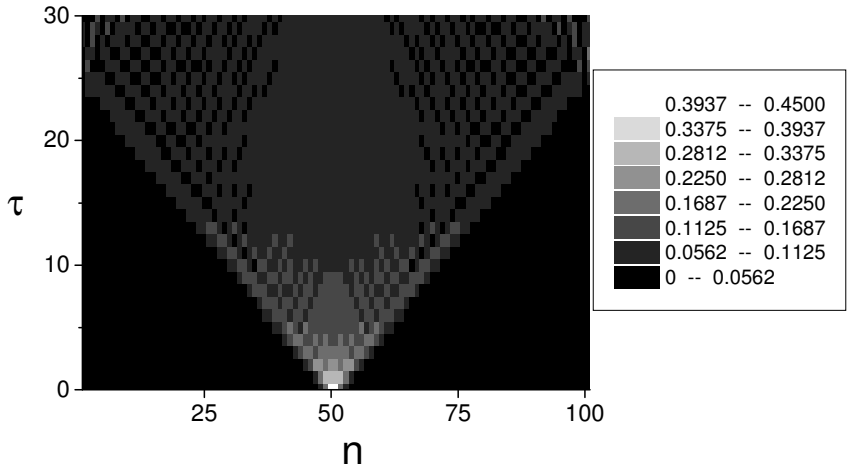

Fig. 5.1 *Discrete diffraction of an even staggered mode in a one-dimensional LN waveguide array. The number of elements in the array is* $N = 101$, $h = 0.5$, $P = 9.68$, *while the initial value of the non-dimensional pulse amplitude is* 0.45.

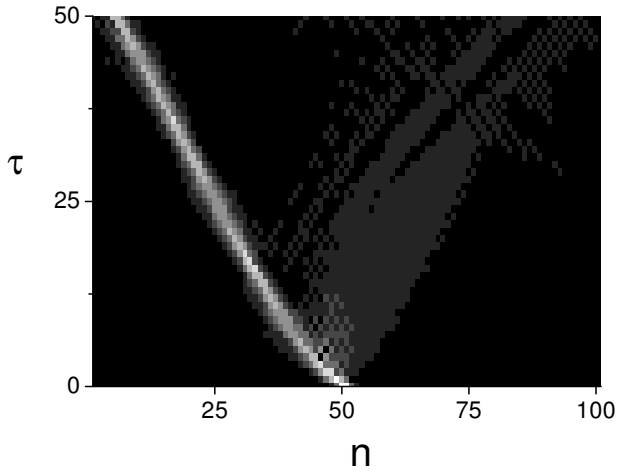

Fig. 5.2 *Diffraction-less propagation of an even staggered mode (with the same parameters as in figure above) in a LN waveguide array.*

5.2 STATIONARY SOLUTIONS

5.2.1 Homogeneous solutions

Similar as in the case of Eq. (4.1), the model equation here possesses two exact homogeneous solutions. The first one is unstaggered where adjacent elements are in phase:

$$U_{HU} = \pm\sqrt{\frac{\nu}{\beta_{PV} - \nu}}\exp(-i\nu\xi), \tag{5.6}$$

while the other one is a staggered solution with adjacent elements out of phase:

$$U_{HS} = \pm\sqrt{\frac{\nu - 2h^{-2}}{\beta_{PV} + 2h^{-2} - \nu}}\exp(-i\nu\xi + in\pi). \tag{5.7}$$

Both solutions have a limited existence range due to the saturable nature of the nonlinearity. As before, v represents the nonlinear frequency shift. The homogeneous staggered solution is represented in Fig. 5.3 for two different values of the parameter β_{PV}. Here, just opposite to the homogeneous solutions, which are obtained in Chapter 4, the amplitude of these array-independent solutions is an increasing function of the nonlinear frequency shift v.

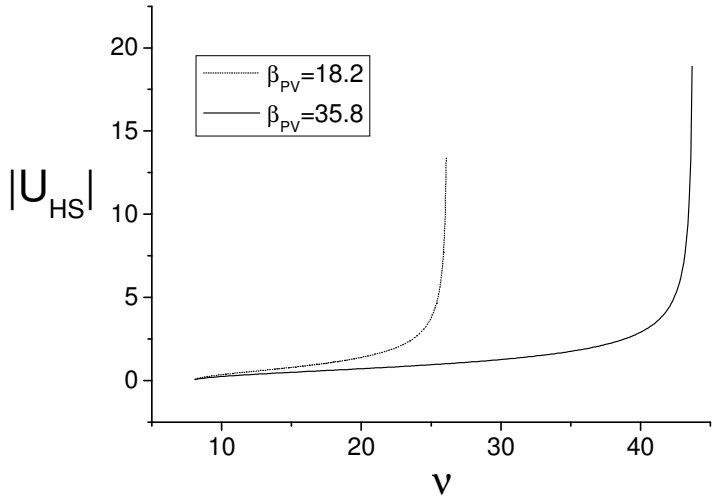

Fig. 5.3 *Homogeneous staggered solution U_{HS} for two different values of the parameter β_{PV}.*

5.2.1.1 Stability of the homogeneous solutions

By introducing a small unstaggered perturbation (see Section 4.2.1.1) in the system (5.4) one finds that the unstaggered homogeneous solution, which is given by Eq. (5.6), is modulationally stable. On the other hand, the staggered homogenous solution, which is given by Eq. (5.7), is unstable with respect to small staggered perturbations. Its dispersion relation reads:

$$\omega^2 = \frac{4}{h^2}\sin^2\left(\frac{\pi}{N}\right)\left(\frac{1}{h^2}\sin^2\left(\frac{\pi}{N}\right)+\frac{(\nu-h^{-2})^2}{\beta_{PV}}-(\nu-h^{-2})\right). \tag{5.8}$$

A sufficient condition for this staggered homogeneous solution to become modulationally unstable is $\omega^2<0$, which, together with the facts that $N\approx 100$ and $h\approx 1$, results in the next instability frequency band:

$$\nu\in\left(2h^{-2}+h^{-2}\sin^2(\pi/N),\ \beta_{PV}+2h^{-2}-h^{-2}\sin^2(\pi/N)\right). \tag{5.9}$$

In the very narrow frequency bands $\Delta\nu = h^{-2}\sin^2(\pi/N)$ (whose width coincides with the corresponding result of unstaggered homogeneous solution from the previous Chapter) at the ends of the existence interval, this solution is stable with respect to the given form of perturbations. However, in these regions instabilities may arise under some other sort of distortions. The above result for the dispersion relation is correct only in the (experimentally justified) limit $4\sin^2(\pi/N)/(\beta_{PV}h^2)\rightarrow 0$. Thus the dispersion relation in Eq. (5.8) defines the instability growth rate spectra for the frequency band in Eq. (5.9).

In the former Chapter we have seen that the modulational instability of the homogeneous unstaggered solution may result in the creation of various stable discrete screening solitons. Analogously, it is logical to suppose that discrete staggered photovoltaic solitons might exist here as an outcome of the modulational instability of the homogeneous staggered solution.

5.2.2 Soliton solutions

Indeed, from the model equation (5.4) it is possible to get the following five analytical expressions for different narrow localized solutions [161]:

a) The symmetric odd staggered (SOS) solution (see Eq. (3.15c) and Fig. 3.4c) reads:

$$|U_0|=\sqrt{\frac{\nu-h^{-2}}{\beta_{PV}+h^{-2}-\nu}},\quad |U_{0\pm m}|=\frac{|U_0|}{2h^2(\nu-h^{-2})^m}, \tag{5.10}$$

where the central element of the array is marked with $n=0$, while $m=1, 2, \ldots$.

b) An antisymmetric odd staggered (AOS) solution, which is given by Eq. (3.4d) and which is illustrated in Fig 3.15d, has the form:

$$U_0=0,\quad |U_{\pm1}|=\sqrt{\frac{\nu-h^{-2}}{\beta_{PV}+h^{-2}-\nu}},\quad |U_{\pm1\pm m}|=\frac{|U_1|}{2h^2(\nu-h^{-2})^m}, \tag{5.11}$$

c) and even staggered (ES) solutions (see Eq. (3.16b) and Fig 3.5b)) are described by:

$$|U_{\pm1}|=\sqrt{\frac{\nu-1.5h^{-2}}{\beta_{PV}+1.5h^{-2}-\nu}},\quad |U_{\pm1\pm m}|=\frac{|U_{\pm1}|}{2h^2(\nu-h^{-2})^m}. \tag{5.12}$$

d) Furthermore, even unstaggered (EU) solutions, which are given by Eq. (3.16a) and Fig. 3.5a, read:

$$|U_{\pm1}|=\sqrt{\frac{\nu-0.5h^{-2}}{\beta_{PV}+0.5h^{-2}-\nu}},\quad |U_{\pm1\pm m}|=\frac{|U_{\pm1}|}{2h^2(h^{-2}-\nu)^m}, \tag{5.13}$$

e) while a twisted staggered (TS) solution (see Eq. (3.16d) and Fig. 3.5d), can be mathematically described by:

$$|U_{\pm 1}|=\sqrt{\frac{\nu-0.5h^{-2}}{\beta_{PV}+0.5h^{-2}-\nu}},\quad |U_{\pm 1\pm m}|=\frac{|U_{\pm 1}|}{2h^{2}(\nu-h^{-2})^{m}}. \tag{5.14}$$

As before, all of them have a limited interval of allowed solitons frequencies. The width of these intervals depends on the two parameters β_{PV} and $0.5\,h^{-2}$. For example, in the case $\beta_{PV} < 0.5h^{-2}$ twisted staggered solitons do not exist. In this thesis we only investigate the case when $\beta_{PV} > 1.5h^{-2}$. The corresponding frequency intervals where these analytical solutions can be found are presented in Table 5.1.

$(0.5\ h^{-2}, h^{-2})$	$(h^{-2}, 1.5\ \mathrm{h}^{-2})$	$(1.5\ h^{-2}, \beta_{PV}+0.5\ h^{-2})$	$(\beta_{PV}+0.5\ h^{-2}, \beta_{PV}+h^{-2})$	$(\beta_{PV}+h^{-2}, \beta_{PV}+1.5\ h^{-2})$
EU	SOS, AOS, TS	SOS, AOS, TS, ES	SOS, AOS, ES	ES

Tab. 5.1 *Frequency intervals for different types of narrow localized modes. For the notation recall the Section 3.4.*

In this thesis a special attention is paid to the two symmetric staggered solutions, namely odd (SOS) and even (ES) one, which stable propagation along the array is illustrated in Fig. 5.4.

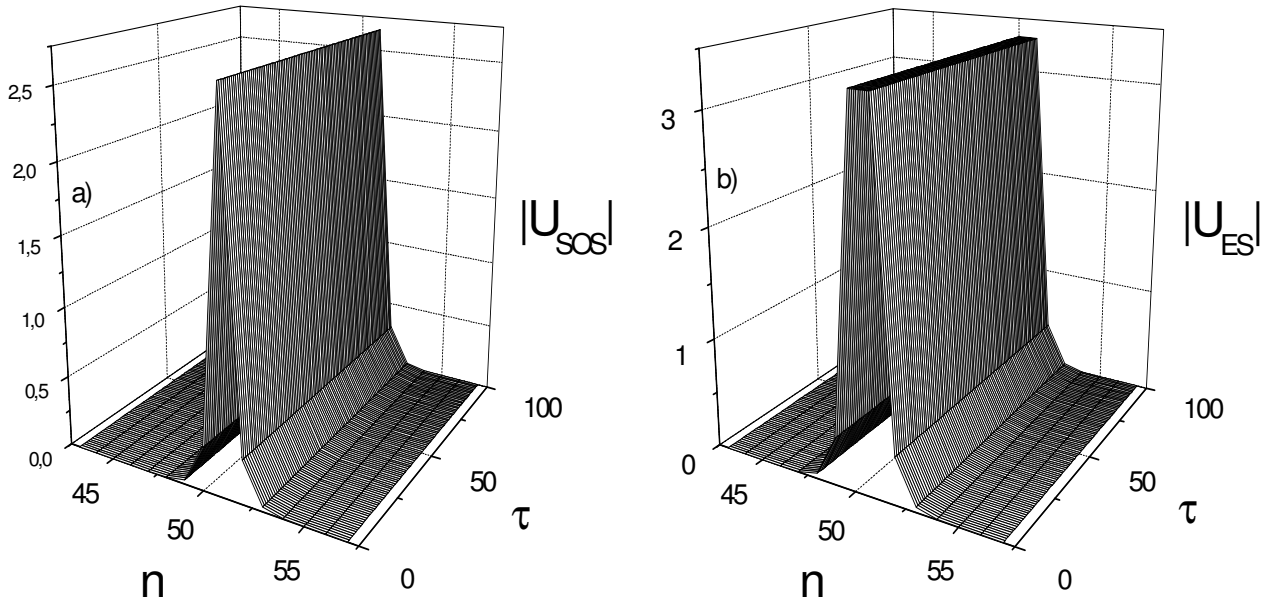

Fig. 5.4 *Propagation of a) odd staggered and b) even staggered discrete photovoltaic soliton for the system parameters a) $h=0.45$, $\beta_{PV}=26.82$, and $P=7.255$, and b) $h=0.5$, $\beta_{PV}=17.89$, and $P=22.5$.*

5.2.2.1 Stability of symmetric staggered soliton solutions

In the case of symmetric odd staggered solutions and an infinite number of elements of the array the total power is equal to:

$$P = |U_0|^2 \frac{(2h^2\nu - 2)^2 + 1}{(2h^2\nu - 2)^2 - 1}, \tag{5.15}$$

where $|U_0|^2$ is given in Eq. (5.10). In all other cases one can get the following result for the soliton power:

$$P = 2|U_1|^2 \frac{(2h^2\nu - 2)^2}{(2h^2\nu - 2)^2 - 1}, \tag{5.16}$$

where the corresponding expressions for $|U_1|^2$ are given by Eq. (5.11-14). From the definition of the power (see Eq. (4.3)) it is clear that $P > 0$ only holds in the regions where $\nu < 0.5h^{-2}$ and $\nu > 1.5\ h^{-2}$, respectively. These conditions expel the even unstaggered soliton solution as physically unreal from the above list of the existing forms of discrete photovoltaic soliton solutions in an infinite nonlinear waveguides array. Additionally, the frequency region where physically real twisted staggered solutions may exist is reduced to the interval ($1.5\ h^{-2}$, $\beta_{SC} + 0.5h^{-2}$).

The dependence of the Hamiltonian of discrete symmetric staggered photovoltaic solitons on the soliton power is presented in Fig. 5.5. According to [107], staggered solitons can be regarded as particles of negative mass. Then, opposite to particles of positive mass (unstaggered solitons), where the particle with the minimal energy is the most stable one, the staggered soliton whose energy is the highest is the most stable soliton. As one may see, it is possible to have a situation in which even staggered soliton is more stable than odd one. That happens in region of very low power and in region of higher power.

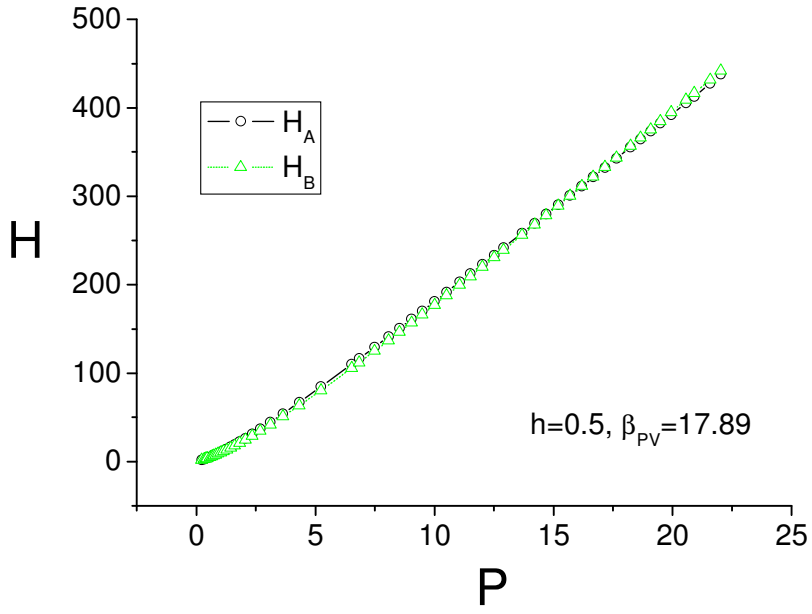

Fig. 5.5 *Power dependence of the Hamiltonian of the symmetric discrete photovoltaic solitons.*

Here, in contrast to the situation in the former Chapter, no cascade processes is observed numerically. In Fig. 5.6, where the dependence of both the odd and even staggered soliton amplitude on the frequency for the central element and its first and second neighbours is presented, one can notice only a weak widening of these localized modes in the region of lower soliton frequencies.

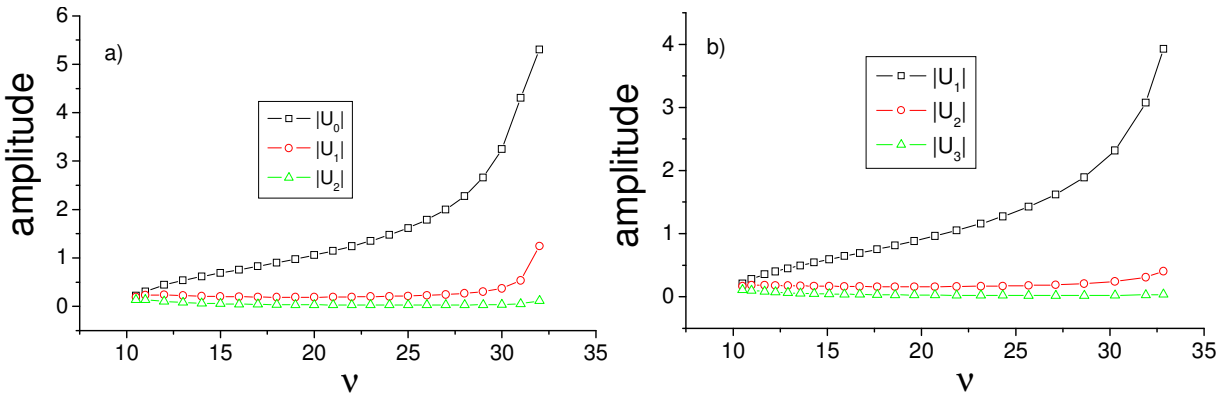

Fig. 5.6 *Amplitude in the central waveguide and its first and second neighbours versus frequency ν for the same system's parameters as in Fig.* 5.4 *for a) odd, and b) even staggered discrete photovoltaic solitons.*

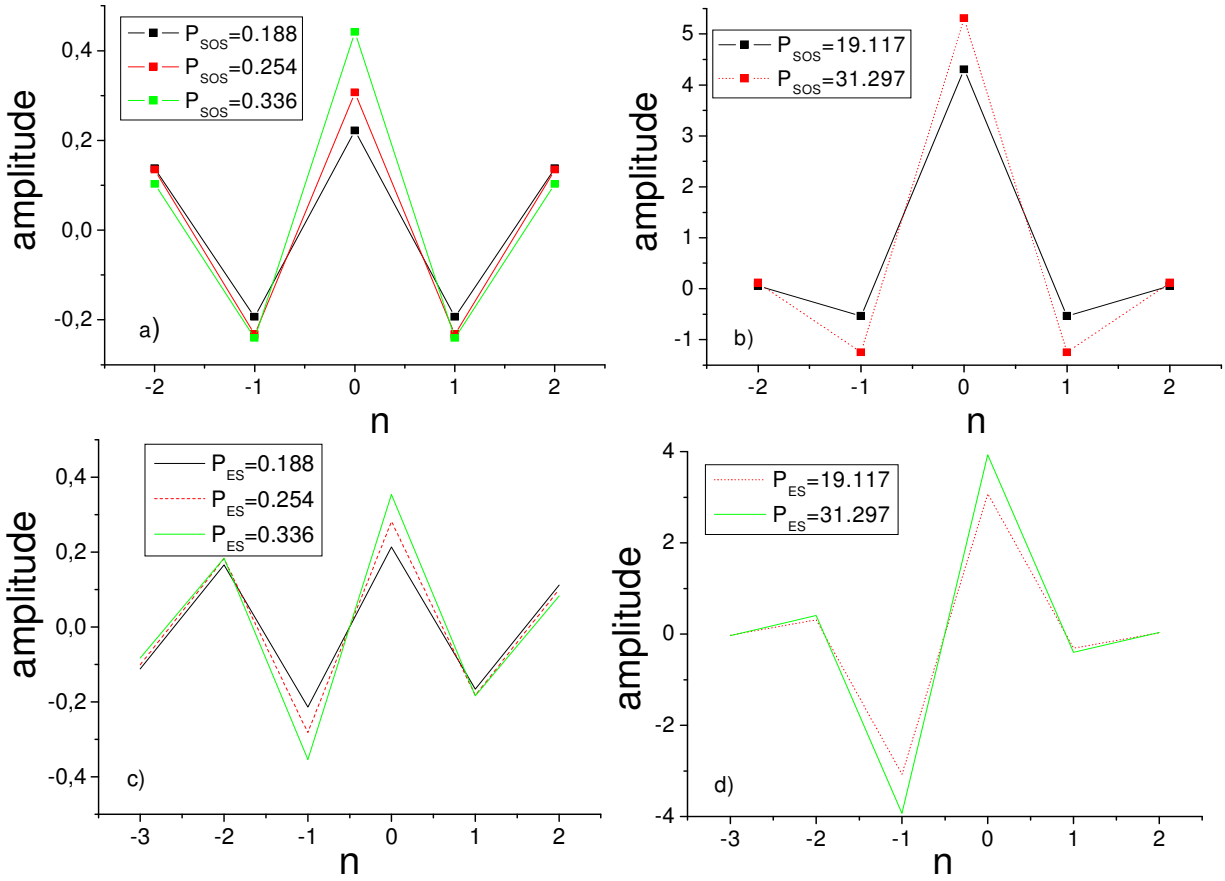

Fig. 5.7 *Amplitude of discrete photovoltaic solitons versus number n: a) odd and c) even soliton in a small power region, b) odd and d) even soliton in region of higher power.*

Redistributions of amplitudes across elements of the array for both symmetric staggered localized solutions are given in Fig. 5.7. In a low power region, where both localized structures are rather wide the effect of discreteness is weak. Due to increased inertia of the system the formation of the narrow even staggered soliton (Fig. 5.7c) is delayed in comparison to the odd one (Fig. 5.7a and Table 5.1). On the other hand, in region of higher soliton power, the odd staggered soliton starts first to widen (Fig. 5.7b) and the even soliton overtakes it energetically (Fig. 5.7d and Table 5.1).

6. PEIERLS-NABARRO POTENTIAL

The link between discrete solitons and intrinsically localized modes in nonlinear lattices is elaborated at the beginning of this Chapter. Being a useful tool for describing the propagation of these localized modes across lattices, the concept of Peierls-Nabarro potential is explained on the example of DNLS equation. The features of this potential are examined in detail in systems with different saturable types of nonlinearity. Finally, switching, steering, and interactions of various solitons in both SBN and LN nonlinear waveguide arrays are investigated, too.

6.1 INTRINSICALLY LOCALIZED MODES

Spatially localized modes may exist in a linear lattice with impurities [162]. The localized mode possesses an amplitude maximum at the impurity site, and it decreases exponentially as a function of the distance from the impurity. Besides these impurity-induced localized structures, a new class of strongly localized modes has been identified in homogeneous nonlinear lattices [97, 163]. Because these lattices do not contain any impurities, Sievers and Takeno called these modes intrinsically localized modes. These modes are the discrete analogue of envelope solitons, with the unique property that their width is only a few lattice spacings.

A seminal model, which shows the main properties of intrinsically localized modes, is a chain with anharmonic inter-atomic interaction, the so-called Fermi-Pasta-Ulam problem [4]. This model describes a one-dimensional lattice composed of atoms with mass *M*, in which each atom interacts only with its nearest neighbours. The corresponding equation of motion is given by:

$$M\,\frac{d^2u_n}{dz^2} - k_2\,(u_{n+1} + u_{n-1} - 2u_n) - k_4\left[(u_{n+1} - u_n)^3 + (u_{n-1} - u_n)^3\right] = 0, \qquad (6.1)$$

where $u_n(z)$ is the displacement of the n-th atom from its equilibrium position, k_2 is the nearest neighbour harmonic force constant, while k_4 is the quartic anharmonic force constant. The Sievers-Takeno mode pattern is $u_n(z) = A\,[...,0,-(1/2),1,-(1/2),0,...]\cos(W\,z)$, where A is the amplitude of the mode. This approximation is valid for large $(k_4/k_2)\,A^2$. The mode frequency W lies above the nonlinear cut-off frequency of the spectrum band. Another type of intrinsic localized modes was introduced by Page [164]. This stationary mode has a pattern of the form $u_n(z) = A\,[...,(1/6),-1,1,-(1/6),...]\cos(W\,z)$. The first mode is dynamically unstable while the latter one is extremely stable.

Intrinsic localized modes are also found in the nonlinear Klein-Gordon chain, where the nonlinearity is produced by an on-site potential [165]. If *C* is the coupling constant, χ is the anharmonicity parameter of the potential, and ω_0 is the frequency of small amplitude on-site vibrations in the nonlinear symmetric on-site potential, the equation of motion is given by:

$$M\,\frac{d^2u_n}{dz^2} - C\,(u_{n+1} + u_{n-1} - 2u_n) + M\,\omega_0^2\,u_n - \frac{1}{3}\chi\,u_n^3 = 0. \qquad (6.2)$$

Linear oscillations of the Klein-Gordon chain of frequency *W* and wave number *k* are described by the following dispersion relation:

$$W^2 = \frac{\omega_0^2}{M} + 4\,\frac{C}{M}\,\sin^2\left(\frac{k}{2}\right), \tag{6.3}$$

where the lattice spacing is taken to be equal to one. This linear spectrum has a gap $\omega_0 / \sqrt{M}$ and is limited by the cut-off frequency $W_{max} = \pm\sqrt{(\omega_0^2 + 4C)/M}$ due to discreteness. Here highly localized modes exist with frequencies lying below the given frequency gap (for $\chi > 0$) or above the cut-off frequency (for $\chi < 0$). The structures of these intrinsically localized modes are $u_n(z) = A\,[...,0, f_1^A, 1, f_1^A, 0, ...]\cos(W z)$ for $\chi > 0$ (where $f_1^A << 1$), and $u_n(z) = A\,[...,0, -f_1^A, 1, -f_1^A, 0, ...]\cos(W z)$ for $\chi < 0$.

These strongly localized modes, which contain only a few excited components, are in fact the discrete solitons from Chapter 3.

6.2 PEIERLS-NABARRO POTENTIAL FOR DNLS MODEL

One of the main problems in the theory of nonlinear localized modes is the description of their propagation through the discrete lattice. During that propagation a mode changes both its position and its structure. In Fig. 6.1 one can see shapes of both high-frequency (a, b) and low-frequency (c, d) localized modes in a nonlinear chain. Modes a) and c) are centred on a site, while modes b) and d) are centred between sites (to be also compared with Figs. 3.4a, b and Figs. 3.5a, b).

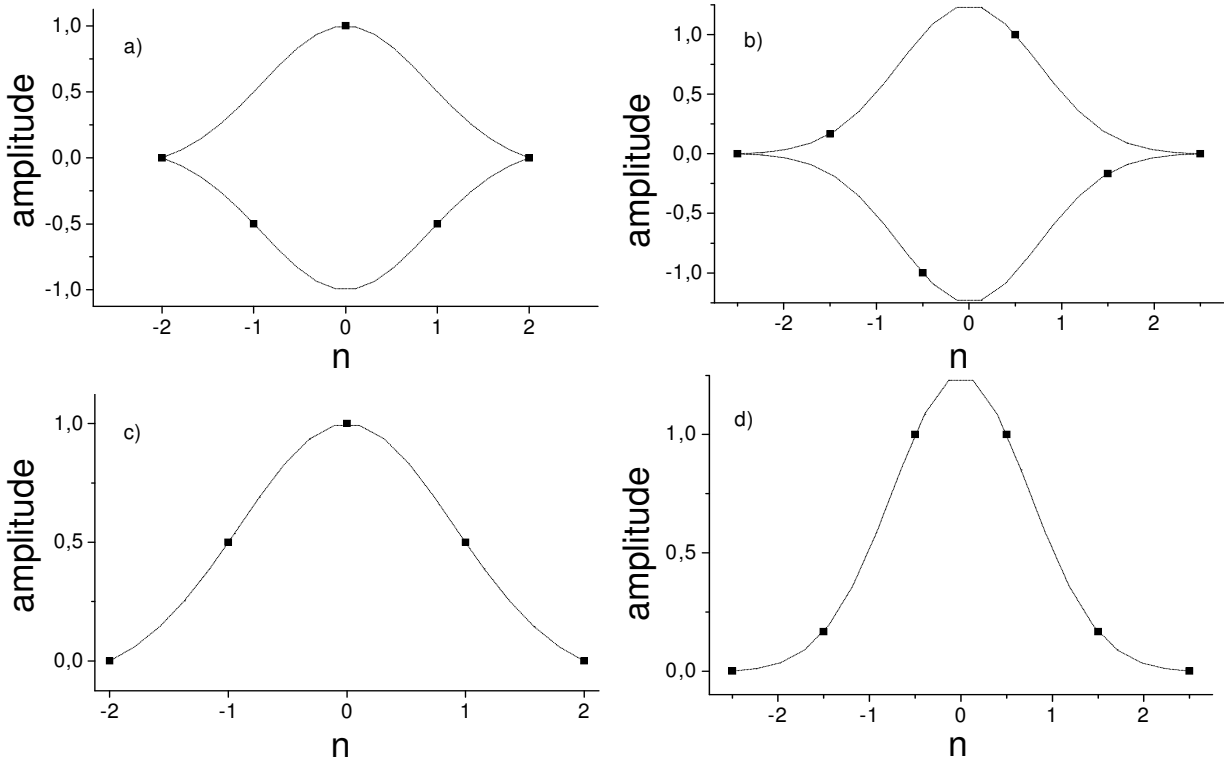

Fig. 6.1 *Localized modes of a nonlinear chain. a, b) Shapes of high-frequency localized modes, and c, d) shapes of low-frequency localized modes.*

Modes a) and b) show an out-of-phase oscillation of adjacent sites and they are related by translations of half the lattice spacing. Therefore, they should both occur as two states of a single mode which propagates through the lattice under a certain angle [166]. The difference in their energies can be attributed to an effective periodic potential which is generated by the lattice discreteness, and which is similar to the Peierls–Nabarro (PN) potential for kinks in the Frenkel-Kantorova model [167]. This potential was discussed for the first time in continuum theory of dislocations [168, 169]. Its existence reflects the fact that the translational invariance in the system is broken by discreteness of the underlying lattice. From the physical point of view, its amplitude can be viewed as the minimum barrier which must be overcome to translate the dislocation by one lattice period.

In this paragraph the accent is put on the Peierls-Nabarro potential in discrete media with cubic nonlinearity. The DNLS equation (3.7) can be, after a simple transformation of the variables, reduced to the following form:

$$i\,\frac{dU_n}{d\xi} + C\,(U_{n+1} + U_{n-1} - 2U_n) + \mathrm{X}\,|U_n|^2\,U_n = 0. \tag{6.4}$$

Depending on the sign of the nonlinearity parameter X, high or low-frequency localized modes may occur. Here a self-focusing nonlinearity $(\mathrm{X} > 0)$ allows for low-frequency (acoustic-like) modes, while, in case of a self-defocusing nonlinearity $(\mathrm{X} < 0)$, high-frequency (optical-like) modes may exist. By recalling the corresponding results from Section 3.3.2 it is easy to obtain an analog spectrum band and the corresponding linear and nonlinear dispersion relations. As mentioned before, one of the principal effects of modulational instability is the creation of localized pulses.

By assuming that a stationary localized solution of Eq. (6.4) has a form $U_n(\xi) = F\,f_n \exp(-i\nu\xi)$ it is possible to get the next set of coupled algebraic equations for the real function f_n

$$\nu\,f_n + C\,(f_{n+1} + f_{n-1} - 2\,f_n) + \mathrm{X}\,F^2 f_n^3 = 0. \tag{6.5}$$

From Eq. (6.5) we can get two types of strongly localized modes. The first one (mode A) is symmetric, centred at the lattice site at $n = 0$, and it is unstaggered. Assuming $F = A$, $f_0 = 1$, $f_{-n} = f_n$, and $|f_{n+1}| << |f_n|$ for $n \geq 0$, this intrinsically localized mode has a pattern in the form:

$$U_n^A(\xi) = A\,(\ldots, 0, f_1^A, 1, f_1^A, 0, \ldots)\,\exp(-i\nu\xi), \tag{6.6}$$

where the parameter $f_1^A = C/(\mathrm{X}A^2)$ is assumed to be small (i.e. all second order terms are neglected) and the lattice elements are indexed with $n = 0, \pm 1, \pm 2, \ldots$ The frequency ν is determined (in the lowest order in f_1^A) to be $\nu \approx -\mathrm{X}A^2$ and lies below the lowest band frequency.

The second strongly localized mode (mode B) is also symmetric, but centred between two neighboured lattice elements $n = \pm 1$, and unstaggered. Assuming $F = B$, $f_{\pm 1} = 1$, $f_{-n} = f_n$, and $f_{n+1} << f_n$ for $n \geq 1$, this intrinsically localized mode has the form:

$$U_n^B(\xi) = B\,(\ldots, 0, f_2^B, 1, 1, f_2^B, 0, \ldots)\,\exp(-i\nu\xi), \tag{6.7}$$

where $\nu \approx -\mathrm{X}B^2$, $f_2^B = C/(\mathrm{X}B^2)$, and the lattice elements are indexed with $n = \pm 1, \pm 2, \ldots$.

If one imagines a localized pulse of fixed shape translated rigidly through the nonlinear lattice, it is obvious that this mode repeatedly changes its symmetry form: When the peak is centred on a lattice site the symmetry is of the form of mode A, while, when the peak is centred between the sites, the symmetry is of the form of mode B. These modes can be viewed as two stationary configurations corresponding to the moving mode at different fixed instants in time provided that their amplitudes are adjusted properly. To compare these amplitudes one may fix the number of quanta or power P. From the condition $P_A = P_B$ it is possible to obtain the following relation between the amplitudes A and B (to lowest order in small parameter f_1^A):

$$A^2 = 2B^2. \tag{6.8}$$

With this condition, one may interpret these two modes as different stationary states of the same localized mode. By virtue of Eq. (6.8) and properly adjusted Eq. (3.9) it is possible to find the difference in energy between these two stationary states. In the lowest order of the tiny parameter f_1^A, one can calculate:

$$\Delta E_{AB}(P) = H_A(P) - H_B(P) = -\frac{1}{2}\mathrm{X}A^4 + \mathrm{X}B^4 = -\frac{1}{4}\mathrm{X}A^4 \neq 0. \tag{6.9}$$

This result reveals that there is an effective energy barrier between modes A and B, which can be considered as the height of the Peierls-Nabarro potential. This potential is always negative, which means that mode A has lower energy than mode B and thus is more stable, and it is proportional to the soliton power level. The existence and stability of modes A and B for the case of the coupled DNLS model describing transport of vibration energy in crystalline acetanilide is discussed in [97]. The power dependent soliton steering studied in [141, 145, 166, 170-173] can be explained with the PN potential regarding it as the minimum barrier which must be overcome to propagate a soliton across the nonlinear lattice [145, 166].

6.3 PEIERLS-NABARRO POTENTIAL IN DISCRETE SYSTEMS WITH SCREENING SATURABLE NONLINEARITY

6.3.1 Theoretical results

In the last chapter it is demonstrated that the model equation (4.1) has two conserved quantities: the Hamiltonian, which is given by Eq. (4.2), and the power, which is given by Eq. (4.3). Furthermore, it is revealed that the stationary homogeneous solution, which is given by Eq. (4.5), is modulationally unstable, and the expression for the growth rate of small perturbations is presented. As already mentioned before, this process of modulation instability is responsible for energy localization and the creation of discrete solitons. Such stationary localized modes can be obtained from Eq. (4.1) by assuming solutions in the form $U_n(\xi) = F f_n \exp(-i\nu\xi)$ and a set of coupled algebraic equations for the real function f_n

$$\nu f_n + \frac{1}{2h^2}\left(f_{n+1} + f_{n-1} - 2f_n\right) - \frac{\beta_{SC} f_n}{1 + F^2 |f_n|^2} = 0. \tag{6.10}$$

In this thesis only two types of strongly localized modes are investigated, which can be obtained from Eq. (6.10). The first one (mode A: a symmetric odd unstaggered soliton) is

centred at the lattice site $n=0$, assuming $F=A, f_0 = 1,\ f_{-n} = f_n$, and $|f_{n+1}|<<|f_n|$ for $n \geq 0$, and has a pattern of the form

$$U_n^A(\xi) = A(..., f_2^A, f_1^A, 1, f_1^A, f_2^A, ...) \exp(-i\nu\xi), \tag{6.11}$$

where the lattice elements are labelled by $n = 0, \pm 1, \pm 2, ...$

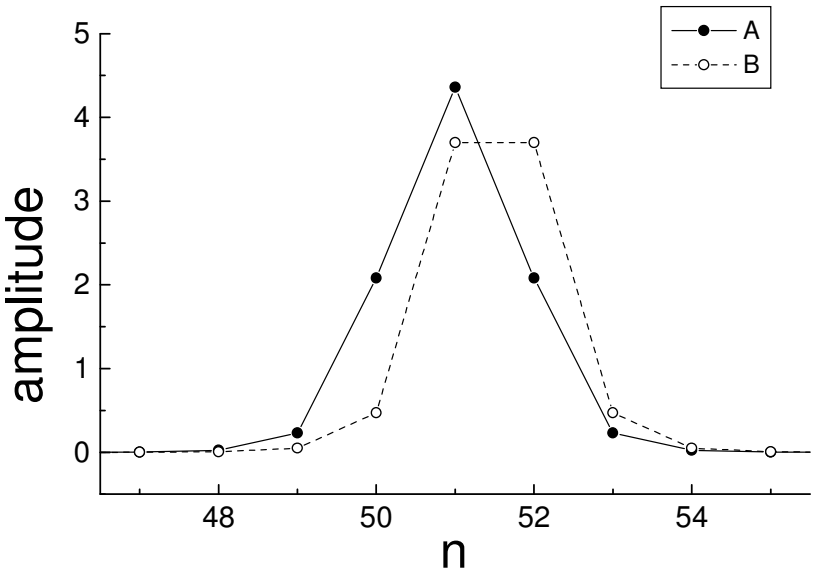

Fig. 6.2 *Odd (A) and even (B) unstaggered symmetric localized modes in a nonlinear array.*

If we consider a linear propagation in the lattice elements with $|n|>1$, the total power P and the Hamiltonian H can be approximately calculated as:

$$P_A = A^2 \frac{(\gamma_{SC} + 2 - \theta)^2 + 1}{(\gamma_{SC} + 2 - \theta)^2 - 1}, \tag{6.12}$$

$$H_A = \gamma_{SC} \ln(1 + A^2) + 2\gamma_{SC} \ln\left[\prod_{j=1}^{\infty}\left(1 + \frac{A^2}{(\gamma_{SC} + 2 - \theta)^{2j}}\right)\right] + 2A^2 \frac{(\gamma_{SC} + 2 - \theta)^2}{(\gamma_{SC} + 2 - \theta)^2 + 1}, \tag{6.13}$$

where $\gamma_{SC} = 2\beta_{SC} h^2,\ \theta = 2\nu h^2,$ and the square of the soliton amplitude A is defined by:

$$A^2 = \frac{(\gamma_{SC} + 2 - \theta)^2 - 2}{(\gamma_{SC} + 2 - \theta)(\theta - 2) + 2}. \tag{6.14}$$

The second strongly localized mode (mode B: a symmetric even unstaggered soliton) is centred between two neighbouring lattice elements $n = \pm 1$. Assuming $F = B,\ f_{\pm 1} = 1,\ f_{-n} = f_n$, and $f_{n+1} << f_n$ for $n \geq 1,$ it can be shown that this mode has a pattern of the form:

$$U_n^B(\xi) = B\ (..., f_3^B, f_2^B, 1, 1, f_2^B, f_3^B, ...) \exp(-i\nu\xi), \tag{6.15}$$

where the lattice elements are indexed with $n = \pm 1, \pm 2, ...$. With the same procedure as applied for the mode A, it is possible to approximately calculate the total power P and the Hamiltonian H for the mode B

$$P_B = 2B^2 \frac{(\gamma_{SC} + 2 - \theta)^2}{(\gamma_{SC} + 2 - \theta)^2 - 1}, \tag{6.16}$$

$$H_B = 2\gamma_{SC} \ln\left[\prod_{j=0}^{\infty}\left(1 + \frac{B^2}{(\gamma_{SC} + 2 - \theta)^{2j}}\right)\right] + 2B^2 \frac{(\gamma_{SC} + 2 - \theta)^2}{(\gamma_{SC} + 2 - \theta)^2 + 1}, \tag{6.17}$$

with the corresponding square of the soliton amplitude:

$$B^2 = \frac{(\gamma_{SC} + 2 - \theta)(\gamma_{SC} + 1 - \theta)}{(\gamma_{SC} + 2 - \theta)(\theta - 1) + 1}. \tag{6.18}$$

These results are obtained in the following way. Firstly, contributions from all neighbouring elements to the chosen one in Eq. (6.10) are neglected. Then, an expression for the small amplitude (linear regime) in the first neighbour is obtained, which is, finally, given back in the equation for the central element. The results of Eqs. (6.12) and (6.13) are presented in Fig. 6.3 for the same parameters as in Fig. 4.9. Here power P is again a decreasing function of the soliton parameter ν, confirming the solitons' stability with respect to small longitudinal perturbations.

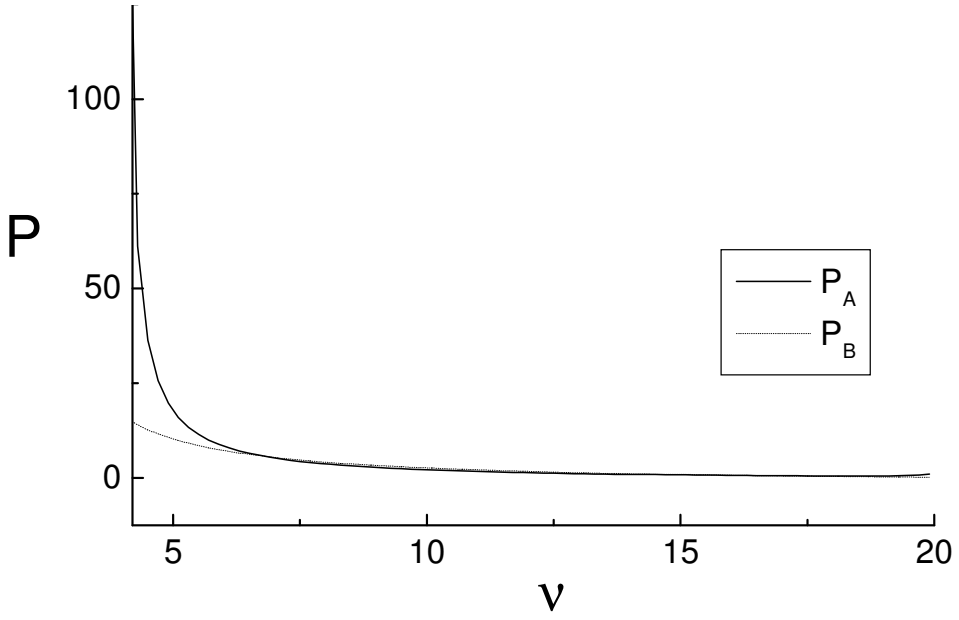

Fig. 6.3 *Analytically obtained* p*ower dependence of localized modes A and B on soliton parameter* ν.

Fig. 6.4 depicts the dependence of the Hamiltonian of modes A and B on the soliton parameter ν, as described by Eqs. (6.13) and (6.17), respectively. One can immediately notice that these two curves intersect each other and, for small values of ν, there exists a region where mode B has lower total energy than mode A. This region does not exist in the case of discrete systems with cubic nonlinearity [145, 174]. It is worthwhile to mention that this transition occurs for a value of the soliton parameter ν which is quite close to the particular value of ν from Chapter 4 when the central element goes into saturation [96].

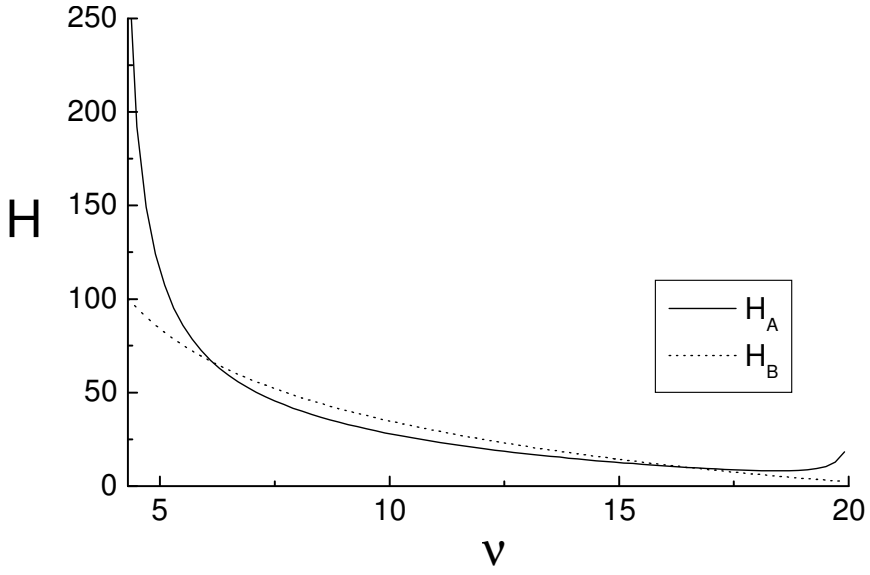

Fig. 6.4 *Analytically calculated Hamiltonian H of the intrinsically localized modes A and B as a function of soliton parameter* ν.

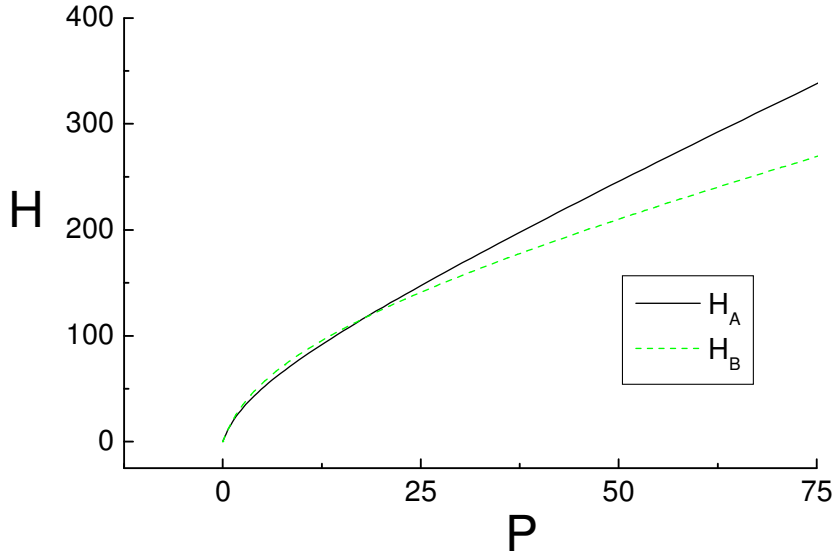

Fig. 6.5 *Analytical dependence of Hamiltonian* H *on soliton power* P *for localized modes A and B. The two curves intersect for powers* $P \approx 20$.

The analytically obtained dependence of Hamiltonian on soliton power is presented in Fig. 6.5. In the small amplitude regime, where the model equation (4.1) is basically reduced to the DNLS equation, mode A has a lower energy for the same power than mode B. Thus, mode A is the favourably localized state of the system. But, for a soliton power $P \approx 20$, mode B starts to be more stable than mode A [174].

The difference in energy between these two stationary localized states for the same power level $P_A = P_B = P$ defines the effective PN potential [145, 166]

$$\Delta E_{AB}(P) = H_A(P) - H_B(P). \tag{6.19}$$

This potential is shown in Fig. 6.6 and Fig 6.7 as a function of soliton frequency and power, respectively. In the first figure region III corresponds to the regime where it is hard to distinguish numerically oscillatory and soliton solutions (see the discussion after Fig. 4.7). Region II with a negative sign of the PN potential covers the domain of applicability of the DNLS model equation, while the first region I of high amplitude exhibits a positive sign of the PN potential.

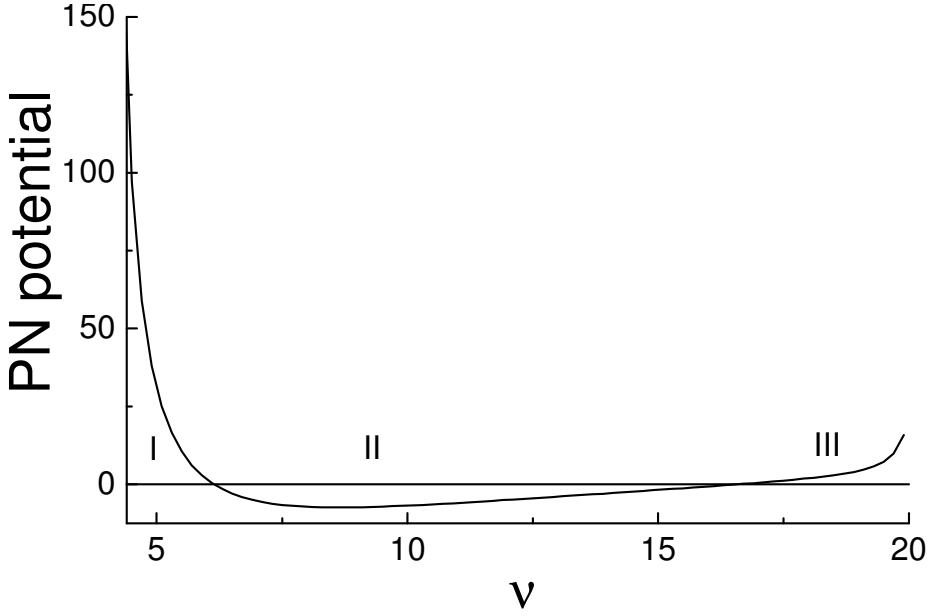

Fig. 6.6 *Peierls-Nabarro potential ΔE_{AB} as a function of soliton parameter ν.*

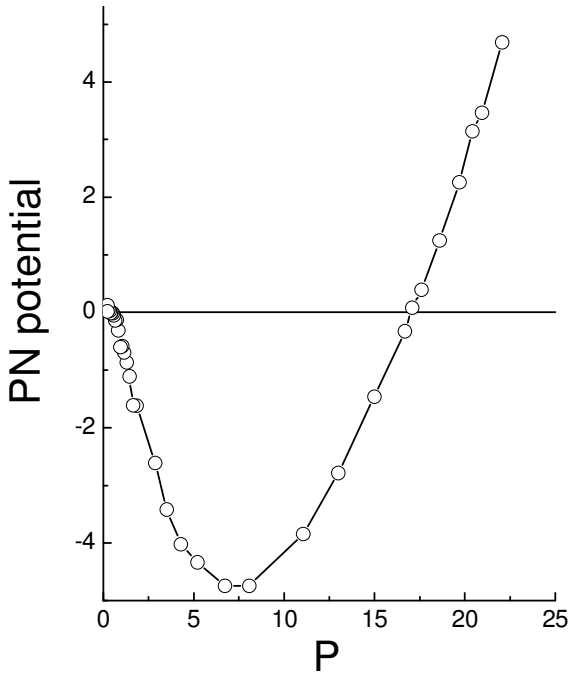

Fig. 6.7 *Dependence of the Peierls-Nabarro potential ΔE_{AB} on soliton power P.*

The shape of the curve $\Delta E_{AB}(P)$, which is presented in Fig. 6.7, indicates the important conclusion that the effective PN potential changes its sign for a critical power $P_C \approx 20$, which brings significant implications on both, the stability properties of the localized modes A and B, and soliton steering across the lattice elements. In the region $0 < P < P_C$ mode A has a lower energy than mode B ($H_A < H_B$) for the same power P, indicating that mode A is stable and mode B is unstable. For this lower power region this coincides with the results obtained in [145, 166] for the DNLS lattices with a Kerr nonlinearity. The obtained agreement is expected because in the small amplitude limit Eq. (4.1) reduces to the cubic DNLS equation. However, in the region $P > P_C$ the situation is opposite ($H_A > H_B$), indicating that now mode B is stable and mode A is unstable. This means, contrary to the DNLS lattices with cubic nonlinearity, a stable propagation of the discrete soliton centred *between* the neighbouring lattice elements (mode B) is possible. The critical power P_{C1}, i.e., a zero of the PN potential, represents marginally stable states for both modes.

6.3.2 Numerical results

As mentioned in Chapter 4, numerical results are irreplaceable in the deep saturation regime, where the approximate analytical solution given by Eq. (4.9) fails. It is numerically revealed there that the elements in the nonlinear array subsequently reach saturation level, so the natural question arises how this cascade mechanism of saturation influences the features of the PN potential. In Fig. 6.8 one can see how the power P of the unstaggered modes A and B depends on the soliton parameter ν. It is obvious that both modes alternately reach the saturation level. The corresponding values of the soliton power where this happens are depicted by crosses.

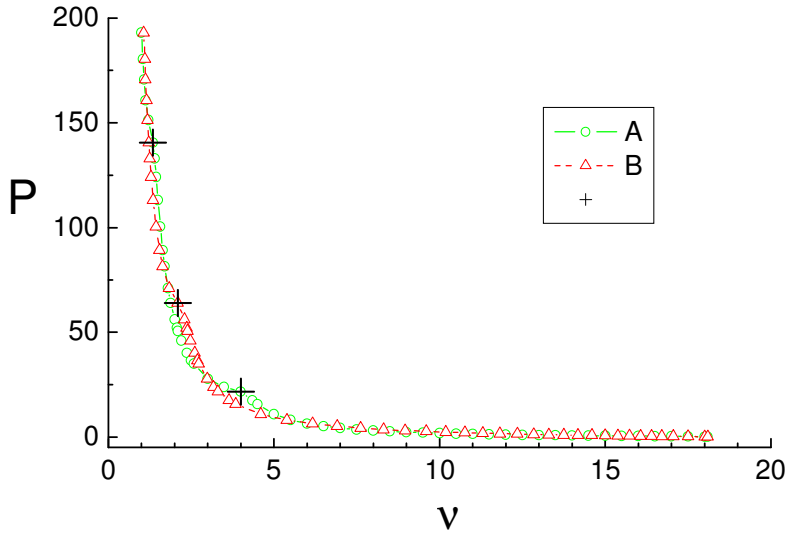

Fig. 6.8 *Numerically calculated power P as a function of soliton parameter ν.*

The numerically obtained dependence of the Hamiltonian H of the localized modes A and B on the soliton parameter ν is presented in Fig. 6.9. While the theory could predict only one intersection of the curves, simulations show the existence of multiple intersections for small ν.

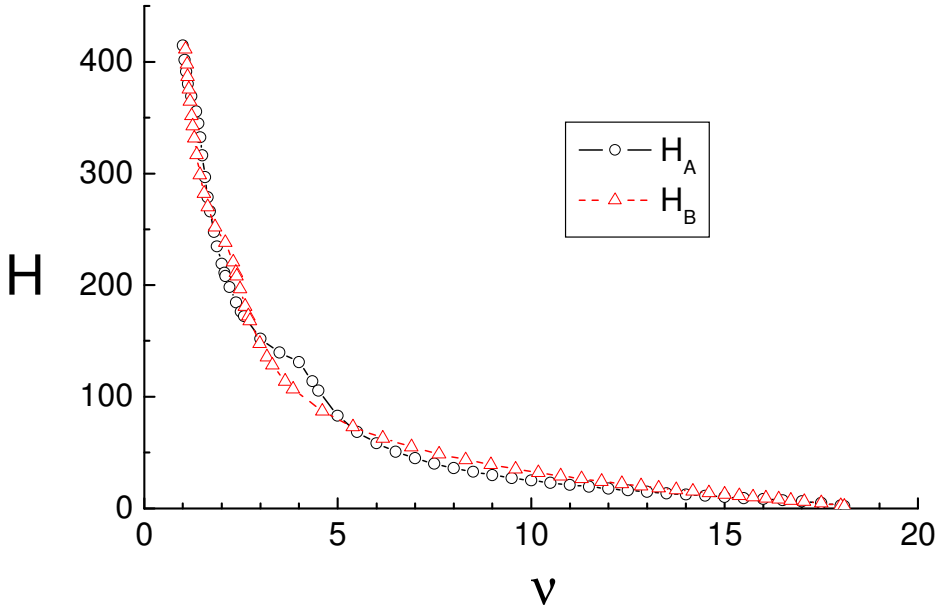

Fig. 6.9 *Numerically calculated dependence of Hamiltonian H of modes A and B on soliton parameter ν.*

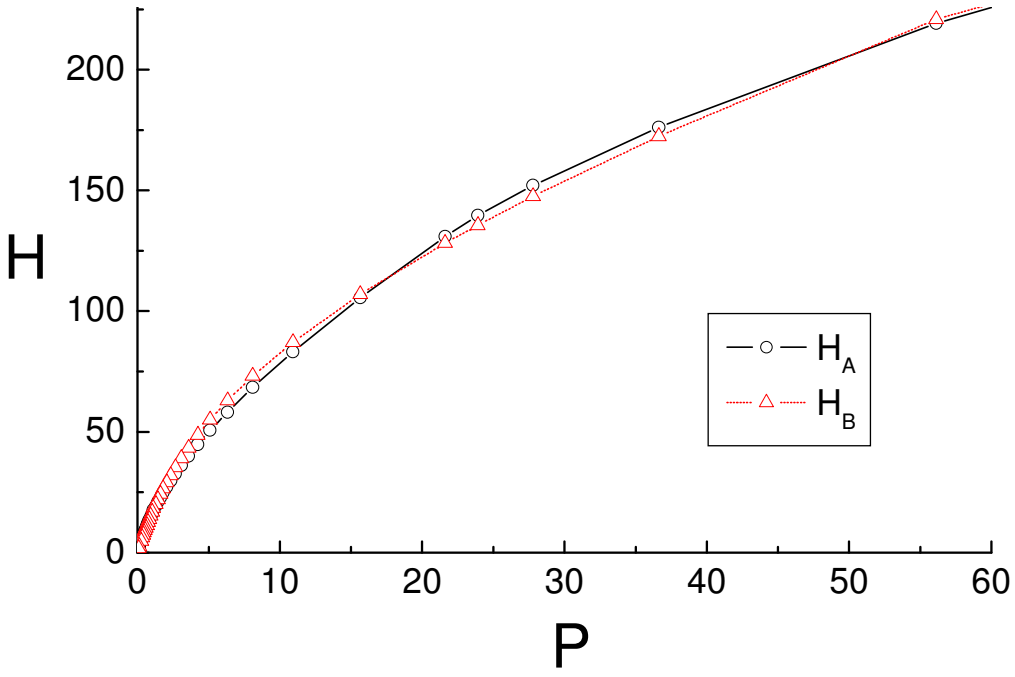

Fig. 6.10 *Numerically estimated dependence of Hamiltonian H on soliton power P.*

In Fig. 6.10 the power dependence of the Hamiltonian for odd and even symmetric, unstaggered modes A and B is depicted. Again, the most prominent result is the existence of three intersections of the curves. Moreover, the smallest value of the soliton power where this novel effect occurs practically coincides with the corresponding analytical result. Another numerical confirmation that the PN potential in discrete media with saturable nonlinearity can be positive is presented in Fig. 6.11.

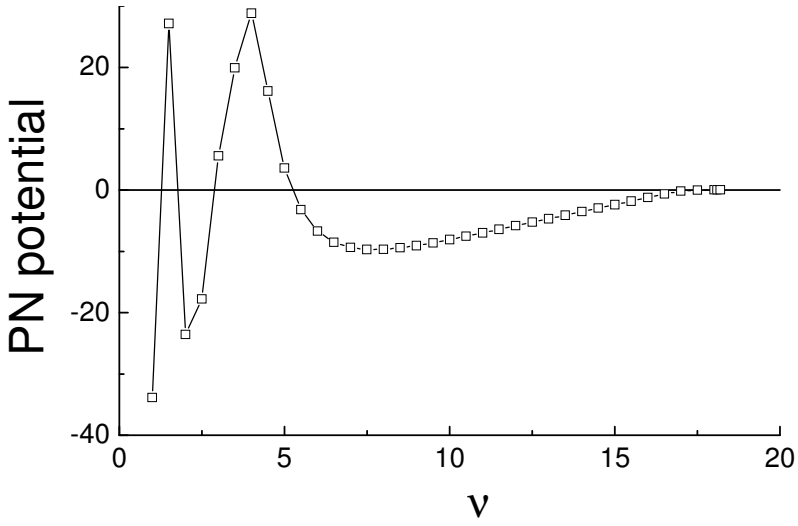

Fig. 6.11 *Numerically calculated Peierls-Nabarro potential as a function of soliton parameter* ν.

The shape of the observed PN potential can be explained by a cascade nature of amplitude saturation in the lattice elements [96]. The amplitude of the central element for mode A increases with increasing power level P up to a point when it reaches the saturation level. A further increase of P is the result of increasing amplitudes in the two neighbouring lattice elements $n = \pm 1$. Consecutively, when the amplitudes in the lattice elements $n = \pm 1$ saturate, the amplitudes of the next lattice elements $n = \pm 2$ contributes to a further increase of P. This cascade process continues with increasing power P, while mode A becomes less and less localized. The same process takes place also for mode B but for larger values of P, because two lattice elements saturate simultaneously. The numerically obtained power dependence of the amplitude in the central and two neighbouring elements for both modes, shown in Fig. 6.12, clearly illustrates the cascade nature of the saturation.

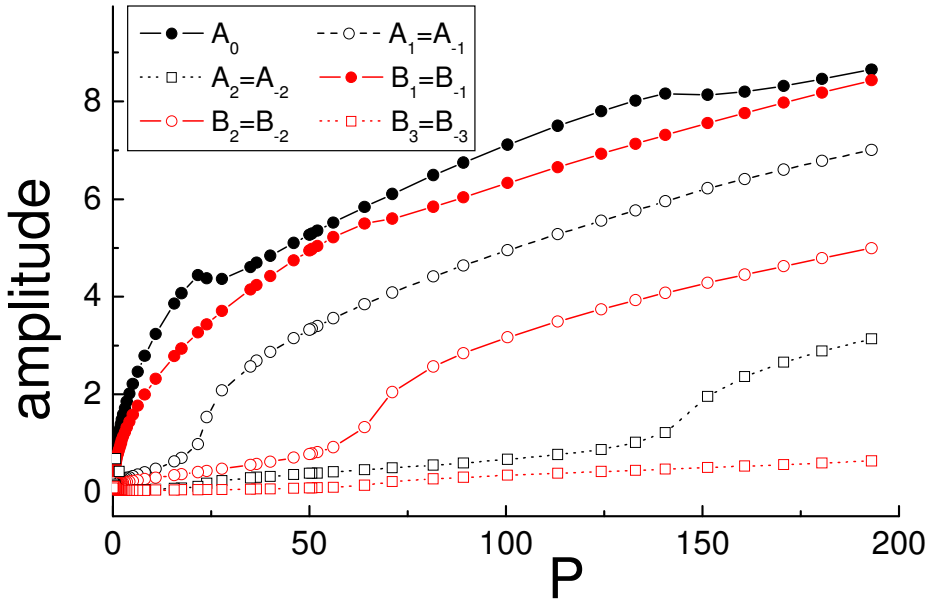

Fig. 6.12 *Cascade mechanism of the saturation (see also Fig. 4.10).*

This means that increasing P does not lead to continuous energy localization into a single lattice element. Instead, the described cascade saturation takes place and suppresses energy localization resulting in the existence of less and less localized modes as P increases.

This explanation indicates the existence of a bounded PN potential with multiple zeros. The numerically obtained PN potential, which is shown in Fig. (6.13), confirms our predictions [174]. A bounded PN potential with multiple zeros ($P_{C1}, P_{C2}, P_{C3}, ...$) is obtained, where the first zero P_{C1} coincides with the analytically predicted value. The other zeros cannot be obtained by the described analytical approach because the approximations for deriving our analytical expressions using Eqs. (6.12), (6.13), (6.16), and (6.17) fail for large values of P.

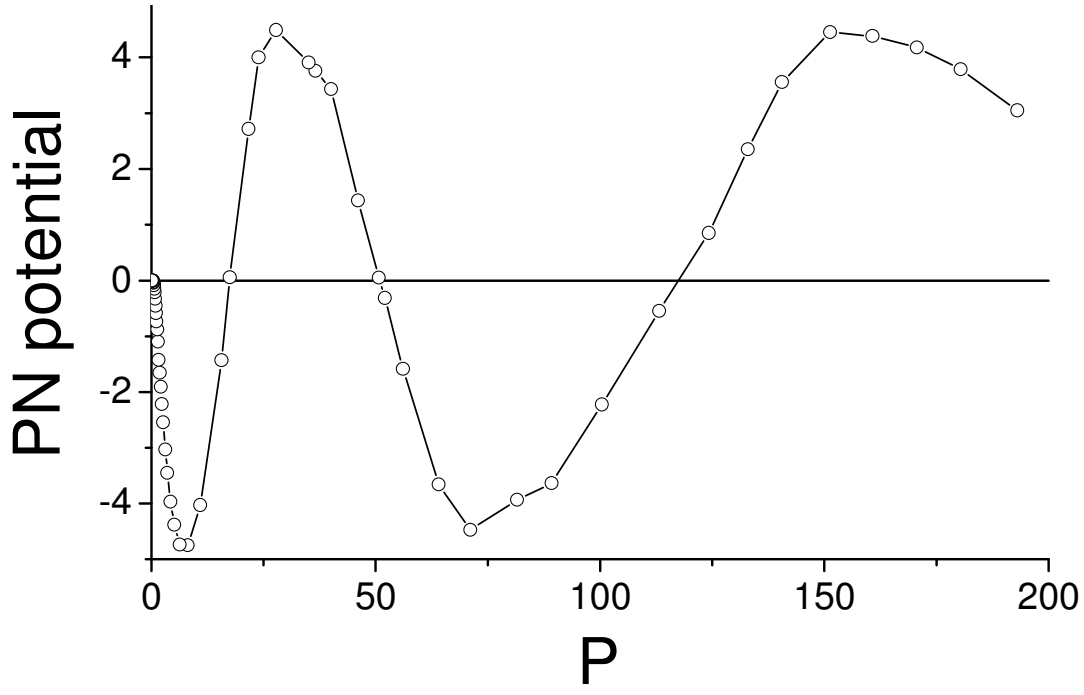

Fig. 6.13 *Numerically estimated dependence of Peierls-Nabarro potential on soliton power P.*

6.3.3 Comparison between theoretical and numerical results

In this paragraph one can see that the obtained analytical results are very well supported with the corresponding numerical results. The approximate results for the power of the unstaggered odd (mode A) and even (mode B) discrete screening solitons are given by Eqs. (6.12) and (6.16). In Fig. 6.14 the comparison of analytical and numerical results of the power dependence of these solitons on the soliton frequency v is presented. The Hamiltonian of these two localized modes is given approximately by Eqs. (6.13) and (6.17). A comparison of analytically and numerically obtained results and their dependence on the soliton frequency v is given in Fig. 6.15.

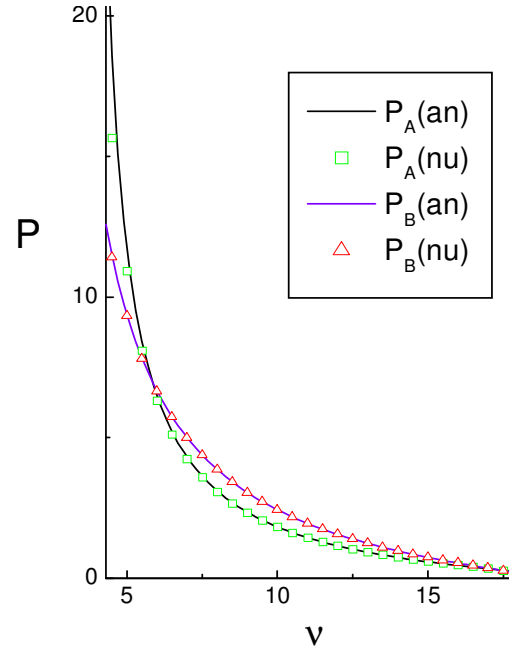

Fig. 6.14 *Comparison of numerically (nu) and analytically (an) obtained power dependence on soliton parameter* ν.

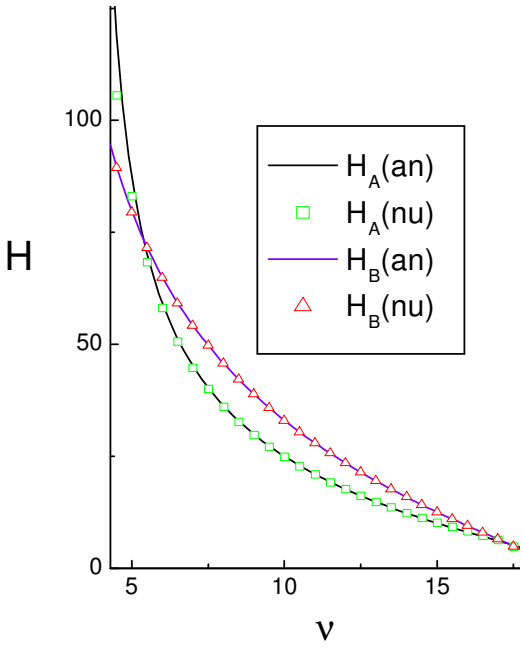

Fig. 6.15 *Comparison of numerically (nu) and analytically (an) obtained dependence of Hamiltonian* H *on soliton parameter* ν.

The analytically and numerically estimated Hamiltonian of these unstaggered discrete screening solitons as a function of the soliton power is presented in Fig. 6.16. Both approaches give almost the same value of the critical power P_{C1}. In Fig. 6.17, where the dependence of the PN potential on the soliton frequency ν is depicted, one may pay attention to the frequency interval ($4<\nu<18$) where both methods are applicable.

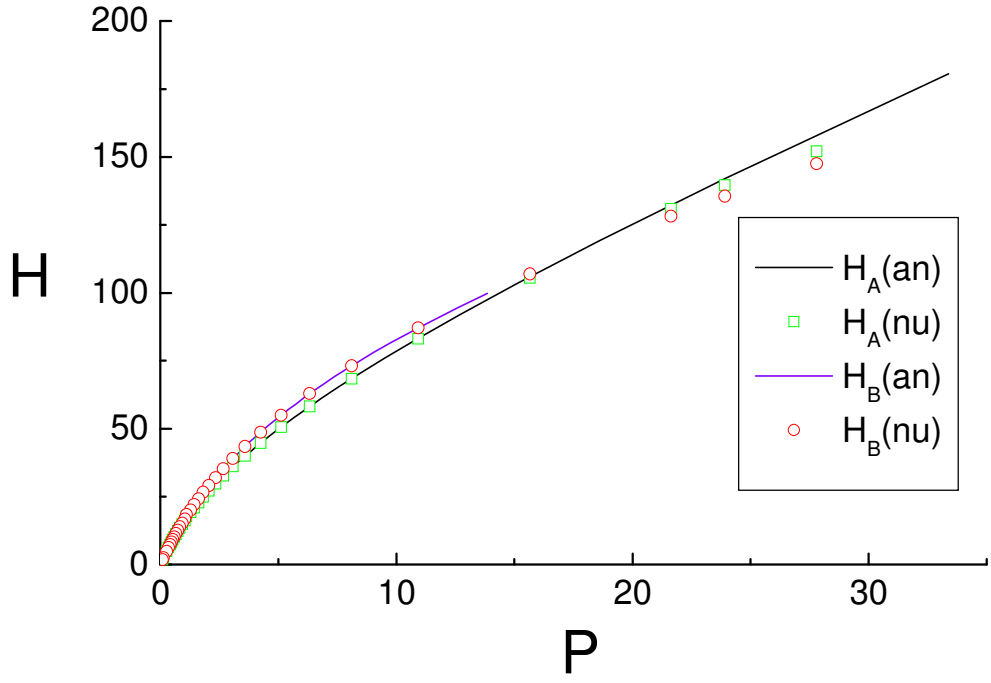

Fig. 6.16 *Analytically and numerically estimated Hamiltonian as a function of power P.*

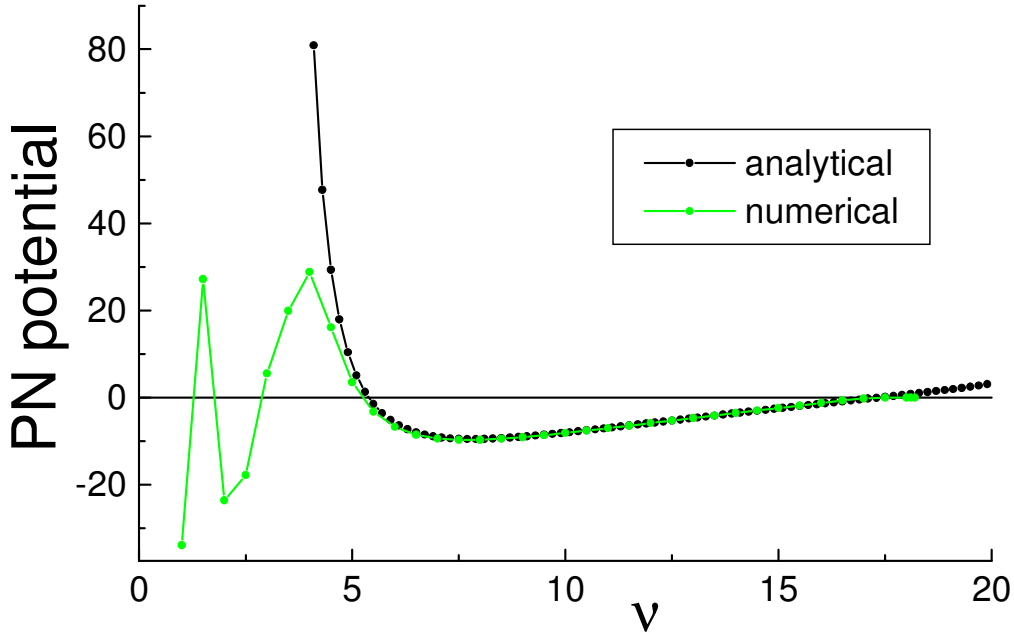

Fig. 6.17 *Comparison of analytically and numerically obtained dependences of Peierls-Nabarro potential on soliton parameter ν.*

Finally, the comparison of analytical and numerical results of the PN potential dependence on soliton power is given in Fig. 6.18. For higher values of the soliton power the approximate solutions, which are given by expressions (4.11) and (4.13), fail.

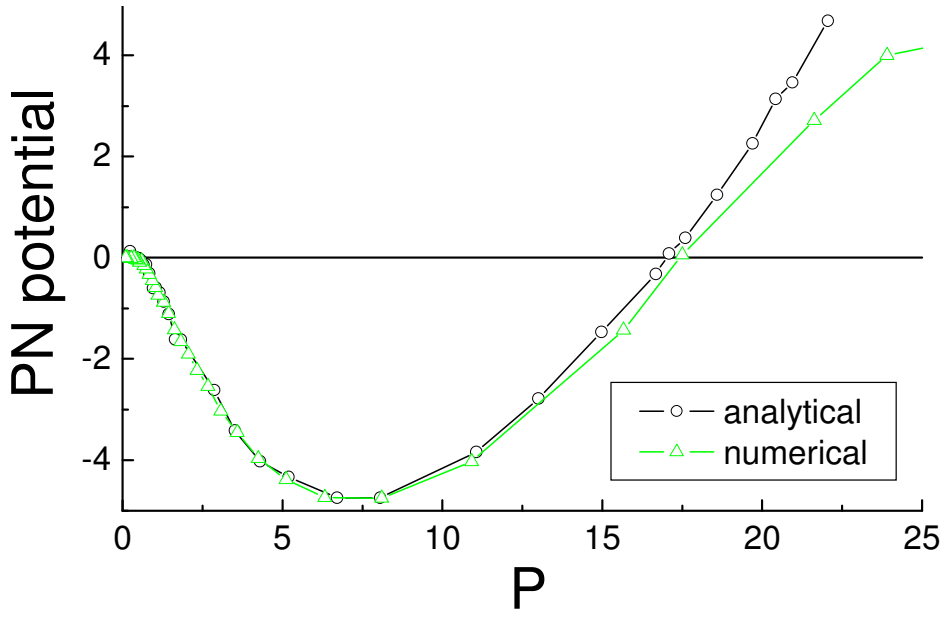

Fig. 6.18 *Comparison of analytically and numerically calculated power dependence of the Peierls-Nabarro potential.*

6.4 PEIERLS-NABARRO POTENTIAL IN DISCRETE SYSTEMS WITH PHOTOVOLTAIC SATURABLE NONLINEARITY

6.4.1 Theoretical results

Discrete photovoltaic solitons (or narrow staggered intrinsically localized modes) can be obtained from the model equation (5.4) by assuming stationary solutions in the form $U_n(\xi) = F f_n \exp(-i\nu\xi + in\pi)$, which results in a set of coupled algebraic equations for the real function f_n [161]:

$$\nu f_n + \frac{1}{2h^2}\left(f_{n+1} + f_{n-1} - 2f_n\right) - \frac{\beta_{PV} F^2 |f_n|^2 f_n}{1 + F^2 |f_n|^2} = 0. \tag{6.20}$$

From these equations one can get many different strongly localized modes, but here only the two simplest types, which are given in Fig. 6.19, are examined. The first one (mode A, or symmetric odd staggered soliton) has a pattern which is given by:

$$U_n^A(\xi) = A(..., f_2^A, -f_1^A, 1, -f_1^A, f_2^A, ...) \exp(-i\nu\xi) \tag{6.21}$$

(see Eq. (6.11)), while the other (mode B, or even staggered soliton) is described by:

$$U_n^B(\xi) = B(..., -f_3^B, f_2^B, -1, 1, -f_2^B, f_3^B, ...) \exp(-i\nu\xi) \tag{6.22}$$

(see also Eq. (6.15)).

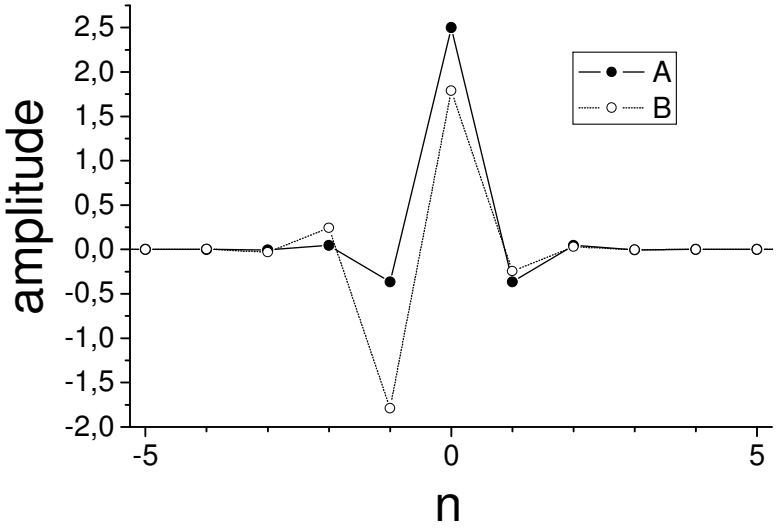

Fig. 6.19 *Odd (A) and even (B) staggered symmetric localized modes in a nonlinear LN waveguide array.*

With the same procedure as above one can get the following approximate results for the total power and the Hamiltonian of the mode A:

$$P_A = A^2 \frac{(\theta-2)^2+1}{(\theta-2)^2-1}, \tag{6.23}$$

$$H_A = \gamma_{PV} P_A - \gamma_{PV} \ln(1+A^2) - 2\gamma_{PV} \ln\left[\prod_{j=1}^{\infty}\left(1+\frac{A^2}{(\theta-2)^{2j}}\right)\right] + 2A^2 \frac{(\theta-1)}{(\theta-3)+1}, \tag{6.24}$$

where $\gamma_{PV} = 2\beta_{PV} h^2$, and, as before, $\theta = 2\nu h^2$, while the square of the soliton amplitude A is defined by:

$$A^2 = \frac{(\theta-2)^2-2}{(\gamma_{PV}+2-\theta)(\theta-2)+2}. \tag{6.25}$$

The corresponding analytical results for the calculated total power P and the Hamiltonian H for mode B are:

$$P_B = 2B^2 \frac{(\theta-2)^2}{(\theta-2)^2-1}, \tag{6.26}$$

$$H_B = \gamma_{PV} P_B - 2\gamma_{PV} \ln\left[\prod_{j=1}^{\infty}\left(1+\frac{B^{2j}}{(\theta-2)^{2(j-1)}}\right)\right] + 2B^2 + 4B^2 \frac{(\theta-2)}{(\theta-3)}, \tag{6.27}$$

with the corresponding square of the soliton amplitude:

$$B^2 = \frac{(\theta-3)(\theta-2)-1}{(\theta-2)(\gamma_{PV}+3-\theta)+1}. \tag{6.28}$$

In Fig. 6.20 the total power of odd and even staggered solitons as a function of the soliton frequency v is presented.

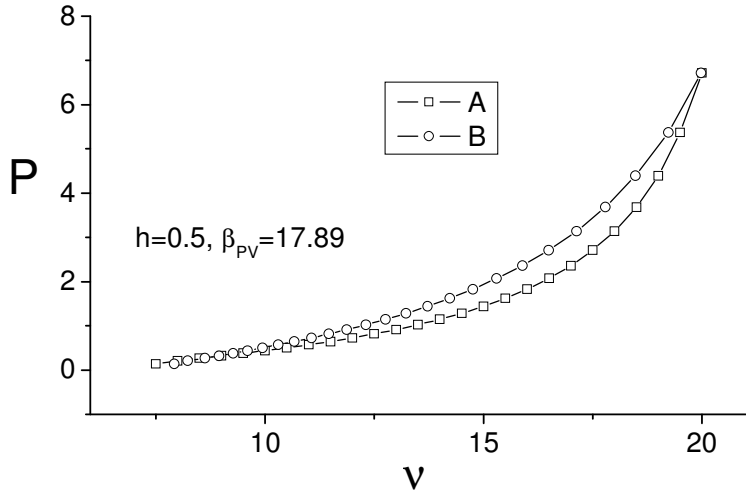

Fig. 6.20 *Analytically obtained* p*ower dependence of staggered localized modes A and B on soliton parameter* ν.

Fig. 6.21 depicts the dependence of the PN potential of these staggered modes A and B on the total soliton power *P*. In a region where the PN potential is positive the odd soliton is more stable, while in regions where this potential is negative the even soliton is more stable (see also Fig. 5.5). Within the DNLS model only the first case exists in literature [107]. Working close to boundaries of these regimes could be fruitful for modelling of new type of optical switch.

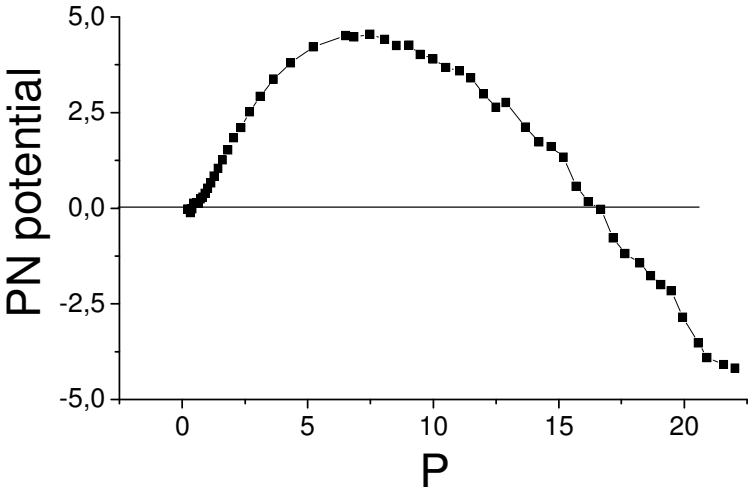

Fig. 6.21 *Analytical dependence of PN potential on soliton power* P *for localized modes A and B. The system parameters are* $h = 0.5$ *and* $\beta_{PV} = 17.89$.

6.4.2 Numerical results

In this section some numerical results about the discrete, symmetric odd and even staggered photovoltaic solitons will be presented. The dependence of total soliton power on soliton

frequency for both symmetric staggered localized modes is depicted in Fig. 6.22. The corresponding system parameters are $h=0.5$, and $\beta_{PV}=17.89$.

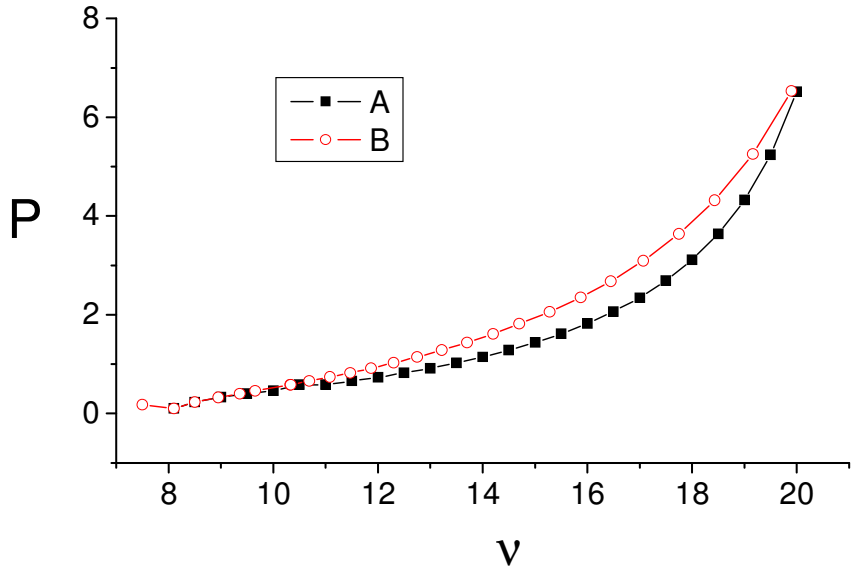

Fig. 6.22 *Power dependence of staggered modes A and B versus soliton frequency ν.*

How the Hamiltonian of these two modes depends on the total soliton power is presented in Fig. 6.23. Only two crossings are observed here, thus the PN potential has two zeros, as can be seen from Fig. 6.24. This behaviour can be explained by different temporal response of modes A and B (which is more inert one, see Fig. 5.7).

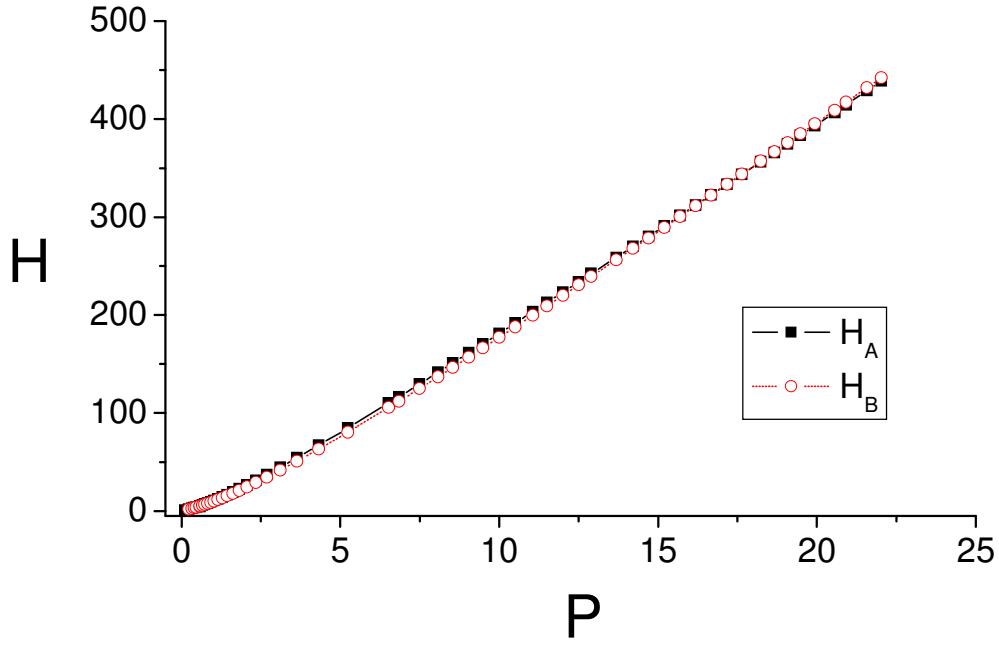

Fig. 6.23 *Hamiltonian of odd and even discrete photovoltaic solitons as a function of the soliton power P.*

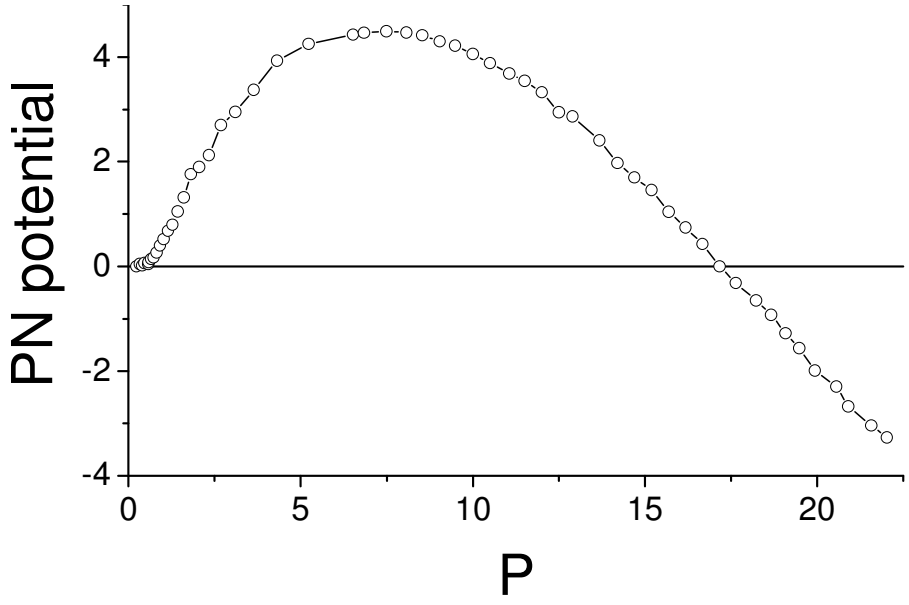

Fig. 6.24 *Dependence of the Peierls-Nabarro potential ΔE_{AB} on soliton power P.*

6.4.3 Comparison between theoretical and numerical results

As in Section 6.3.3, one can see that here the agreement between the analytical and numerical results is very good, too. This is verified in Fig. 6.25, where the corresponding comparison of Eqs. (6.23) and (6.26) is given, and in Fig. 6.26, where the expressions (6.24) and (6.27) are compared analytically and numerically. The system parameters are the same as in Fig. 6.21.

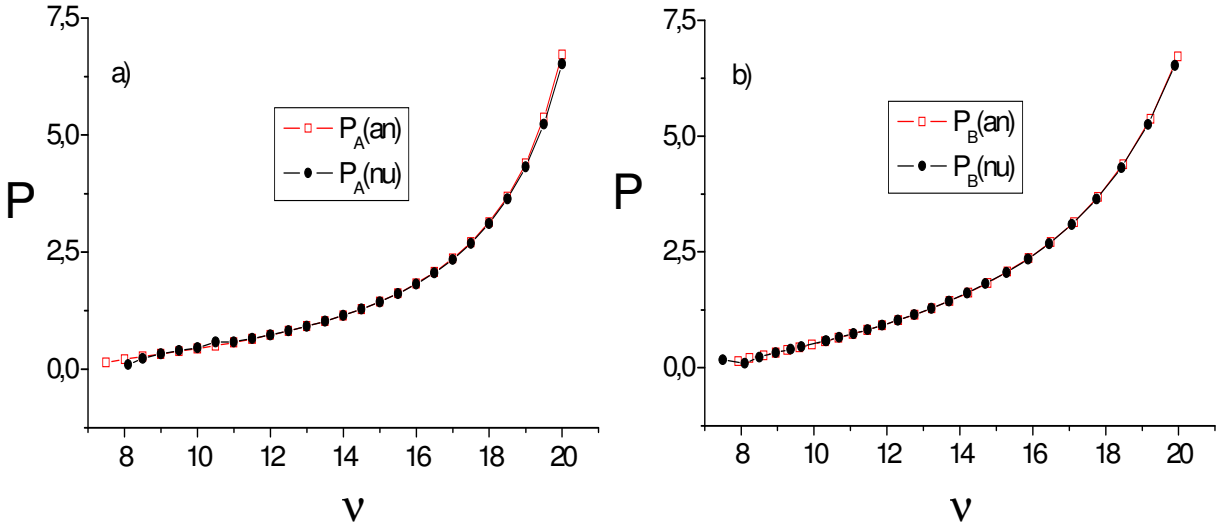

Fig. 6.25 *Dependence of the soliton power on the soliton frequency: comparison of analytics and numerics for a) mode A and b) mode B.*

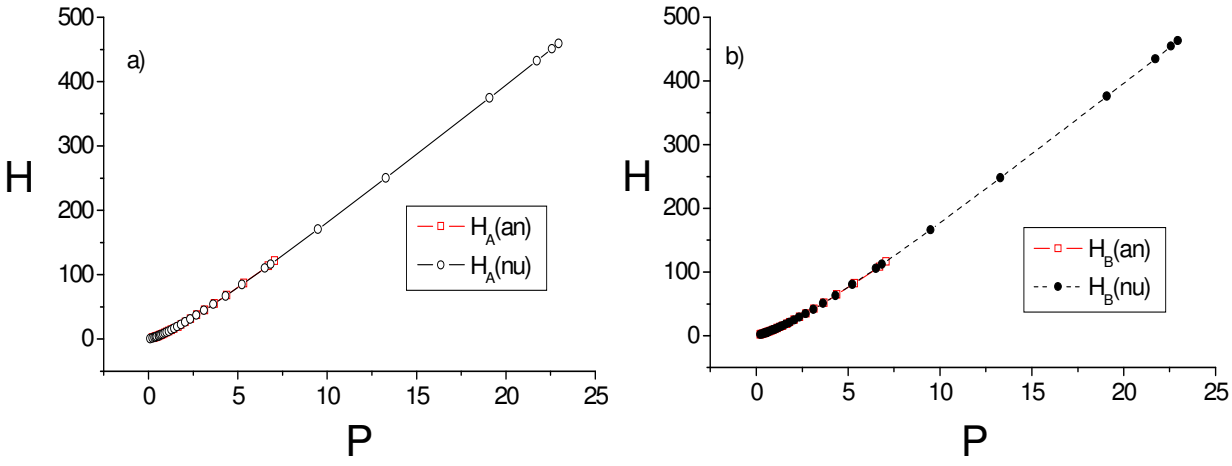

Fig. 6.26 *Comparison of analytically and numerically obtained dependence of the Hamiltonian on the soliton power for a) mode A and b) mode B.*

Collation of analytically and numerically calculated form of PN potential for the values of system parameters as above is shown in Fig. 6.27. Apart from the small difference in region of higher power, the agreement between these results is rather good.

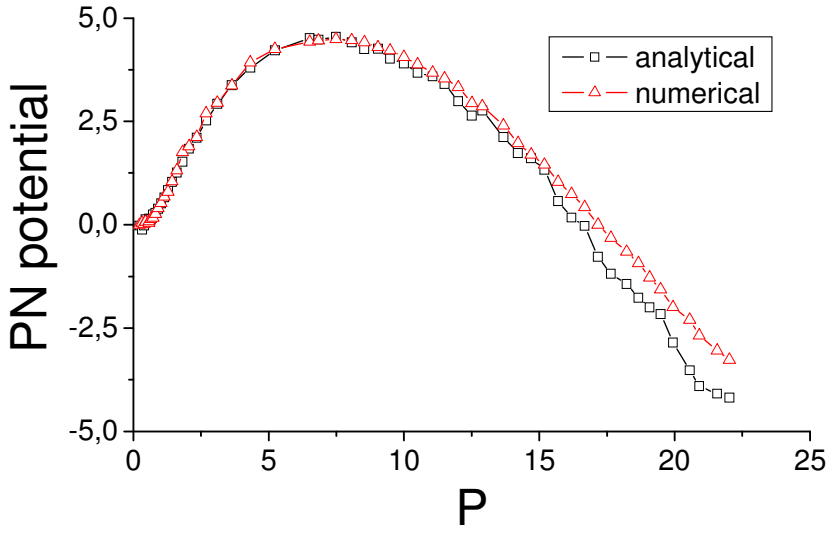

Fig. 6.27 *PN potential of symmetric discrete photovoltaic solitons, analytics vs. numerics.*

6.5 POWER DEPENDENT SWITCHING BETWEEN MODES A AND B

In order to verify our analytical results about the stability of the localized modes A an B, as well as to estimate the influence of the PN potential barrier on the mobility of the solitons across the lattice elements, we have performed a set of numerical simulations of Eqs. (4.1) and (5.4), based on a 6th-order Runge-Kutta procedure with regular checking of the conserved quantities P and H.

In the case of discrete staggered solitons, which have only two zeroes of PN potential, it is possible to observe stable propagation of both localized modes. Numerical simulations reveal that even staggered solitons will always pass spontaneously into the odd staggered solution in region with positive PN potential, as shown in Fig. 6.28a. The opposite spontaneous transition, where mode A converts into mode B, is allowed in regions with negative PN potential, as illustrated in Fig. 6.28b.

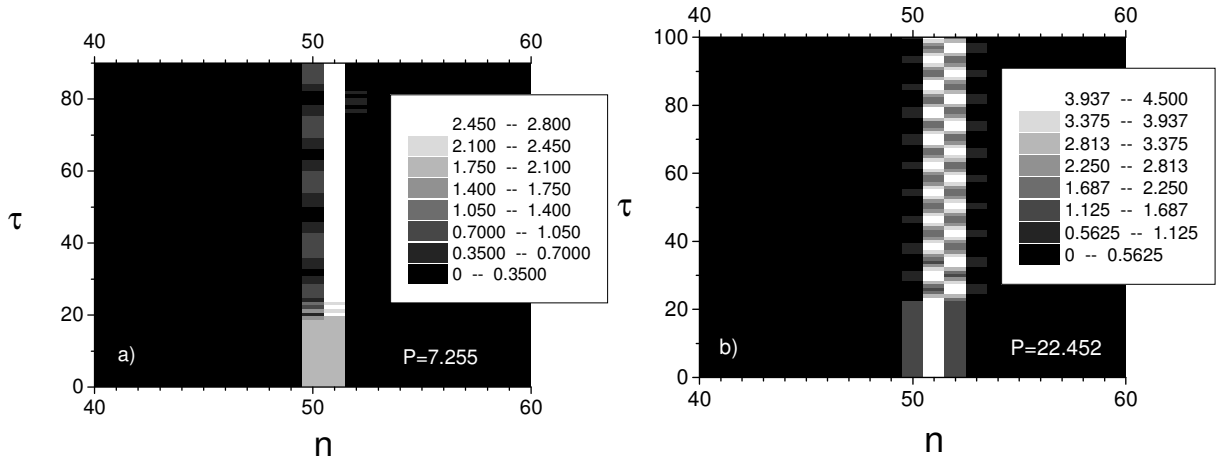

Fig. 6.28 *a) Unstable propagation of even staggered soliton across the nonlinear LN waveguide array in region with positive PN potential, and b) unstable propagation of odd symmetric staggered soliton in region with negative PN potential (top view). System parameters are:* $h = 0.5$, $\beta_{PV} = 17.89$, *and* $N = 101$.

In the case of discrete screening solitons, due to existence of multiple zeroes of the PN potential, the situation is more interesting. But now, in the regions with negative PN potential barrier, it is possible to observe stable propagation of unstaggered mode A, as shown in Fig 6.29a. An additionally applied numerical perturbation does not have any influence on the propagation of this mode. An example of a simulation including perturbations is presented in Fig. 6.29b.

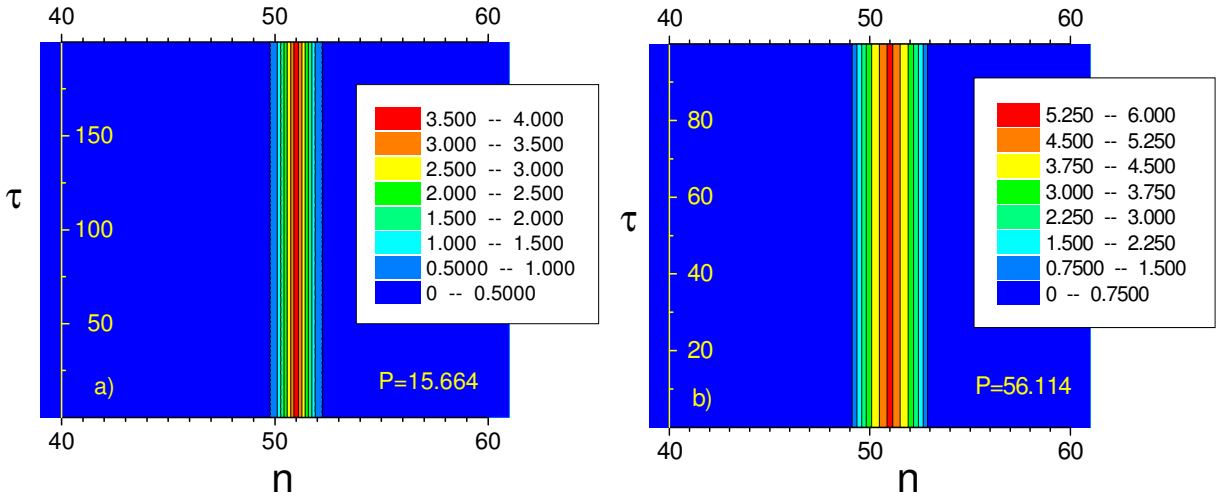

Fig. 6.29 *a) Unperturbed and b) perturbed propagation of unstaggered mode A in regions with a negative PN potential.*

In the region with negative PN potential unstaggered mode B, which has the higher energy when compared to mode A, is unstable and quickly relaxes into the stable mode A. One example of such switching is given in Fig. 6.30, where the parameters $N = 101$ and $\nu = 4$ are used. The process of mode transfer is accompanied with simultaneous pulse amplification.

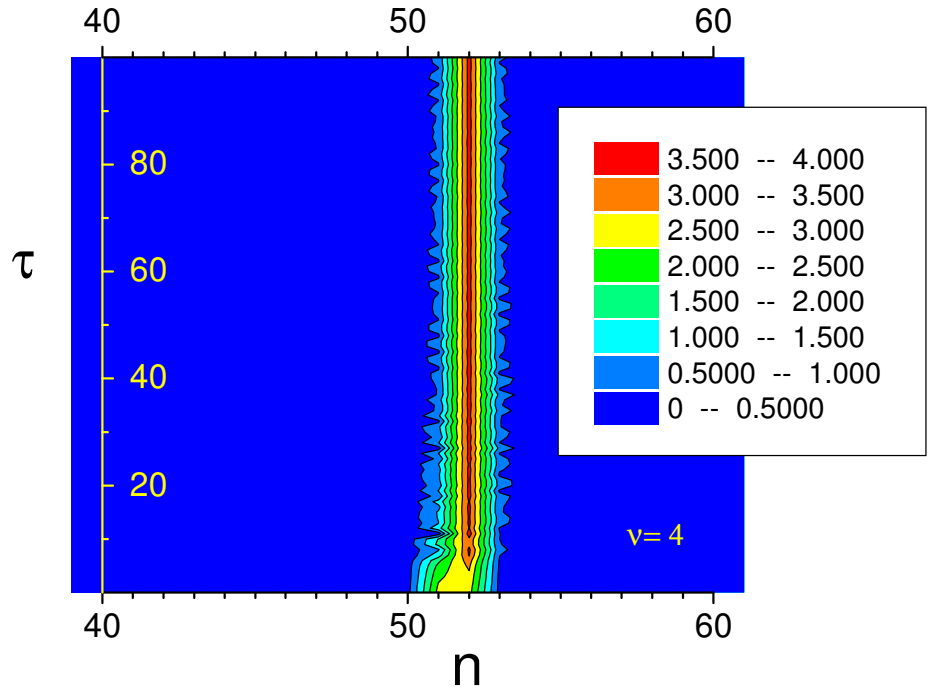

Fig. 6.30 *Unstable propagation of unstaggered mode B in a region where the PN potential is negative.*

On the other hand, in the regions with positive PN potential barrier one might observe a stable propagation of unstaggered mode B. This new phenomenon, which may be utilized for a new class of all-optical switching devices, is presented in Fig. 6.31.

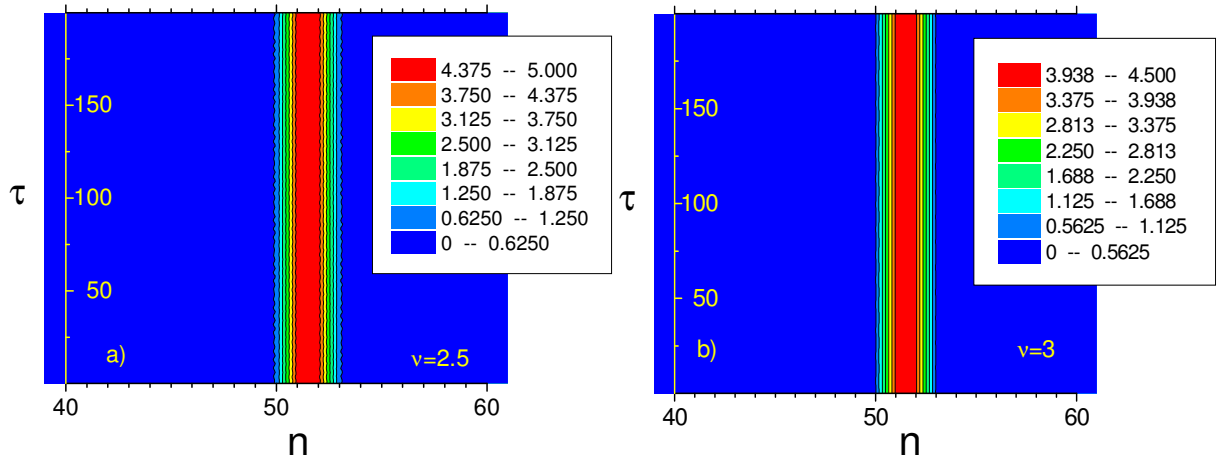

Fig. 6.31 a) *Unperturbed propagation of an even, symmetric unstaggered mode B in a region with positive PN potential.* b) *Propagation of mode B under the influence of perturbations. The soliton parameter ν belongs to the region where the PN barrier is positive.*

In this region with positive PN potential the unstable odd unstaggered mode A quickly relaxes into the stable even mode B. An example of this process, which does not occur in the corresponding system with cubic nonlinearity, is presented in Fig. 6.32.

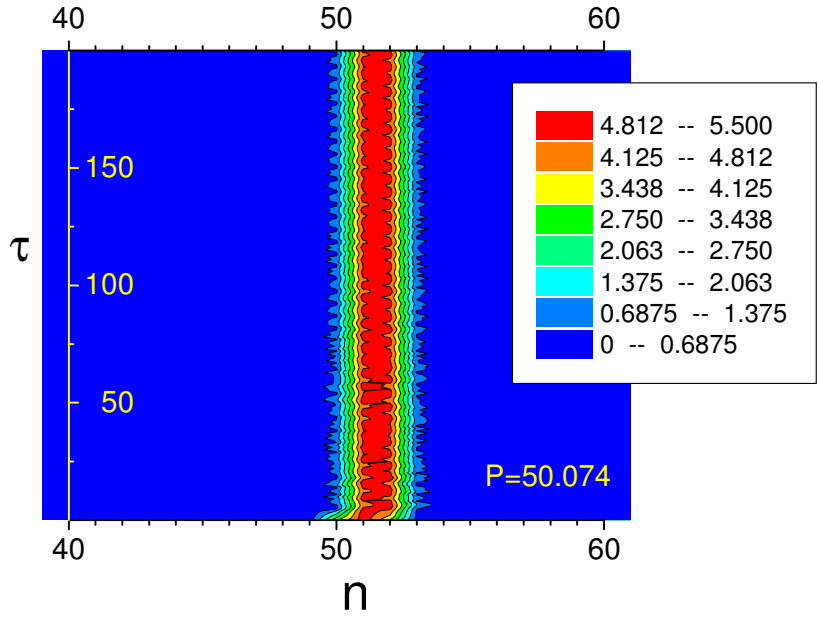

Fig. 6.32 *Transition of the unstable unstaggered mode A into the more stable configuration of mode B in a region with positive PN potential.*

Finally, when the intrinsically localized unstaggered modes A and B have a power equal to the one of the values of critical power (P_{C1}, P_{C2}, P_{C3},…), it is possible to observe stable propagation of both modes.

6.6 STEERING OF DISCRETE SOLITONS

In this section numerical results, concerning beam steering in nonlinear SBN and LN waveguide arrays, will be presented. Up to date, beam steering was investigated only in discrete systems which can be described by virtue of DNLS equation [141-143]. According to the scenario which is described in [145, 166] the modes A and B can be approximately viewed as dynamical states of the same moving localized mode. Therefore, one can expect that the shape of the PN potential strongly affects the power dependent soliton steering across the lattice elements.

The fact that the amplitude of the PN potential barrier in the case of discrete screening solitons is bounded brings the general conclusion that the ability of large power discrete screening solitons to move across the lattice is considerably higher than in the case of DNLS lattices with cubic nonlinearity. These solitons forced to move sideways may propagate or may be trapped inside the potential barrier, thus exhibiting oscillations of the soliton velocity. Moreover, the existence of zeros of the PN potential indicates the possibility for the existence of unlimited soliton steering across the lattice. However, unstaggered localized modes A and B represent pure solitons without internal oscillations but with different self frequencies v_A, v_B for a fixed soliton power P. During the periodic transition of the moving mode through modes A an B, its

frequency oscillates between v_A and v_B. Therefore, the moving modes are not pure solitons but breathers with an additional internal mode of freedom [175-177]. Thus, one can conclude that the PN barrier is only one of the factors influencing the mobility effect.

Discrete screening solitons are numerically forced to move sideways by introduction of a small phase difference offset between adjacent lattice elements. The observed dynamics is complex and strongly depends on both, soliton power and introduced phase offset Φ.

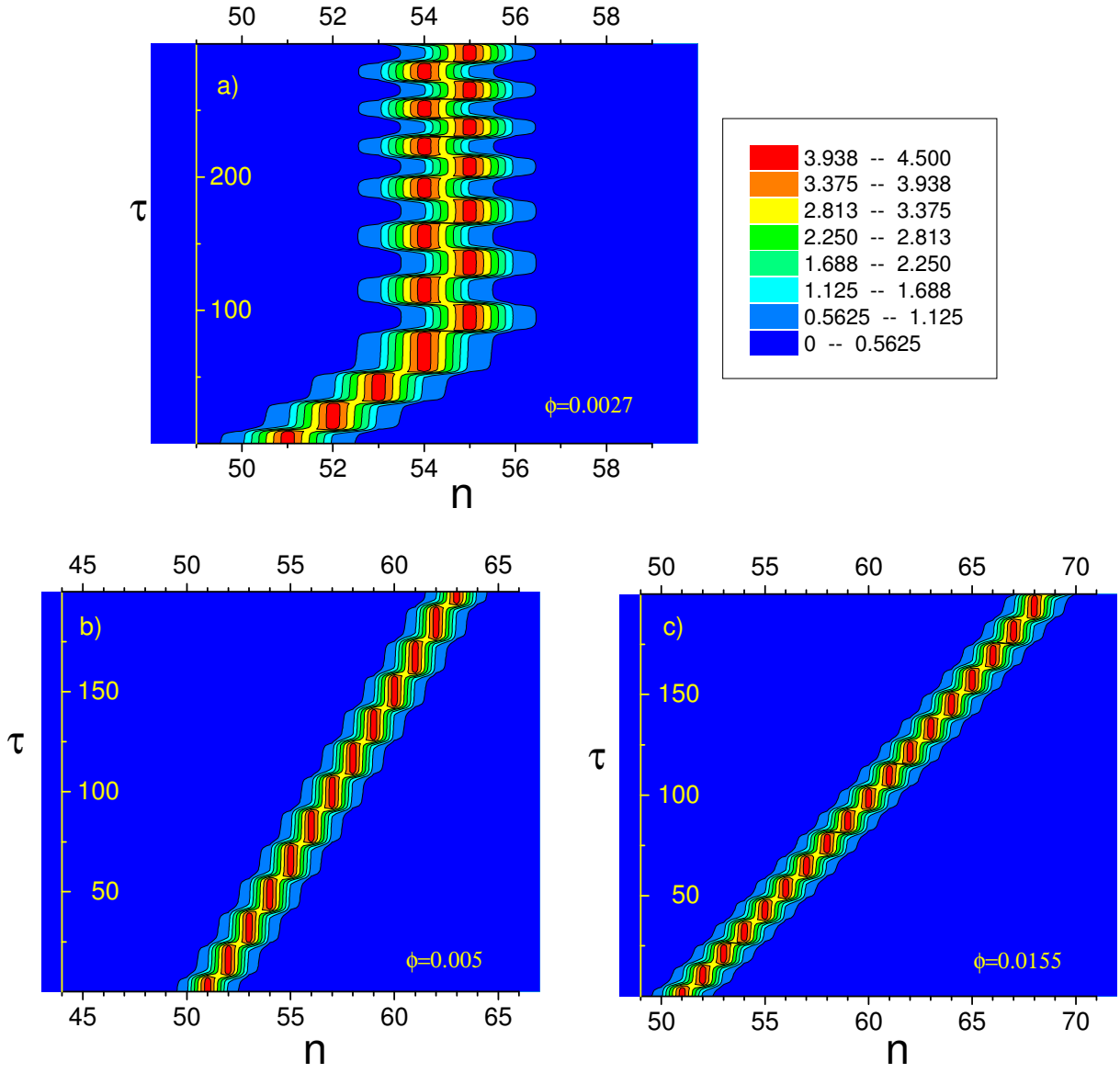

Fig. 6.33 *Illustration of the steering dynamics of discrete odd screening solitons with* $P = 21.63$ *and* $N = 101$, $\beta_{PV} = 18.2$, $h = 0.5$, *that are launched under a small angle into the lattice. Soliton steering is initiated from the unstable mode A with the following initial phase offsets: a)* $\Phi = 0.0027$, *b)* $\Phi = 0.005$, *and c)* $\Phi = 0.0155$.

In general, the results that are shown below confirm the conclusion that a moving mode is a breather as well as the prediction that the PN potential strongly affects its dynamics causing an enhanced mobility of large power discrete screening solitons. Here, in order to illustrate these conclusions, some of the most instructive examples are presented. First, a large power soliton

with $P = 21.63 > P_{C1}$, i.e., a region where unstaggered mode A is unstable and unstaggered mode B is stable (opposite situation than for DNLS lattices with cubic nonlinearity), is launched. Soliton steering is initiated from the unstable mode A by introducing a small phase offset. The introduced phase difference increases the Hamiltonian and as result we get an initial state with the same P but with a Hamiltonian H above the value H_A for the unstable mode A. As a consequence of the conservation of the power and the Hamiltonian, the energy difference is transferred partly into the internal mode of freedom and partly into the kinetic energy enabling soliton steering across the lattice. Figure 6.33a-c demonstrates the propagation of discrete odd screening solitons across the lattice for three different values of the initial phase offset. As can be seen, the soliton with a small initial phase offset (Fig. 6.33a) starts to steer, slows down, and is finally trapped by the potential barrier composing a complex breather type of localized mode, where the energy mainly oscillates between two lattice elements. Solitons with larger initial phase offset propagate across the lattice with a constant transverse velocity (Fig. 6.33b). Further increasing of the initial phase offset induces a weak soliton steering and a larger transverse velocity (Fig. 6.33c). An analogue dynamical behaviour of the unstaggered mode B for the case of a negative PN potential is shown in Fig. 6.34.

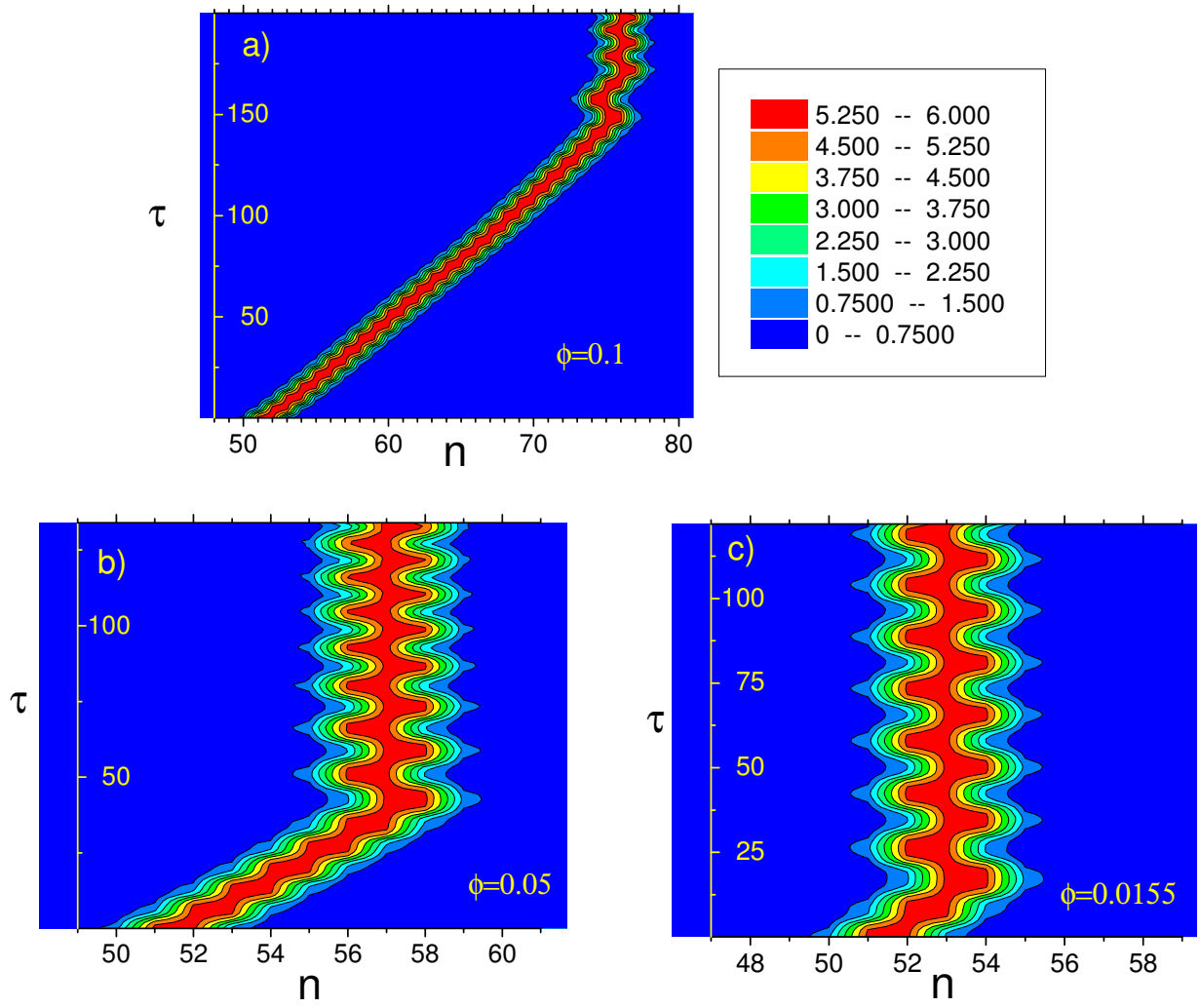

Fig. 6.34 *Illustration of the dynamics of solitons with* $v = 2.1$ *and* $N = 101$, $\beta_{PV} = 18.2$, $h = 0.5$ *that are launched under small angles into the lattice. Soliton steering is initiated from the unstable mode B with the following initial phase offsets: a)* $\Phi = 0.1$, *b)* $\Phi = 0.05$, *and c)* $\Phi = 0.0155$.

Steering of discrete photovoltaic solitons is also investigated within this thesis. By contemplating Fig. 5.5 and Fig. 6.23, where analytically and numerically achieved dependence of the Hamiltonian on the soliton power is presented, one can conclude that here the PN potential is rather small for almost any values of the power *P*. Thus, it should be quite easy to initiate steering of both symmetric staggered modes across the nonlinear LN waveguide array. In the thesis only some numerical results from a low-power region are exposed in Fig.6.35 and Fig. 6.36. An input in the form of an either even (Fig. 6.35) or odd (Fig. 6.36) staggered soliton, with small power $P<0.5$ and having a linear-phase gradient in the transverse plane (i.e. phase tilt), can excite moving odd breathers, which propagate at an angle to the waveguides. The propagation angle is higher for higher phase tilts (see Fig. 6.35b, c).

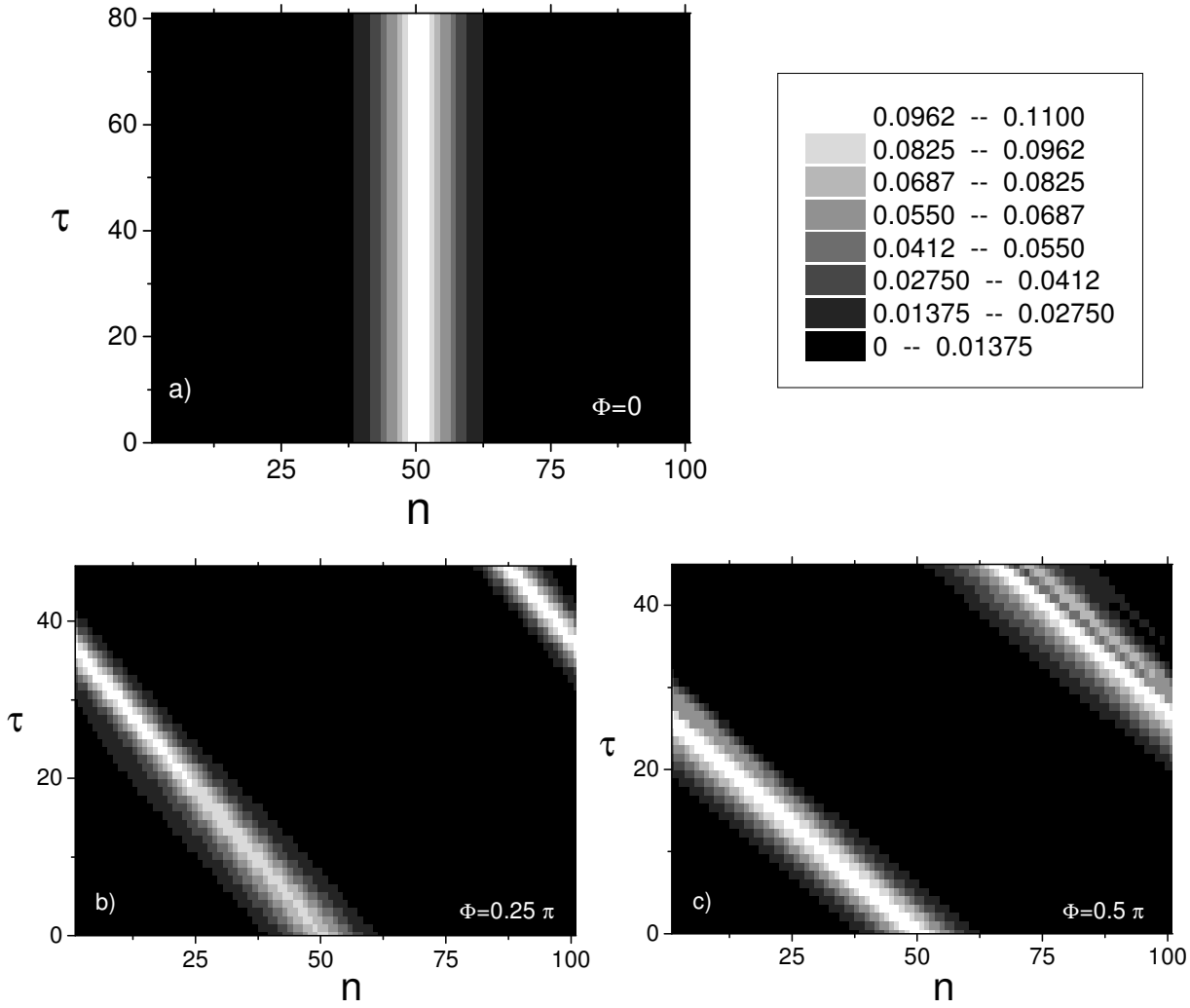

Fig. 6.35 *Steering of the even discrete photovoltaic soliton with* $P=0.1$ *as a function of the relative phase offset* Φ*: a) stable propagation for* $\Phi=0$*, b) moving breather for* $\Phi=0.25\pi$*, and c) moving breather faster than the previous one for* $\Phi=0.5\pi$*.*

As the power of discrete staggered soliton is increased, the direction of propagation may change and, finally, when the soliton can not overcome the PN potential, it is trapped on one of the waveguides as in the example in Fig. 6.36b. Odd modes with higher power are stable with respect to a transversal translational shift [161].

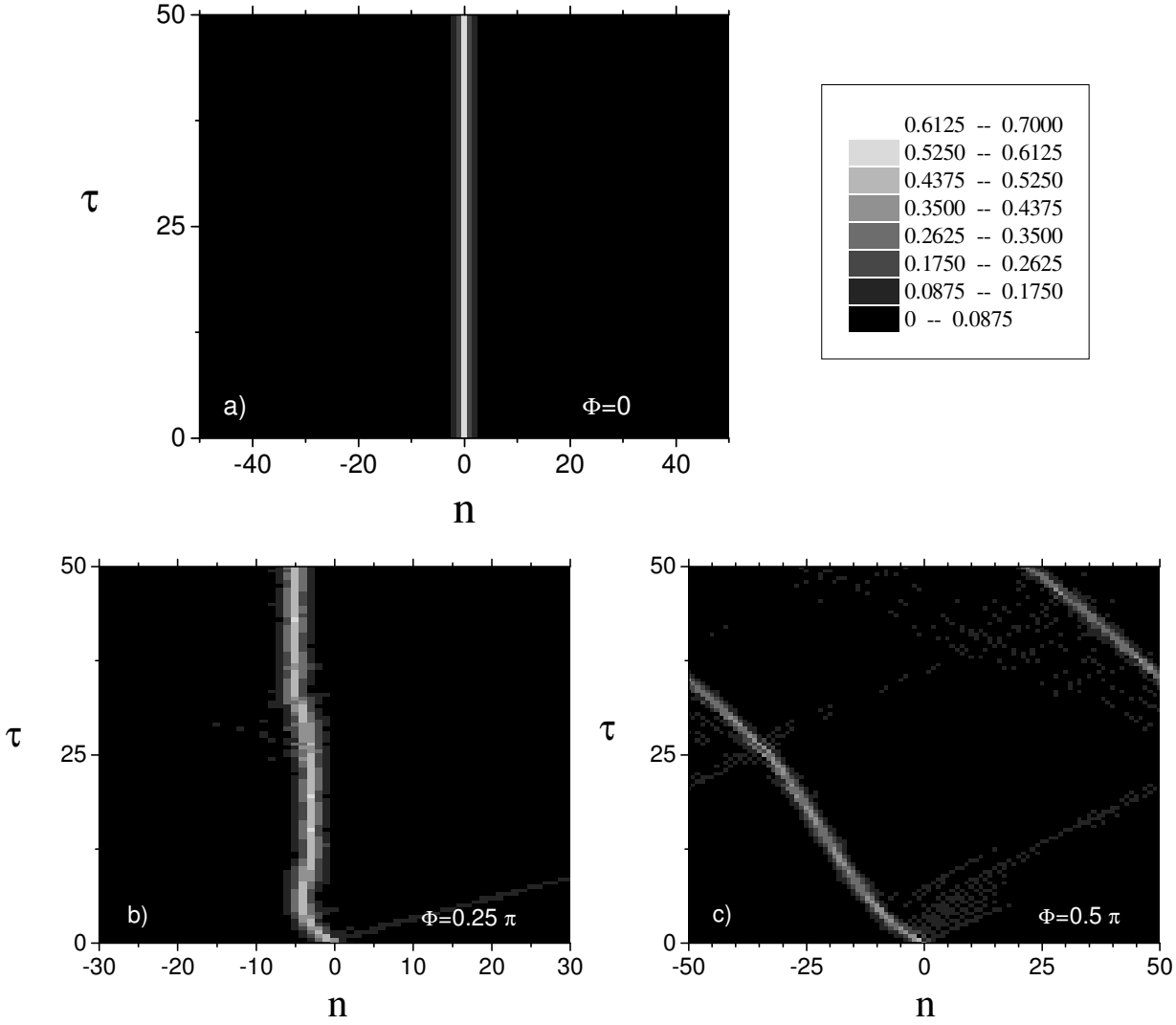

Fig. 6.36 *Steering of odd symmetric staggered soliton with P = 0.582 as a function of the relative phase offset Φ: a) straightforward propagation, b) trapping, and c) free propagation across the lattice.*

6.7 INTERACTIONS OF DISCRETE SOLITONS

Collisions of solitary waves are an important problem both mathematically and physically. For example, in a wavelength-division multiplexing system (which is a popular technology in fiber communication systems) optical pulses in different frequency channels collide with each other all the time [178]. Usually, as the problem of soliton interactions is sufficiently complex, it is necessary to apply detailed numerical calculations for predictions. These interactions of solitons can be divided in two main classes: coherent and incoherent. In photorefractive waveguides [179-182] and optical fibres [183-184] collisions are being used to achieve instant beam steering and signal control, respectively. More information about soliton interactions can be found, for instance, in a recent review paper by Stegeman and Segev [54]. Till now collisions between discrete solitons are investigated only in media with quadratic [185] and cubic nonlinearity [141, 186-188]. Depending on the initial distance between two solitons, their

amplitudes, and their phase difference, soliton fusion, repulsion as well as quasi-elastic collisions are observed.

In this thesis collisions between either two odd or two even, unstaggered discrete solitons are numerically investigated. An example of bright, odd solitons fusion is given in Fig. 6.37. Here two unstaggered solitons that propagate under symmetric angles of different sign inside the lattice fuse together and form a single soliton.

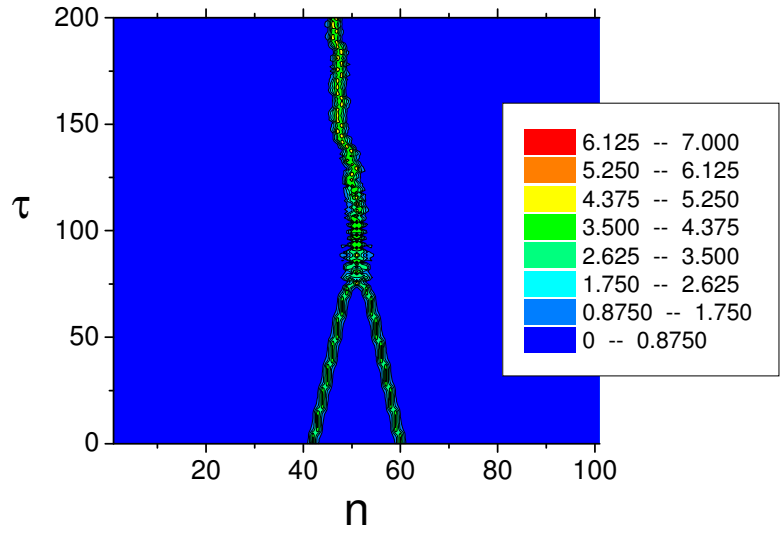

Fig. 6.37 *Fusion of two unstaggered solitons centred on sites with* $n = 42$ *and* $n = 60$*. The initial value of the amplitude of the solitons is* $A = 4.439$*, while the initial phases are* $\Phi = \pm 0.0155$*, respectively.*

In Fig. 6.38 one might see some possible results of the interaction of even, symmetric, unstaggered bright solitons. In part a), which depicts a soliton fusion after multiple collisions, a quite similar behaviour is observed as the one reported in [187]. In parts b) and c) where the symmetric phase offset of the beams has been increased, elastic collisions of the two solitons are observed. These results may be experimentally verified using waveguide lattices fabricated in photorefractive crystals like strontium-barium niobate SBN61 soon.

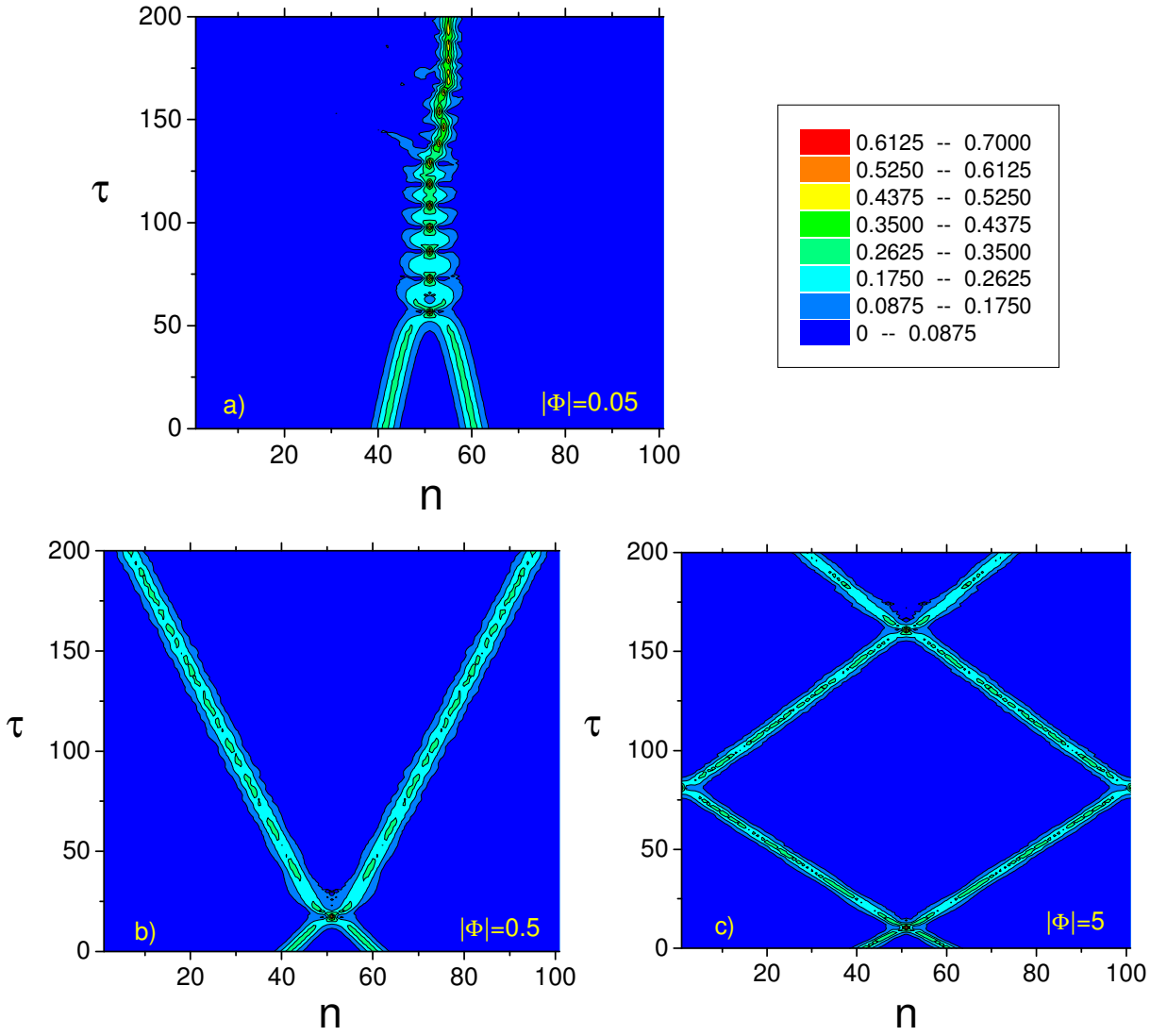

Fig. 6.38 *Interactions of even unstaggered solitons in a nonlinear waveguide array with* $N = 101$ *elements that are launched with symmetric phase offsets* $\pm\Phi$. *The solitons are initially centred between elements with* $n = 41–42$ *and* $n = 60–61$, *while the soliton amplitude is* $B = 0.276$. *a) Fusion of discrete solitons with the* $\Phi = \pm 0.05$ *after multiple collisions, and elastic interaction of discrete solitons with b)* $\Phi = \pm 0.5$ *and c)* $\Phi = \pm 5$.

7. FIRST EXPERIMENTAL RESULTS

At the beginning of this Chapter the fabrication procedure of nonlinear waveguide arrays in photorefractive lithium niobate and strontium-barium niobate crystals is briefly explained. Then the used experimental setup is described and, finally, results which confirm the effects of discrete diffraction, diffraction-less propagation, self-focusing, self defocusing, and steering of symmetric odd staggered solitons in nonlinear lithium niobate waveguide arrays are presented.

7.1 CHANNEL WAVEGUIDE PREPARATION

7.1.1 Lithium niobate

Single-crystalline lithium niobate ($LiNbO_3$) is probably the most frequently used electro-optic material for investigations of photorefractive phenomena. It can be grown up to a length of tens of centimeters and with diameters up to four inches. This crystal has excellent optical properties, rather high electro-optic coefficients, and good mechanical and chemical resistance. At the same time, crystals are available in wafer form for rather moderate cost. On the one hand, $LiNbO_3$ substrates allow for the relatively easy formation of high-quality low-loss optical waveguides, which makes this material a preferred candidate for new nonlinear and electro-optic components in integrated optics. On the other hand, the photorefractive properties of $LiNbO_3$ crystals can be tailored in a wide range by additional doping with impurities like iron, copper, or manganese. Such doped crystals are of considerable interest for applications that use the photorefractive effect of the material, like optical phase conjugation by four-wave mixing, or volume holographic storage.

For the experimental confirmation of our results on discrete solitons in materials with saturable nonlinearity, photorefractive waveguide arrays have been fabricated in $LiNbO_3$. Up to date, there are a few well-developed methods for the fabrication of waveguides in $LiNbO_3$, such as ion exchange, ion implantation, ion in-diffusion, and thin film deposition [155]. Experimental results, which represent the core of this Chapter, are obtained from titanium in-diffused waveguides in samples that have been additionally diffusion-doped with copper.

The corresponding fabrication procedure is as follows. Before forming waveguide arrays in $LiNbO_3$ wafers, one has to perform either iron or copper doping. This is necessary in order to increase the photorefractive response of the material and thus the value of the nonlinearity in $LiNbO_3$. The diffusion coefficient of copper ions in $LiNbO_3$ is much larger than that of iron ions, thus allowing for shorter diffusion times. On the other hand, the surface roughness of the wafers may be increased because of copper ions that are diffused into $LiNbO_3$, while this effect is almost absent for iron in-diffusion. As a consequence, copper ions are diffused into the whole wafer that has a thickness of 1 mm from the back-side, while iron ions are diffused into $LiNbO_3$ from the waveguide surface for a depth of only 20 μm (width of the Gaussian diffusion profile). In our experiments x-cut crystal wafers of sizes 1 mm × 7.8 mm × (10 – 25) mm are used. First copper layers with a thickness of (5 – 50) nm are deposited onto the surface of the substrate using thermal evaporation. These layers act as a finite diffusion source and are in-diffused for (24 – 30) hours at 1000 °C in a wet argon atmosphere. In this way the doping levels range from $(5 - 50) \times 10^{24}$ m^{-3}. Similarly, the alternative in-diffusion of several

nanometers-thick iron layers for (20 – 40) hours at 1000 °C may form a 10–30 µm-thick doped substrate with iron concentrations of (5 – 70) $\times 10^{24}$ m^{-3}.

Then, lithographic techniques are used to pattern the titanium film into narrow stripes with widths of (3 – 4) µm and separations of (2.2 – 4.4) µm. First, a titanium layer with a typical thickness of 10 nm is deposited onto the polished surface using electron beam evaporation. The titanium in-diffusion is performed for 2 hours at a temperature of 1000 °C in air. In this way single mode waveguides with low losses (less than 1 dB/cm) are formed for both TE and TM modes. The photographs of a few single-mode $LiNbO_3$:Ti:Fe and $LiNbO_3$:Ti:Cu waveguides are shown in Fig. 7.1.

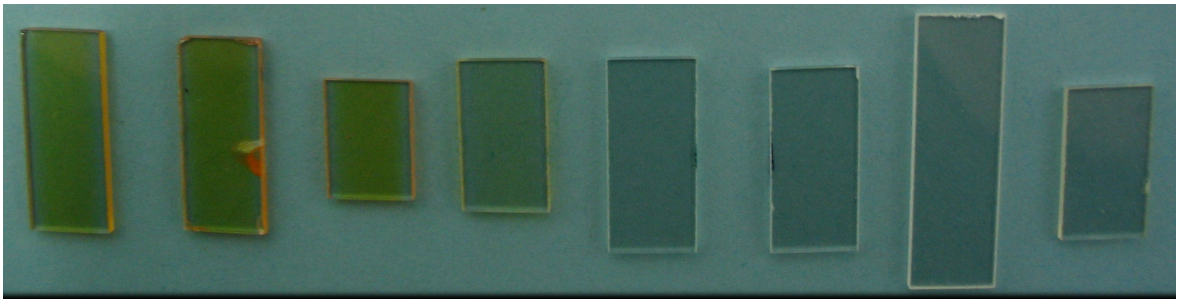

Fig. 7.1 *$LiNbO_3$:Ti:Cu (yellow) and $LiNbO_3$:Ti:Fe (transparent) waveguides.*

7.1.2 Strontium-barium niobate

Much faster but, unfortunately, more expensive photorefractive crystals than lithium niobate are strontium-barium niobate crystals (SBN, $Sr_y Ba_{1-y} Nb_2O_6$, where $0.25 \leq y \leq 0.75$). The most utilized crystal compositions among them are those of the congruently melting composition with $y=0.61$, or samples with $y=0.75$, which have a very high electrooptic tensor element r_{33} of about 1400 pm/V [189]. Although the congruently melting composition has smaller electrooptic coefficients of about r_{33} = 280 pm/V, SBN61 possesses still values that are about ten times larger than in case of $LiNbO_3$. SBN crystals also have a high photorefractive sensitivity, which is artificially increased by suitable doping with, e.g., rhodium, cerium, or chromium [190].

Waveguide formation in SBN crystals can be performed by virtue of sulphur or zinc in-diffusion, the static strain-optic effect, proton and helium ion implantation, and thin layers can be also prepared by sputtering (pulsed laser deposition). Samples that may be used for future investigations following the predictions of this thesis are currently fabricated by helium ion implantation and by using the strain-optic effect.

7.2 DISCRETE DIFFRACTION

The experimental setup that is used in this thesis is sketched in Fig. 7.2. The green light of an argon ion laser ($\lambda_0 = 514.5$ nm) is divided into two beams by virtue of a Mach-Zehnder interferometer, where the optical power can be controlled by a combination of polarizer and half-wave plate. The two beams of equal power are overlapped under a small angle and are

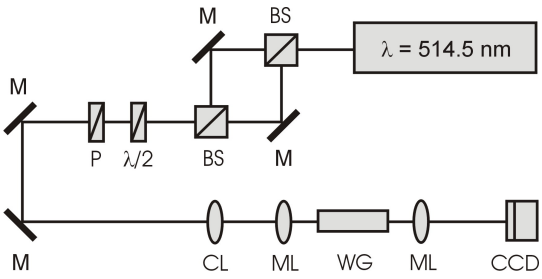

Fig. 7.2 *Experimental setup. BS's, beam splitters; M's, mirrors; λ/2, half wave plate; P, polarizer; CL, cylindrical lens; ML's, microscope lenses; WG, waveguide array; CCD, CCD camera.*

coupled into the waveguide array using a 40× microscope lens. A cylindrical lens forms the elliptical shape of the input light beam to optimize the in-coupling efficiency. A 20× or 10× microscope lens collects the light from the other facet of the crystal. A CCD camera system serves for monitoring of the intensity distribution on the rear face of the array. A personal computer is connected to the CCD, which collects and analyzes the experimental data.

The argon ion laser can also work in the blue light regime, which will be an advantage for the planned experiments with SBN crystals. Beside the Runge-Kutta method (compare with Fig. 5.2) the pulse propagation in the $LiNbO_3$ waveguide array is also simulated by a program based on BPM (beam propagation method). Fig. 7.3 shows the simulation result when a 35 µm-broad beam is launched into a $LiNbO_3$ waveguide array with a propagation length of 17 mm. Here the channel width is 4 µm and the separation between the adjacent channels is 3.6 µm. In the inset the corresponding experimental result is presented, and the corresponding intensity distribution measured at the rear side of the waveguides array is given in Fig. 7.4.

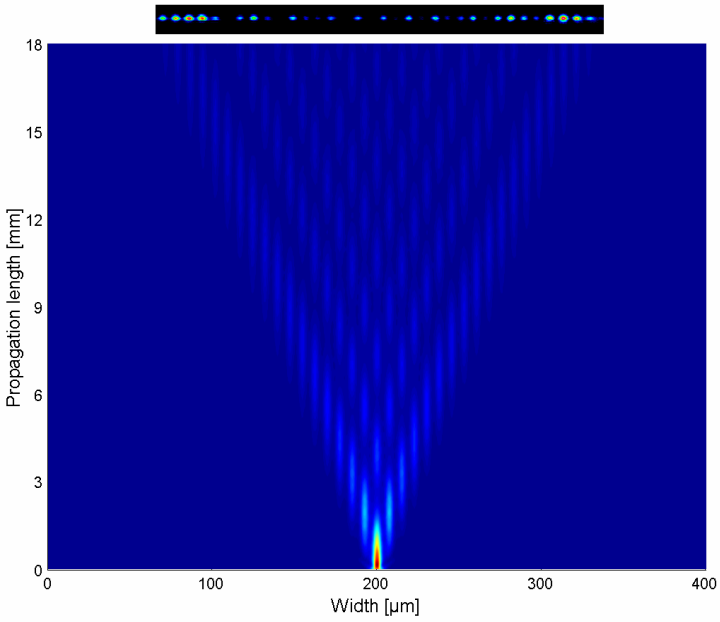

Fig. 7.3 *Comparison between numerically and experimentally obtained results of the discrete diffraction in $LiNbO_3$ waveguides array.*

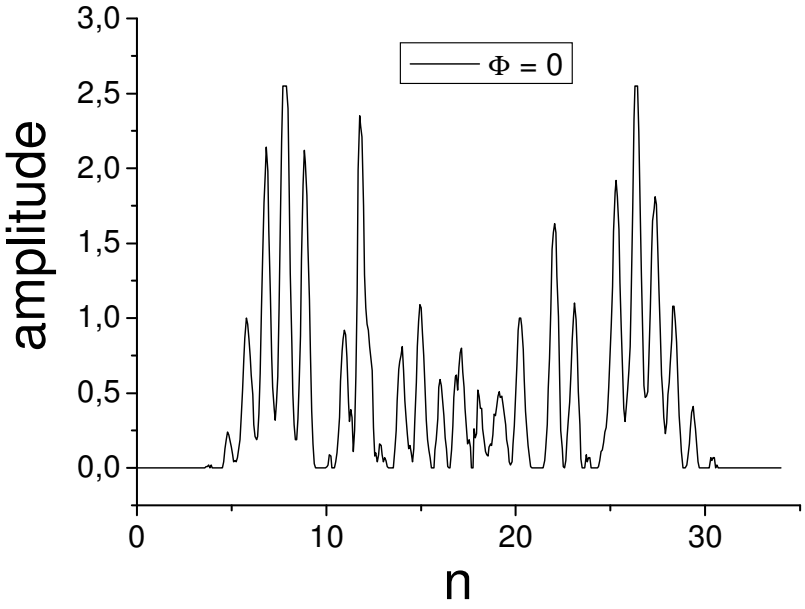

Fig. 7.4 *Intensity distribution (in arbitrary units) at the end facet of the crystal (see Fig.* 7.3*).*

As mentioned in Paragraph 3.1, when the wave front propagates under the angles with a Bloch momentum $| k_x d | \leq \pi$ the discrete diffraction vanishes. Fig. 7.5 shows the photographs from the output facet of the waveguide arrays for discrete diffraction ($k_x d \approx 0$) and for $k_x d$ close but little smaller than $\pm \pi$. As one can see, the beam widths of (b) and (c) are much less than that of (a). It is obvious that the experimental result, which is given in Fig. 7.5c, is quite similar to the corresponding numerical result, which is presented in Fig. 5.2. Neither numerically nor experimentally a pure diffraction-less propagation (compare these results with Fig. 1c from Ref. [76]) could be obtained. The corresponding intensity distribution is presented in Fig. 7.6.

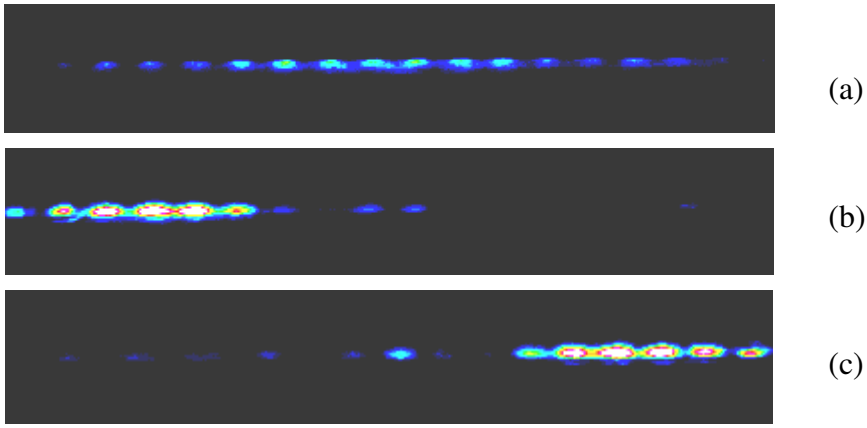

Fig. 7.5 *a) Discrete diffraction ($k_x d \approx 0$), and b-c) diffraction-less propagation $k_x d$ close but smaller than $\pm \pi$. See also Fig.* 3.1*b.*

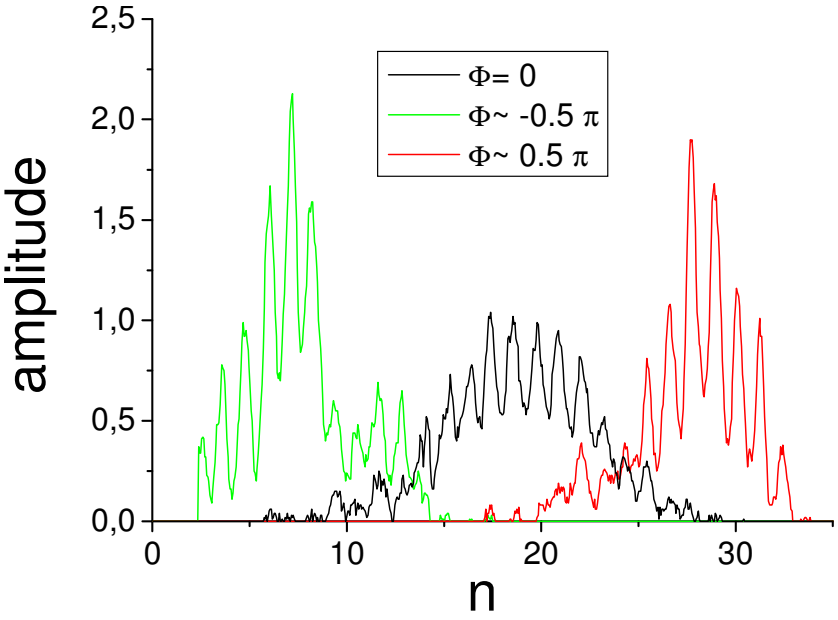

Fig. 7.6 *Intensity distribution at the end facet of the crystal (see Fig. 7.5).*

7.3 FORMATION OF DISCRETE PHOTOVOLTAIC SOLITONS

As suggested in [72], in nonlinear waveguide arrays, due to their periodical dispersion relation, it is possible to observe both, self-focusing and self-defocusing effects, by simple change of the input angle of the beam. These results are experimentally verified in our $LiNbO_3$ channel waveguides and a typical example is presented in Fig. 7.7. Here the initial pulse is given in (a), linear regime and the discrete diffraction is shown in (b), while (c) and (d) illustrate the nonlinear self-defocusing and self-focusing.

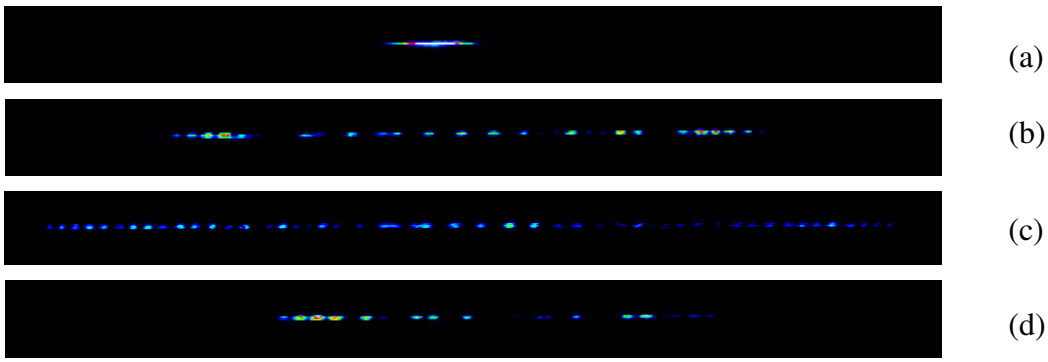

Fig. 7.7 *Comparison of (a) initial input beam, (b) discrete diffraction, (c) self-defocusing, and (d) self-focusing images.*

As indicated in (c) and (d), nonlinear self-defocusing and self-focusing are observed at higher powers when the beam is launched into the waveguide arrays normally ($k_x d \approx 0$) or tilted by a small angle of about 1.5° with respect to the normal direction ($\pi/2 < k_x d < \pi$).

Bright discrete soliton-like structure formation in Cu-doped nonlinear $LiNbO_3$ waveguide arrays is presented in Fig. 7.8. Here the used waveguide array is 17 mm long while the waveguide width and waveguides separation are 4 μm and 4.4 μm, respectively. A focused laser beam with a width of 5 μm is launched into the array with normal propagation direction. At low input power (about 5 μW, measured in front of the input lens) a linear behavior is demonstrated. By increasing the power of the light to about 200 μW, which corresponds to a power of about 10 μW inside the waveguides, a nonlinear behavior is observed. The output beam becomes narrower and narrower, until a discrete soliton-like structure forms after 230 min. We also investigate the case of higher light power up to 500 μW (25 μW in the waveguides) before the input lens. In this case the formation time for discrete soliton-like structures is decreased to about 120 min.

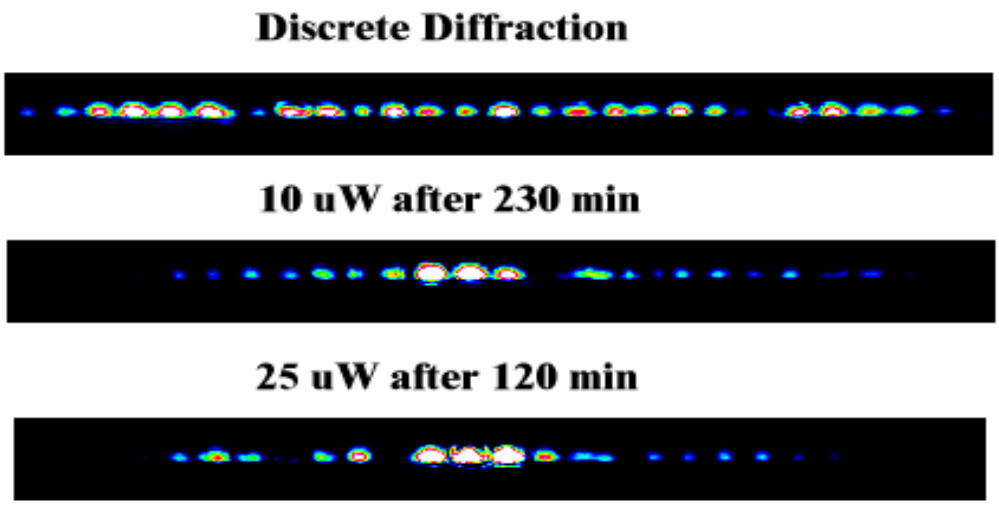

Fig. 7.8 *Discrete bright soliton-like structure formation in Cu-doped $LiNbO_3$ waveguide arrays.*

7.4 STEERING OF THE ODD SYMMETRIC DISCRETE PHOTOVOLTAIC SOLITONS

In this section experimental results which confirm the steering effect of symmetric odd staggered solitons are presented [160]. The used sample was 18 mm long and additionally doped by copper in-diffusion with a concentration of 5×10^{24} m^{-3} [193]. The distance between the adjacent channels in this sample is 3.6 μm while the width of the single mode channel waveguides is 4 μm. The grating period of the interference pattern of two beams of the equal power is carefully adjusted to match the inter-waveguide distance of the array. In this way a staggered input pattern, that consists of a central maximum and two first neighbours which are out of phase relative to the center, is obtained.

Both linear and nonlinear light propagation in the waveguide array is shown for an input power of about 4 μW in Fig. 7.9. Because the sample has a rather large time constant, linear wave propagation can be observed immediately after switching on the input beams in Fig. 7.9b. This profile, which represents the regime of discrete diffraction, is slightly asymmetric due to a small initial phase offset of the two input beams. After a few minutes of illumination light-induced phase changes lead to self-focusing of the beam, which finally results in the formation of a steady-state odd symmetric staggered soliton (Fig. 7.9c), which is recorded up to steady

state within one hour of illumination. This soliton is shifted with respect to the input beam demonstrating steering of the soliton across the array (compare with the numerical result from Fig. 6.36b). This localized structure was monitored for almost two hours without any changes.

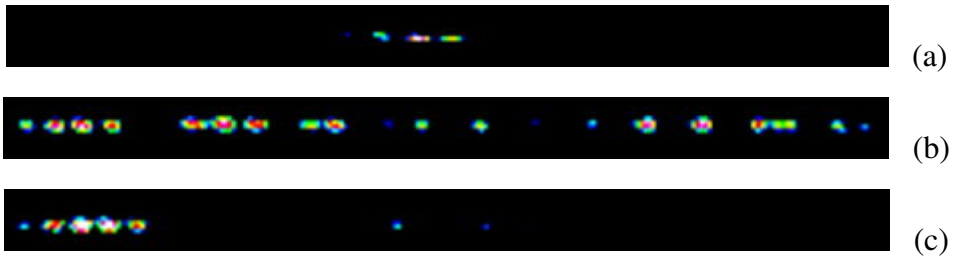

Fig. 7.9 *Images from the CCD camera taken at the front (a) and at the rear face (b, c) of the nonlinear $LINbO_3$ waveguide array.*

The corresponding intensity graphs are presented in Fig. 7.10. The discrete symmetric odd staggered soliton is trapped by the channel waveguide which is indexed with $n=-9$.

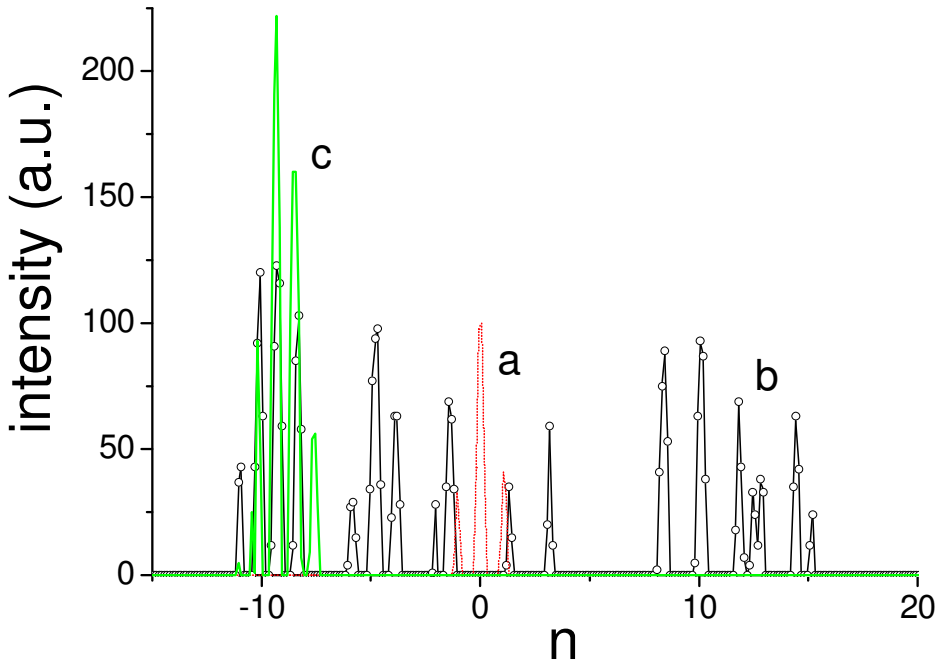

Fig. 7.10 *Intensity profiles which correspond to the experimentally obtained data from Fig.* 7.9.

8. CONCLUSIONS

In this thesis the nonlinear dynamics of spatial solitons in inherently discrete systems with saturable types of nonlinearity are investigated, which can be presented mathematically as a system of coupled ordinary differential equations. These equations represent special cases of the discrete nonlinear Schrödinger equation with either focusing or defocusing nonlinearity of a saturable type. Various stationary solutions of these nonlinear differential-difference equations are investigated analytically, numerically, and experimentally within the thesis.

Discrete solitons can exist due to an exact balance between nonlinearity and linear coupling effects among adjacent potential wells. Although they can be found in quite different nonlinear systems in nature such as Josephson junctions, Bose-Einstein condensates, DNA molecules, Scheibe aggregates, or electrical lattices, in this thesis the accent is put on bright coherent optical solitons in nonlinear waveguide arrays. It is believed that these periodic waveguide structures, which can be precisely fabricated in quite different media, together with optical solitons are going to be irreplaceable elements of future all-optical networks and devices, such as optical reconfigurable interconnects, beam modulators and deflectors, as well as amplifiers and all-optical switches.

In the small amplitude or linear regime the optical field travelling in a homogeneous waveguide array is subjected to a periodic potential and, as a result, the corresponding dispersion relation is periodic and organized as a succession of allowed bands and band gaps. Waves can only travel if their eigenvalues fall within an allowed band. This band structure of the dispersion relation is the underlying physical mechanism leading to discrete diffraction. Discrete diffraction may be completely controlled by launching a beam at a particular angle relative to the array. As a result diffraction in a waveguide array can become anomalous or even vanishes completely. Both, numerical and experimental evidences of discrete diffraction and diffraction-less propagation across the nonlinear waveguide array are given within the thesis.

The discretized Vinetskii-Kukhtarev equation, which is suggested as a model equation for optical pulse propagation in one-dimensional photorefractive waveguides with screening saturable nonlinearity, is found to have uniform unstaggered (adjacent elements are in-phase) and staggered (adjacent elements are out-of-phase) stationary solutions. Only the first array-independent solution is modulationaly unstable with respect to small unstaggered perturbations. Modulation instability can lead to the generation of various strongly localized unstaggered stationary modes or discrete screening solitons, such as symmetric odd and even solitons, twisted solitons, and antisymmetric odd ones. Within the thesis only the two first solutions were examined in detail, both analytically and numerically. The ultimate demand for an application of discrete solitons in real all-optical devices is that they have to be stable. Therefore, their stability is confirmed analytically and numerically within the thesis, while the corresponding experimental proof is still under way.

In the high amplitude or deep saturation regime, in which the discovered approximate analytical solution fails, a cascade mechanism of saturation is revealed by virtue of numerical simulations. A predetermined element of the array (in fact an arbitrary one, because an almost full control of the relevant parameters can be obtained in the experiments) goes first into saturation, while the amplitude in its neighbours keeps rising monotonically until it also reaches the saturation level. This procedure is repeated for the next neighbours, which finally leads to a widening of the localized structure. This is opposite to the situation in discrete media with cubic (Kerr) nonlinearity, in which a further increase in power results in continuous energy localization into a single element and its decoupling from the rest of the array.

Two types of solitons are considered: an odd symmetric unstaggered soliton (or mode A) is centred on the site while an even symmetric unstaggered soliton (or mode B) is centred between the sites of the array. The difference of their energies is attributed to the Peierls-Nabarro effective periodic potential generated by the lattice discreteness. A power dependent soliton steering can be explained with this potential assuming it as the minimum barrier which must be overcome to propagate a soliton across the nonlinear lattice. During the work on these systems it is discovered that this potential may change its sign as a function of optical power, which is opposite to discrete media with cubic nonlinearity where the potential is always negative and proportional to the soliton power level. This property of the screening saturable nonlinearity has a strong influence on the stability of the above mentioned unstaggered modes A and B. It is numerically demonstrated that a stable soliton propagation between waveguides (mode B) is possible, thus enabling a new type of all-optical switch. Due to the cascade mechanism of saturation the corresponding Peierls-Nabarro potential has multiple zeroes, which enables an increased mobility of large symmetric unstaggered discrete solitons across the system. It is also revealed that at these zeroes discrete screening solitons do not fuse but interact elastically. Such a fusion of solitons is observed for spatial solitons in saturable bulk media.

A mathematical model which can describe the optical pulse propagation in homogeneous one-dimensional and lossless photovoltaic photorefractive waveguide arrays is also proposed. Here, the uniform staggered stationary solution is modulationally unstable with respect to small staggered perturbations. As the outcome of modulation instability, various strongly localized staggered modes can occur. Within this thesis only symmetric odd and even staggered solitons are studied. Discrete photovoltaic solitons do not express the cascade mechanism of saturation. However, it is possible to find two zeroes of the Peierls-Nabarro potential and thus a stable propagation of mode B across array becomes possible. The reason for the existence of these zeroes is a different pace of the energy redistribution between adjacent elements of the localized modes A and B.

For the first time discrete diffraction, discrete self-focusing and self-defocusing phenomena in one-dimensional channel waveguide arrays in lithium niobate ($LiNbO_3$) are experimentally observed. Both narrow input beams with widths of about 4 μm, where only one channel is excited, and broad input beams with widths of 30-60 μm to excite 5-7 channels at the same time are used to explore the linear and nonlinear dynamics in the nonlinear arrays. Seminal observation of discrete soliton-like structure formation in Cu-doped $LiNbO_3$ waveguides is also reported. Steering of odd discrete photovoltaic solitons across the array is demonstrated, too.

As usual, each discovery triggers an avalanche of new questions. Here, one can think about a development of a theory which includes a phase dependence of the soliton. This can be useful for a better understanding of steering and collisions of these localized structures. Besides the symmetric, unstaggered and staggered odd and even modes, which are investigated thoroughly within this thesis, it will be interesting to examine the properties of other types of localized modes which these nonlinear lattices can support, such as antisymmetric odd and twisted modes. Theoretical predictions of stable propagation of mode B and enhanced mobility of large power solitons across the waveguide array challenge our experimental abilities to prove or to rebut them. Also, it will be interesting to investigate the influence of point and line defects within the array on the dynamics of discrete solitons, as well as their interactions with each other. In addition, a generalization of the suggested model equations, in order to comprise both soliton dynamics in higher bands and the influence of dispersion, will be desirable. Finally, experiments with modes A and B as well with other possible stationary modes may pave the way for the fabrications of realistic principal all-optical devices such as routers and switches.

9. REFERENCES

[1] J. S. Russel, Rep. Meet. British Assoc. Adv. Sci. **14**, 311 (1844).

[2] D. J. Korteweg and G. de Vries, Philos. Mag. Ser. **5**, 422 (1895).

[3] C. S. Gardner and G. J. Morikawa, Courant Inst. of Math. Sc.Rept.N^0 **40**, 9082 (1962).

[4] E. Fermi, J. Pasta, and S. Ulam, "*Nonlinear Wave Motion*", Ed. A. C. Newell, Am. Math. Soc., Providence (1974).

[5] N. J. Zabusky and M. D. Kruskal, Phys. Rev. Lett. **15**, 240 (1965).

[6] C. S. Gardner, J. M. Greene, M. D. Kruskal, R. M. Miura, Phys. Rev. Lett. **19**, 1095 (1967).

[7] P. D. Lax, Commun. Pure Appl. Math. **21**, 467 (1968).

[8] V. E. Zakharov and A. B. Shabat, Sov. Phys. JETP **34**, 62 (1972).

[9] M. J. Ablowitz, D. J. Kaup, A. C. Newell, H. Segur, Stud. Appl. Math. **53**, 249 (1974).

[10] A. S. Davydov, J. Theor. Biol. **38**, 559 (1973).

[11] P. L. Christiansen, O. Bang, S. Pagano, and G. Vitiello, Nanobiology **1**, 229 (1992).

[12] P. A. Franken, A. E. Hill, C. W. Peters, and G. Weinreich, Phys. Rev. Lett **7**, 118 (1961).

[13] G. A. Askar'yan, Sov. Phys. JETP **15**, 1088 (1962).

[14] M. Hercher, J. Opt. Soc. Am. **54**, 563 (1964).

[15] J. E. Bjorkholm and A. Ashkin, Phys. Rev. Lett. **32**, 129 (1974).

[16] A. Hasegawa and F. D. Tappert, Appl. Phys. Lett. **23**, 142 (1973).

[17] L. F. Mollenauer and K. Smith, Opt. Lett. **13**, 675 (1988).

[18] D. N. Christodoulides and R. I. Joseph, Opt. Lett. **13,** 794 (1988).

[19] H. S. Eisenberg, Y. Silberberg, R. Morandotti, A. R. Boyd, and J. S. Aitchinson, Phys. Rev. Lett. **81**, 3383 (1998).

[20] Y. Silberberg, Opt. Lett. **15**, 1282 (1990).

[21] A. Hasegawa and F. D. Tappert, Appl. Phys. Lett. **23**, 171 (1973).

[22] R. Y. Chiao, E. Garmire, and C. H. Townes, Phys. Rev. Lett. **13**, 479 (1964).

[23] Yu. S. Kivshar, Opt. Lett. **18**, 1147 (1993).

[24] K. Tai, A. Hasegawa, and A. Tomita, Phys. Rev. Lett. **56**, 135 (1986).

[25] S. Darmanyan, I. Relke, and F. Lederer, Phys. Rev. E **55**, 7662 (1997).

[26] Yu. Kivshar and X. Yang, Phys. Rev. E **49**, 1657 (1994).

[27] J. M. Soto-Crespo, D. R. Heatley, E. M. Wright, and N. N. Akhmediev, Phys. Rev. A **44**, 636 (1991).

[28] D. N. Christodoulides, T. H. Coscun, M. Mitchell, and M. Segev, Phys. Rev. Lett. **80**, 2310 (1998).

[29] A. V. Buryak, Yu. S. Kivshar, M. Shih, and M. Segev, Phys. Rev. Lett. **82**, 81 (1999).

[30] L. P. Pitaevskii, Zh. Eksp. Teor. Fiz. **40**, 646 (1961).

[31] A. W. Snyder, L. Poladian, and D. J. Mitchell, Opt. Lett. **17**, 789 (1992).

[32] J. J. Garcia-Ripoll, V. M. Perez Garcia, E. A. Ostrovskaya, and Yu. S. Kivshar, Phys. Rev. Lett. **85**, 82 (2000).

[33] M. A. Karpierz, "Spatial solitons in liquid crystals" in *Soliton-driven Photonics*, Eds. A. D. Boardman and A. P. Sukhorukov, Kluwer Academic Publishers, pp. 41 (2001).

[34] R. Uzdin, M. Segev, and G. J. Salamo, Opt. Lett. **26**, 1547 (2001).

[35] Y. N. Karamzin and A. P. Sukhorukov, Sov. Phys. JETP **41**, 414 (1976).

[36] W. E. Torruellas, Z. Wang, D. J. Hagan, E. W. VanStryland, G. I. Stegeman, L. Torner, and C. R. Menyuk, Phys. Rev. Lett. **74**, 5036 (1995).

[37] R. A. Fuerst, M. T. G. Canva, D. Baboiu, G. I. Stegeman, Opt. Lett. **22**, 1748 (1997).

[38] G. I. Stegeman, D. J. Hagan, and L. Torner, J. Opt. Quantum Electron. **28**, 1691 (1996).

[39] R. Schiek, Y. Baek, and G. I. Stegeman, Phys. Rev. E **53**, 1138 (1996).

[40] M. Segev, B. Crosignani, A. Yariv, and B. Fischer, Phys. Rev. Lett. **68**, 923 (1992).

[41] G. C. Valley, M. Segev, B. Crosignani, A. Yariv, M. M. Fejer, and M. C. Bashaw, Phys. Rev. A **50**, R4457 (1994).

[42] M. Taya, M. C. Bashaw, M. M. Fejer, M. Segev, and G. C. Valley, Phys. Rev. A **52**, 3095 (1995).

[43] M. Segev, A. Yariv, B. Crosignani, P. DiPorto, G. Duree, G. Salamo, and E. Sharp, Opt. Lett. **19**, 1296 (1994).

[44] M. D. Iturbe-Castillo, P. A. Marquez-Aguilar, J. J. Sánchez-Mondragón, S. Stepanov, and V. Vysloukh, Appl. Phys. Lett. **64**, 408 (1994).

[45] M. Segev, G. C. Valley, B. Crosignani, P. DiPorto, and A. Yariv, Phys. Rev. Lett. **73**, 3211 (1994).

[46] M. Jeganathan and L. Hesselink, J. Opt. Soc. Am. B **11**, 1791 (1994).

[47] D. N. Christodoulides and M. I. Carvalho, J. Opt. Soc. Am. B **12**, 1628 (1995).

[48] M. Morin, G. Duree, G. Salamo, and M. Segev, Opt. Lett. **20**, 2066 (1995).

[49] M. Klotz, H. Meng, G. Salamo, M. Segev, and S. R. Montogmery, Opt. Lett **24**, 77 (1998).

[50] F. Derrien, J. F. Henninot, M. Warenghem, and G. Abbate, J. Opt. A: Pure Appl. Opt. **2**, 332 (2000).

[51] M. Mitchell, Z. Chen, M. Shih, and M. Segev, Phys. Rev. Lett. **77**, 490 (1996).

[52] M. Mitchell and M. Segev, Nature **387**, 880 (1997).

[53] M. Segev and D. N. Christodoulides, Optics & Photonics News **13**, 70 (2002).

[54] G. I. Stegeman and M. Segev, Science **286**, 1518 (1999).

[55] S. V. Manakov, Sov. Phys. JETP **38**, 248 (1974).

[56] J. U. Kang, G. I. Stegeman, J. S. Aitchinson, and N. Akhmediev, Phys. Rev. Lett. **76**, 3699 (1996).

[57] S. Trillo, S. Wabnitz, E. M. Wright, and G. I. Stegeman, Opt. Lett. **13**, 871 (1998).

[58] D. N. Christodoulides, S. R. Singh, M. I. Carvalho, and M. Segev, Appl. Phys. Lett. **68**, 1763 (1996).

[59] M. V. Tratnik and J. E. Sipe, Phys. Rev. A **38**, 2001 (1988).

[60] M. Mitchell, M. Segev, and D. N. Christodoulides, Phys. Rev. Lett. **80**, 4657 (1998).

[61] E. A. Ostrovskaya, Yu. S. Kivshar, D. V. Skryabin, and W. J. Firth, Phys. Rev. Lett. **83**, 296 (1999).

[62] M. Shalaby and A. J. Barthelemy, IEEE J. Quantum. Electron. **28**, 2736 (1992).

[63] Z. Chen, M. Segev, T. H. Coskun, D. N. Christodoulides, Yu. S. Kivshar, and V. V. Afanasjev, Opt. Lett. **21**, 1821 (1996).

[64] T. Carmon, C. Anastassiou, S. Lan, D. Kip, Z. Musslimani, M. Segev, and D. N. Christodoulides, Opt. Lett. **25**, 1113 (2000).

[65] M. Brambilla, L. A. Lugiato, F. Prati, L. Spinelli, and W. J. Firth, Phys. Rev. Lett. **79**, 2042 (1997).

[66] W. W. Rigrod, Appl. Phys. Lett. **2**, 51 (1963).

[67] F. T. Arecchi, S. Boccaletti, and P. L. Ramazza, Phys. Rep. **318**, 1 (1999).

[68] E. A. Kuznetsov, A. M. Rubenchik, and V. E. Zakharov, Phys. Rep. **142**, 103 (1986)

[69] J. J. Rasmussen and K. Rypdal, Phys. Scr. **33**, 481 (1986).

[70] X. Liu, L. J. Qian, and F. W. Wise, Phys. Rev. Lett. **82**, 4631 (1999).

[71] A. Yariv, "*Optical Electronics"*, Saunders College Publishing, Philadelphia, pp.519 (1991).

[72] H. S. Eisenberg, Y. Silberberg, R. Morandotti, and J. S. Aitchinson, Phys. Rev. Lett. **85**, 1863 (2000).

[73] N. W. Ashcroft and N. D. Mermin, "*Solid state physics*", Holt, Reinhart, and Winston, New York, 182 (1976).

[74] R. Morandotti, H. S. Eisenberg, Y. Silberberg, M. Sorel, and J. S. Aitchinson, Phys. Rev. Lett. **86**, 3296 (2001).

[75] M. J. Ablowitz and Z. H. Musslimani, Phys. Rev. Lett. **87**, 254102 (2001).

[76] F. Lederer and Y. Silberberg, Optics & Photonics News **2**, 48 (2002).

[77] F. Bloch, Z. Phys. **52**, 555 (1928).

[78] C. Zener, Proc. R. Soc. London A **145**, 523 (1934).

[79] C. Waschke, H. Roskos, R. Schwendler, K. Leo, H. Kurz, and K. Kohler, Phys. Rev. Lett. **70**, 3319 (1993).

[80] R. Morandotti, U. Peschel, J. S. Aitchinson, H. S. Eisenberg, and Y. Silberberg, Phys. Rev. Lett. **83**, 4756 (1999).

[81] D. Mandelik, H. S. Eisenberg, Y. Silberberg, R. Morandotti, and J. S. Aitchinson, Phys. Rev. Lett. **90**, 053902 (2003).

[82] Yu. I. Voloschchenko, Yu. N. Ryzhov, V. E. Sotin, Sov. Phys. Tech. Phys. **26**, 541 (1981).

[83] H. Kogelnik and C. V. Shank, J. Appl. Phys. **42**, 2327 (1972).

[84] T. Holstein, Ann. Phys. **8**, 343 (1959).

[85] R. Sharf and A. R. Bishop, Phys. Rev. A **43**, 6535 (1991).

[86] S. Mookherjea and A. Yariv, Opt. Express **9**, 91 (2001).

[87] I. R. Durrani, G. Murtaza, and H.U. Rahman, Plasma Physics **22**, 719 (1980).

[88] S. V. Vladimirov, S. I. Popel, and V. N. Tsytovich, Phys. Fluids B **5**, 4109 (1993).

[89] Yu. S. Kivshar and D. E. Pelinkovsky, Phys. Rept. **331**, 117 (2000).

[90] A. B. Aceves, G. G. Luther, C. De Angelis, A. M. Rubenchik, and S. K. Turitsyn, Phys. Rev. Lett. **75**, 73 (1995).

[91] I. Relke, Phys. Rev. E **57**, 6105 (1998).

[92] D. Kip, M. Soljačić, M. Segev, E. Eugenieva, and D. N. Christodoulides, Science **290**, 495 (2000).

[93] D. Kip, M. Soljačić, M. Segev, S. M. Sears and D. N. Christodoulides, J. Opt. Soc. Am. B **19**, 502 (2002).

[94] S. F. Mingaleev, Yu. S. Kivshar, and R. A. Sammut, Phys. Rev. E **62**, 5777 (2000).

[95] A. A. Sukhorukov and Yu. S. Kivshar, Phys. Rev. E **65**, 036609 (2002).

[96] M. Stepić, D. Kip, Lj. Hadžievski, and A. Maluckov, Phys. Rev. E **69**, 066618 (2004).

[97] J. C. Eilbeck, P. S. Lomdahl, and A. C. Scott, Phys. Rev. B **30**, 4703 (1984).

[98] Yu. S. Kivshar and M. Peyrard, Phys. Rev. B **46**, 3198 (1992).

[99] J. Pouget, M. Remoissenet, and M. Tamga, Phys. Rev. B **47**, 14866 (1993).

[100] S. Darmanyan, A. Kobyakov, and F. Lederer, Sov. Phys. JETP **86**, 682 (1998).

[101] Lj. Hadžievski, M. Stepić, and M.M. Škorić, Phys. Rev. B **68**, 014305 (2003).

[102] G. B. Whitham, Proc. R. Soc. London A **283**, 238 (1965).

[103] T. B. Benjamin and J. E. Feir, J. Fluid Mech. **27**, 417 (1967).

[104] F. Lederer, S. Darmanyan, and A. Kobyakov, *"Discrete Solitons"* in *Spatial Solitons,* eds. S. Trillo and W. Torruellas, Springer Series on Optical Sciences, Vol. 82, Springer, Berlin, New York, pp. 269 (2001).

[105] N. M. Naumova, S. V. Bulanov, T. Zh. Esirkepov, D. Farina, K. Nishihara, F. Pegoraro, H. Ruhl, and A. S. Sakharov, Phys. Rev. Lett. **87**, 185004 (2001).

[106] Lj. Hadžievski, M. S. Jovanović, M.M. Škorić, and K. Mima, Physics of Plasmas **9**, 2569 (2002).

[107] D. Cai, A. R. Bishop, and N. Grønbech-Jensen, Phys. Rev. Lett. **70**, 591 (1993).

[108] B. L. Swanson, J. A. Brozik, S. P. Love, G. F. Strouse, A. P. Shreve, A. R. Bishop, W. Z. Wang, and M. I. Salkola, Phys. Rev. Lett. **82**, 3288 (1999).

[109] M. Peyrard and A. R. Bishop, Phys. Rev. Lett **62**, 2755 (1989).

[110] M. Peyrard, T. Dauxois, H. Hoyet, and C. R. Willis, Physica **68D**, 104 (1993).

[111] G. Lapenta, Phys. Rev. Lett **90**, 135005 (2003).

[112] G. P. Agrawal, P. L. Baldeck, and R. R. Alfano, Phys. Rev. A **39**, 3406 (1989).

[113] W. Królikowski, O. Bang, J. J. Rasmussen, J. Wyller, Phys. Rev. E **64**, 016612 (2001).

[114] M. Stepić, Lj. Hadžievski, and M.M. Škorić, Phys. Rev. E **65**, 026604 (2002).

[115] C. Anastassiou, M. Soljačić, M. Segev, D. Kip, E. D. Eugenieva, D. N. Christodoulides, Phys. Rev. Lett. **85**, 4888 (2000).

[116] Z. H. Musslimani and J. Yang, Opt. Lett. **26**, 1981 (2001).

[117] D. Neshev, A. A. Sukhorukov, Yu. S. Kivshar, W. Królikowski, Opt. Lett. **29**, 259 (2004).

[118] K. Motzek, F. Kaiser, W. Chu, M. Shih, and Yu. S. Kivshar, Opt. Lett. **29**, 280 (2004).

[119] D. Anderson, M. Bondeson, and M. Lisak, Phys. Lett. **67A**, 331 (1978).

[120] V. E. Zakharov and E. A. Kuznetsov, Sov. Phys. JETP **64**, 773 (1986).

[121] K. Rypdal and J. J. Rasmussen, Phys. Scr. **40**, 192 (1989).

[122] Lj. R. Hadžievski, M.M. Škorić, A. M. Rubenchik, E. G. Shapiro, and S. K. Turitsyn, Phys. Rev. A **42**, 3651 (1990).

[123] A. Hasegawa, Chaos **10**, 475 (2000).

[124] V. I. Karpman and E. M. Maslov, Phys. Lett. **60A**, 307 (1977).

[125] E. S. Benilov, Sov. Phys. JETP **61**, 70 (1985).

[126] J. Carr and J. C. Eilbeck, Phys. Lett. **109A**, 201 (1985).

[127] E. W. Laedke, K. H. Spatschek, V. K. Mezentsev, S. L. Musher, I. V. Ryzhenkova, and S. K. Turitsyn, Pis'ma v ZhETF **62**, 652 (1995).

[128] L.M. Floría, J.L. Marín, P.J. Martínez, F. Falo, S. Aubry, Europhys. Lett. **36**, 539 (1996).

[129] A. B. Aceves, C. De Angelis, A. M. Rubenchik, S. K. Turitsyn, Opt. Lett. **19**, 329 (1994).

[130] M. I. Weinstein, Nonlinearity **12**, 673 (1999).

[131] P. G. Kevrekidis, B. A. Malomed, and Yu. B. Gaididei, Phys. Rev. E **66**, 016609 (2002).

[132] S. Trillo, S. Wabnitz, E. M. Wright, and G. I. Stegeman, Opt. Lett. **13**, 672 (1988).

[133] J. M. Soto-Crespo and E. M. Wright, J. Appl. Phys. **70**, 7240 (1991).

[134] Yu. S. Kivshar, Opt. Lett. **18**, 7 (1993).

[135] W. Królikowski, U. Trutschel, M. Cronin-Golomb, and C. Schmidt-Hattenberger, Opt. Lett. **19**, 320 (1994).

[136] X. Yang, Yu. S. Kivshar, B. Davies, and D. R. Andersen, Opt. Lett. **19**, 344 (1994).

[137] W. Królikowski and Yu. S. Kivshar, J. Opt. Soc. Am. B **13**, 876 (1996).

[138] O. Bang and P. D. Miller, Phys. Scr. **T67**, 26 (1996).

[139] A. B. Aceves and M. Santagiustina, Phys. Rev. E **56**, 1113 (1997).

[140] R. A. Vicencio, M. I. Molina, and Yu. S. Kivshar, Opt. Lett. **28**, 1942 (2003).

[141] A. B. Aceves, C. De Angelis, T. Peschel, R. Muschall, F. Lederer, S. Trillo, and S. Wabnitz, Phys. Rev. E **53**, 1172 (1996).

[142] U. Peschel, R. Morandotti, J. M. Arnold, J. S. Aitchison, H. S. Eisenberg, Y. Silberberg, T. Pertsch, and F. Lederer, J. Opt. Soc. Am. B **19**, 2637 (2002).

[143] T. Pertsch, T. Zentgraf, U. Peschel, A. Bräuer, and F. Lederer, Appl. Phys. Lett. **80**, 3247 (2002).

[144] A. B. Aceves, C. De Angelis, S. Trillo, and S. Wabnitz, Opt. Lett. **19**, 332 (1994).

[145] R. Morandotti, U. Peschel, J. S. Aitchinson, H. S. Eisenberg, and Y. Silberberg, Phys. Rev. Lett. **83**, 2726 (1999).

[146] V. O. Vinetskii and N. V. Kukhtarev, Sov. Phys. Solid State **16**, 2414 (1975).

[147] O. Bang, J. J. Rasmussen, and P. L. Christiansen, Nonlinearity **7**, 205 (1994).

[148] B. Malomed and M. I. Weinstein, Phys. Lett. A **220**, 91 (1996).

[149] J. C. Eilbeck, P. S. Lomdahl, and A. C. Scott, Physica D **16**, 318 (1985).

[150] E. Trías, J. J. Mazo, and T. P. Orlando, Phys. Rev. Lett. **84**, 741 (2000).

[151] S. Pekar, J. Phys. (USSR) **10**, 341 (1946).

[152] L. A. Ostrovskii, V. V. Papko, and Yu. A. Stepanyants, Sov. Phys. JETP **51**, 417 (1980).

[153] P. Marquie, J. M. Bilbault, and M. Remoissenet, Phys. Rev. E **51**, 6127 (1995).

[154] P. V. Lenzo, E. G. Spencer, and A. A. Bailman, Appl. Phys. Lett. **11**, 23 (1967).

[155] D. Kip, Appl. Phys. B:Lasers Opt. **67**, 131 (1998).

[156] A. C. Scott and L. Macneil, Phys. Lett. **98A**, 87 (1983).

[157] E. W. Laedke, K. H. Spatschek, and S. K. Turitsyn, Phys. Rev. Lett. **73**, 1055 (1994).

[158] F. Kh. Abdullaev, S. A. Darmanyan, and J. Garnier, Prog. Opt. **44**, 303 (2002).

[159] M. G. Vakhitov and A. A. Kolokolov, Radiophys. Quantum Electron. **16**, 783 (1975).

[160] M. Stepić, A. Maluckov, F. Chen, and D. Kip, will be submited to J. Opt. Soc. Am. B.

[161] A. Maluckov, M. Stepić, D. Kip, and Lj. Hadžievski, submited to Phys. Rev. E

[162] A. A. Maradudin, *Theoretical and Experimental Aspects of the Effects of Point Defects and Disorder on the Vibrations of Crystals*, Academic, New York (1966).

[163] A. J. Sievers and S. Takeno, Phys. Rev. Lett. **61**, 970 (1988).

[164] J. B. Page, Phys. Rev. B **41**, 7835 (1990).

[165] Ch. Claude, Yu. S. Kivshar, O. Kluth, K. H. Spatschek, Phys. Rev. B **47**, 14228 (1993).

[166] Yu. S. Kivshar and D. K. Campbell, Phys. Rev. E **48**, 3077 (1993).

[167] O. M. Braun and Yu. S. Kivshar, Phys. Rept. **306**, 1 (1998).

[168] R. F. Peierls, Proc. R. Soc. London **52**, 34 (1940).

[169] F. R. Nabarro, Proc. R. Soc. London **59**, 256 (1947).

[170] G. I. Stegeman, D. N. Christodoulides, and M. Segev, IEEE J. on Select. Topics in Quantum Electron. **6**, 1419 (2000).

[171] A. Sukhorukov, Yu. S. Kivshar, H. S. Eisenberg, and Y. Silberberg, IEEE J. of Quantum Electron. **39**, 31 (2003).

[172] D. N. Christodoulides, F. Lederer, and Y. Silberberg, Nature **424**, 817 (2003).

[173] H. Feddersen, in *Nonlinear Structures in Physics and Biology*, Ed. M. Remoissenet and M. Peyrard, Springer Verlag, Berlin, 159 (1991).

[174] Lj. Hadžievski, A. Maluckov, M. Stepić, and D. Kip, Phys. Rev. Lett. **93**, 033901 (2004).

[175] S. Flach and C. R. Willis, Phys. Rept. **295**, 182 (1998).

[176] R. S. MacKay and S. Aubry, Nonlinearity **7**, 1623 (1994).

[177] G. P. Tsironis, Chaos **13**, 657 (2003).

[178] G. P. Agrawal, *Nonlinear Fiber Optics*, Academic Press, San Diego (1989).

[179] W. Królikowski and S. A. Holmstrom, Opt. Lett. **22**, 369 (1997).

[180] H. Meng, G. Salamo, M. Shih, and M. Segev, Opt. Lett. **22**, 448 (1997).

[181] W. Królikowski, M. Saffman, B. Luther-Davies, C. Denz, Phys. Rev. Lett. **80**, 3240 (1998).

[182] D. Kip, M. Wesner, C. Herden, and V. Shandarov, Appl. Phys. B **68**, 971 (1999).

[183] S. Kumar, M. Wald, F. Lederer, and A. Hasegawa, Opt. Lett. **23**, 1019 (1998).

[184] G. E. Falkovich, M. G. Stepanov, and S. K. Turitsyn, Phys. Rev. E **64**, 067602 (2001).

[185] T. Peschel, U. Peschel, and F. Lederer, Phys. Rev. E **57**, 1127 (1998).

[186] D. Cai, A. R. Bishop, and N. Grønbech-Jensen, Phys. Rev. E **56**, 7246 (1997).

[187] I. E. Paracharalampous, P. G. Kevrekidis, B. A. Malomed, and D. J. Frantzeskakis, Phys. Rev. E **68**, 046604 (2003).

[188] J. Meier, G. I. Stegeman, Y. Silberberg, R. Morandotti, and J. S. Aitchison, Phys. Rev. Lett. **93**, 093903 (2004).

[189] J. W. Fleischer, T. Carmon, M. Segev, N. K. Efremidis, and D. N. Christodoulides, Phys. Rev. Lett. **90**, 023902 (2003).

[190] D. Kip, B. Kemper, I. Nee, R. Pankrath, and P. Moretti, Appl. Phys. B **65**, 511 (1997).

[191] J. F. Ziegler, J. P. Biesack, and U. Littmark, *Stopping and ranges of Ions in Matter*, Pergamon, New York (1985).

[192] P. J. Chandler and F. L. Lama, Opt. Acta **33**, 127 (1986).

[193] K. Peithmann, J. Hukriede, K. Buse, and E. Krätzig, Phys. Rev. B **61**, 4615 (2000).

List of personal publications which are partially used in preparation of this thesis

In journals:

- A. Maluckov, M. Stepić, D. Kip, and Lj. Hadžievski, submitted to Phys. Rev. E.
- M. Stepić, A. Maluckov, F. Chen, and D. Kip, will be submitted to J. Opt. Soc. Am. B.
- Lj. Hadžievski, A. Maluckov, M. Stepić, and D. Kip, Phys. Rev. Lett. **93**, 033901 (2004).
- M. Stepić, D. Kip, Lj. Hadžievski, and A. Maluckov, Phys. Rev. E **69**, 066618 (2004).
- Lj. Hadžievski, M. Stepić, and M.M. Škorić, Phys. Rev. B **68**, 014305 (2003).
- M. Stepić, Lj. Hadžievski and M. M. Škorić, NIFS reports **772**, (2003).
- M. Stepić, Lj. Hadžievski, and M.M. Škorić, Phys. Rev. E **65**, 026604 (2002).

At conferences:

- M. Stepić, A. Maluckov, V. Shandarov, F. Chen, D. Runde, C. Rüter, and D. Kip, 10. International Conference Nonlinear optics of liquid and photorefractive crystals, Alustha, Crimea, Ukraine (2004).
- V. Shandarov, D. Kip, F. Chen, M. Stepić, D. Runde, and C. Rüter, Tomsk, Russia, s4_02 (2004).
- F. Chen, D. Kip, V. Shandarov, D. Runde, M. Stepić, and C. Rüter, 4. Asia-Pacific Conference, Fundamental problems of Opto- and Microelectronics, Khabarovsk, Russia, p. 108 (2004).
- F. Chen, M. Stepić, D. Runde, D. Kip, and V. Shandarov, 10. Microoptics Conference, Jena, Germany, L-25 (2004).
- A. Maluckov, M. Stepić, Lj. Hadžievski, and D. Kip, 11. Congress of Physicists of Serbia and Montenegro, Petrovac by the sea, Serbia and Montenegro, s2_06 (2004).
- A. Maluckov, M. Stepić, Lj. Hadžievski, and D. Kip, 11. Congress of Physicists of Serbia and Montenegro, Petrovac by the sea, Serbia and Montenegro, s2_07 (2004).
- A. Maluckov, M. Stepić, and Lj. Hadžievski, The Fifth General Conference of the Balkan Physical Union, Vrnjačka Banja, Serbia and Montenegro, p. 943 (2003).
- M. Stepić, D. Kip, and Lj. Hadžievski, The Fifth General Conference of the Balkan Physical Union, Vrnjačka Banja, Serbia and Montenegro, p. 929 (2003).
- M. Stepić, D. Kip, and Lj. Hadžievski, The Ninth International Conference on Photorefractive Effects, Materials, and Devices, Le Colle sur Loup, France, PD4 (2003).
- Lj. Hadžievski, M. Stepić, and M. M. Škorić, 3. Yu-Japan joint Workshop on computer simulation science, Belgrade, Yugoslavia, published in abstract p. 4 (2002).
- M. S. Stepić, Lj. R. Hadžievski, and M. M. Škorić, 21. Summer School and International Symposium of the Physics of Ionized Gases, Sokobanja, Yugoslavia, p. 637 (2002).
- M. S. Stepić, Lj. R. Hadžievski, and M. M. Škorić, 3. Nonlinear Science Festival, Technical University of Denmark, Lyngby, Denmark, published in abstract p. 42 (2001).

- Lj. R. Hadžievski, M. S. Stepić, M. M. Škorić, and T. Sato, 20. Summer School and International Symposium of the Physics of Ionized Gases, Zlatibor, Yugoslavia, p. 575 (2000).

LIST OF USED ABBREVIATIONS AND SYMBOLS

Abbreviations

NLS equation	nonlinear Schrödinger equation
DNLS equation	discrete nonlinear Schrödinger equation
PN potential	Peierls-Nabarro potential
LN	lithium niobate ($LiNb0_3$)
SBN	strontium barium niobate ($Sr_yBa_{1-y}Nb_2O_6$, $0.25 \leq y \leq 0.75$)
1D	one-dimensional
2D	two-dimensional
MI	modulational instability
SOU soliton	symmetric odd unstaggered soliton
AOU solton	antisymmetric odd unstaggered soliton
SOS soliton	symmetric odd staggered soliton
AOS solton	antisymmetric odd staggered soliton
EU soliton	even unstaggered soliton
ES soliton	even staggered soliton
TU soliton	twisted unstaggered soliton
TS soliton	twisted staggered soliton

Symbols

I	light intensity
n_r	refractive index
Δn_r	local refractive index change
n_2	Kerr coefficient
U	slowly varying envelope of wave function
x	transversal coordinate
z	propagation coordinate
i	imaginary unit $\left(i = \sqrt{-1}\right)$
A_0	amplitude of slowly varying envelope
U_∞	background amplitude $\left(U_\infty = \lvert U(x \to \pm\infty) \rvert\right)$

π	Ludolph's number $(\pi \approx 3.141592...)$
m	natural number
E_n	complex amplitude of the electrical field envelope at lattice site n
n	index of element of an array
Π	propagation constant
C	coupling constant
E_0	amplitude of the envelope in $n = 0$
J_n	Bessel's function of the first kind of order n
$\vec{r}$	radius vector
$\vec{k}$	wave vector
k	wave number
λ_0	wavelength of light in vacuum
k_x	transverse component of the wave vector
k_z	longitudinal component of the wave vector
Φ	phase
Δx	transversal shift
D	diffraction coefficient
D_{FP}	diffraction coefficient in free space
d	distance between centers of two adjacent elements of an array
$k_x d$	Bloch momentum
p	strength of linear potential
X	nonlinear coefficient
P	power
H	Hamiltonian
N	number of elements in array
E_H	amplitude of homogeneous solution
q	discrete wave number
ν_H	frequency of homogeneous stationary solution
η	$\eta = \cos(q)$
δ_n	small perturbation of amplitude of uniform solution
δ	amplitude of small perturbation $(\delta = a + ib)$

Q wave number of perturbation

W frequency

F_n amplitude of wave function at site n $\left(F_n = F\, f_n^{A,B}\right)$

$f_{1,2,\ldots}^{A}$ small numbers $\left(0 \le f_{1,2,\ldots}^{A} << 1\right)$

$f_{1,2,\ldots}^{B}$ small numbers $\left(0 \le f_{1,2,\ldots}^{B} << 1\right)$

F arbitrary constant: $F = A$ for odd symmetric mode, while $F = B$ for even symmetric mode

U_n envelope of wave function in n-th element of array

w width of single waveguide

h normalized distance between two elements in an array $\left(h = (L - Nw)/(Nx_0)\right)$

L length of the crystal in transversal direction

x_0 arbitrary spatial width

ξ dimensionless propagation coordinate $\left(\xi = z/(kx_0^2)\right)$

τ normalized dimensionless propagation coordinate $\left(\tau = \xi/2h^2\right)$

n_{reo} extraordinary refractive index

n_{ro} ordinary refractive index

β_{SC} positive parameter $\left(\beta_{SC} = (k\, x_0\, n_{reo})^2\, r_{33} E_{ext}\right)$

r_{33} electro-optic coefficient

E_{ext} external applied electric field

V constant bias voltage

U_{OSC} wave function of oscillatory solution

ν nonlinear frequency shift (or soliton frequency)

$|U_{HU}|$ amplitude of homogeneous unstaggered solution

$|U_{HS}|$ amplitude of homogeneous staggered solution

ε small parameter

Γ growth rate of perturbation $\left(\omega = \Omega + i\Gamma\right)$

Ω real part of growth rate

A_x slowly varying amplitude of the optical field

I_D dark irradiance

G dark generation rate

c_p	photo-ionization cross section
α	constant $\left(\alpha = -n_{ro}^3 \, r_{33} E_{PV} / 2\right)$
E_{PV}	photovoltaic field constant
β_{PV}	positive parameter $\left(\beta_{PV} = k^2 \, x_0^2 \mid \alpha \mid / n_{ro}\right)$
s	dimensionless transverse coordinate $\left(s = x / x_0\right)$
M	mass of an atom
u_n	displacement of atom from the equilibrium position
k_2	nearest neighbour harmonic force constant
k_4	quartic anharmonic force constant
χ	anharmonicity parameter of potential
ω_0	frequency of small amplitude on-site vibrations
ΔE_{AB}	Peierls-Nabarro potential $\left(\Delta E_{AB} = H_A - H_B\right)$
θ	normalized nonlinear frequency shift $\left(\theta = 2\nu h^2\right)$
γ_{SC}	normalized nonlinear screening constant $\left(\gamma_{SC} = 2\beta_{SC} h^2\right)$
γ_{PV}	normalized nonlinear photovoltaic constant $\left(\gamma_{PV} = 2\beta_{PV} h^2\right)$
$P_{C,C1,\ldots}$	critical power (zeroes of PN potential)
y	number $\left(0.25 \le y \le 0.75\right)$

ACKNOWLEDGMENTS

A core of this thesis consists of research results that are obtained in last two years, during my stay at Group of Optical Technologies, Institute of Physics and Physical Technologies, Technical University Clausthal in Germany. First of all I would like to thank my supervisor Prof. Dr. D. Kip for giving me a chance to work in his research group, teaching me first lessons at optical table, improving readability of my manuscripts, giving me freedom in work and helping me whenever it was necessary. I also would like to express my deep gratitude to D. Runde who helped me decisively to acclimatize on life abroad. Their help, as well a help from Dr. H. Rosher and our marvellous secretary Mrs. B. Bühler, has exceeded by far all my expectations. In time, the group starts to grow so I met Dr. F. Chen, who helped me a lot with experiments, and C. Rüter, who provided my research with excellent crystal samples. Prof. Dr. V. Shandarov, who has visited our group a few times, gave me a lot of useful advices related to work in Soliton Laboratory of our group and I am indebted to him on that. I acknowledge a work of our IT Team and our technicians, too. Work with F. Werunsky was an interesting experience for me. I am also thankful to young colleagues S. Breuer, C. Wirth, and S. Brunkler for their patient during my language practice. I am grateful to Prof. Dr. W. Lücke who agreed to review my thesis and participate in the work of the advisory Committee. This thesis is carried out under the auspices of the German Federal Ministry of Education and Research (BMBF, grant DIP-E6.1), INTAS (contract 01-0481), and, in part, by the Ministry of Science, Development and Technologies of Republic Serbia, Project 1964.

However, part of my gratitude should be paid to people from my homeland Serbia, who are surely deserved for my decision to work in science, ranging from my gymnasium physics teacher Prof. Lj. Jovanović and Prof. Dr. Božidar Milić from Faculty of Physics in Belgrade, to Prof. Dr. Miloš Škorić who received me in his research group at Vinča Institute of Nuclear Sciences in Belgrade. There I met my first supervisor, Dr. Lj. Hadžievski, who has introduced me patiently in canons of scientific work and who helped me a lot to accomplish my M. Sc. studies on time. I am glad that he is the member of the advisory Committee, too. I also would like to mention two others extraordinary persons from my former Institute: Dr. V. Miljević, whose still youthful spirit fascinate me over and over again and Dr. M. Rajković whose altruism give me an additional stimulation to work as a researcher. And last but not least, I would to gratefully acknowledge a magnificent cooperation with Dr. A. Maluckov who has checked numerically almost all of my theoretical predictions.

Apart from all my teachers and colleagues, I would like to thank all friends of mine, my family and the family of my wife, too, for great help, constant support and interest in my work. Finally, I am indescribable grateful to my dear wife Aleksandra and our wonderful daughter Mitra for all love and happiness that they are bringing in my life.

AFFIDAVIT:

Hereby I declare on oath that I compose presented work single-handed without any illegal help and with all used resources fully indicated. This dissertation is neither partially nor as a whole submitted for survey to any other University and I am trying to obtain a PhD degree for the first time.

In Clausthal-Zellerfeld, 25.10.2004 Milutin Stepić